



GEORG-AUGUST-UNIVERSITÄT
GÖTTINGEN IN PUBLICA COMMODA
SEIT 1737

Molecular Mechanisms of Sound Frequency Discrimination in the *Drosophila* Ear

Dissertation

for the award of the degree

“Doctor rerum naturalium” (Dr.rer.nat.)

of the Georg-August-University Göttingen

within the doctoral program Biology

of the Georg-August University School of Science (GAUSS)

submitted by

Xiaowei Zhang

from Changzhi, Shanxi, The People’s Republic of China

Göttingen, 2022

Thesis Committee

Prof. Dr. Martin Göpfert (supervisor)

Department Cellular Neurobiology, Georg-August-University Göttingen

Prof. Dr. André Fiala

Department of Molecular Neurobiology of Behavior, Georg-August-University Göttingen

Dr. Jan Clemens

European Neuroscience Institute, Georg-August-University Göttingen

Members of Examination Board

Reviewer: Prof. Dr. Martin Göpfert

Department Cellular Neurobiology, Georg-August-University Göttingen

Second reviewer: Prof. Dr. André Fiala

Department of Molecular Neurobiology of Behavior, Georg-August-University Göttingen

Further members of Examination Board

Dr. Jan Clemens

European Neuroscience Institute, Georg-August-University Göttingen

Prof. Dr. Andreas Stumpner

Department Cellular Neurobiology, Georg-August-University Göttingen

Prof. Dr. Carolin Wichmann

Center for Biostructural Imaging of Neurodegeneration, University Medical Center Göttingen

Prof. Dr. Nicola Strenzke

Institute for Auditory Neuroscience & Inner Ear Lab, University Medical Center Göttingen

Date of oral examination: 28.11.2022

Declaration

I herewith declare that my PhD thesis entitled “Molecular Mechanisms of Frequency Discrimination in the *Drosophila* Ear” was written independently and with no other sources and aids than quoted.

Xiaowei Zhang

Göttingen, October 2022

Table of Contents

Preface	7
I. Nature of sound	7
I. I Generation of sound	7
I. II Sound waveform and frequency filter.....	8
I.III Harmonic oscillation and resonance in acoustics	9
II. Sound perception	11
II. I Sound propagation and perception in human ear.....	11
Abstract	13
Chapter 1. Molecular Mechanisms of Sound Frequency Discrimination in the Drosophila Ear	14
1.1 Introduction	14
1.1.1 The model organism of <i>Drosophila melanogaster</i>	14
1.1.2 Parallels between vertebrate and <i>Drosophila</i> ear.....	15
1.1.3 Mechanism basis of <i>Drosophila</i> hearing	16
1.1.3.1 Mechanics of sound perception and anatomy of JO	16
1.1.3.2 Transduction of sound signals and chordotonal organ.....	17
1.1.3.3 Auditory signal processing in brain	19
1.1.4 Sound frequency dependent of JO neurons.....	20
1.1.4.1 Classification of JO neurons and their functions	20
1.1.4.2 Classification of auditory JO neurons.....	21
1.1.5 Frequency discrimination in cochlea	23
1.1.5.1 What is frequency discrimination and why it is important?.....	22
1.1.5.2 Cochlea frequency selectivity	23
1.1.5.3 The mechanisms of frequency discrimination in cochlea	24
1.1.6 The comparison between hair cells and JO neurons	26
1.2 Materials & Methods	27
1.2.1 Genetic approaches for the studies of genetics in <i>Drosophila</i>	27
1.2.1.1 Transposable Elements	27
1.2.1.2 GAL4 / UAS system	27
1.2.2 Immunohistochemistry.....	28
1.2.2.1 Johnston's organ staining in adult flies.....	28
1.2.2.2 Larva <i>lch5</i> organ staining.....	30
1.2.2.3 The whole antenna and brain staining.....	30
1.2.3 Polymerase Chain Reaction (PCR).....	30
1.2.3.1 Reverse Transcription (RT) – PCR.....	30

1.2.3.2 Rapid amplification of cDNA ends – PCR	32
1.2.4 Cell- or tissue- specific cell ablation and eyFLP	35
1.2.5 Maintenance of fly stock.....	37
1.2.6 Drosophila hearing assessment by Laser Doppler Vibrometry.....	40
1.2.6.1 Fly mounting.....	40
1.2.6.2 Mechanical measurement.....	40
1.2.6.3 Free fluctuation recording of sound receiver	41
1.2.6.4 Sound-induced intensity measurement at iBF.....	41
1.2.6.5 Sound-induced intensity measurement at different frequencies	43
1.2.7 Images analysis and data statistical analysis.....	43
1.2.8 Additional information for antibody	43
1.3 Results	45
1.3.1 Auditory performance of fly’s ear in wild-type strains.....	45
1.3.1.1 Anatomical analysis of JO neurons.....	45
1.3.1.2 Hearing performance at an individual best frequency (iBF).....	46
1.3.1.3 Hearing performance at different frequencies.....	50
1.3.1.3.1 Mechanical and electrical response at different frequencies.....	50
1.3.1.3.2 Responses at Iso-Intensity and Iso-Displacement.....	50
1.3.2 Effects of ablated auditory JO neurons	53
1.3.2.1 Distribution and localization of auditory JO neurons	53
1.3.2.2 Auditory performance of JO neurons at different frequencies.....	55
1.3.3 Candidate genes for regulationg frequency tuning of JO neurons	58
1.3.3.1 The voltage-gated calcium channels in fly’s hearing.....	58
1.3.3.1.1 The voltage-gated calcium channels expression in JO.....	58
1.3.3.1.2 The voltage-gated calcium channels in fly’s hearing.....	60
1.3.3.2 BK _c channel in fly’s hearing	62
1.3.3.3 Potassium channels in fly’s hearing.....	64
1.3.3.3.1 Voltage-gated channels expression in JO	64
1.3.3.3.2 Voltage-gated potassium channels in fly’s hearing.....	65
1.3.3.4 Other related genes (<i>Irkl</i> , <i>piezo</i> , <i>prestin</i>) in fly’s hearing	68
1.3.3.4.1 <i>Irkl</i> , <i>piezo</i> , and <i>prestin</i> expression in JO	68
1.3.3.4.2 <i>Irkl</i> , <i>piezo</i> , and <i>prestin</i> effects in fly’s hearing.....	69
1.3.4 Summary from genetic screen (Q factor and F ₀).....	72
1.3.5 Alternative splicing in electrical tuning modulation.....	73
1.4 Discussion	75
1.4.1 Damped simple harmonic oscillation.....	75
1.4.2 Frequency discrimination: from cells to genes	76

1.4.3 Gene-specific patterns of expression in JO.....	77
1.4.4 Diversification of channel gating kinetics.....	77
Chapter 2. Genetic screen of potassium channels in Johnston's Organ (JO).....	79
2.1 Introduction.....	79
2.1.1 Background and genetic screen in <i>Drosophila</i>	79
2.1.2 Potassium channels: diversity, classification, and physiology.....	81
2.1.3 Potassium channels: recirculation in cochlea.....	83
2.1.4 Potassium channels: diversity and functions in <i>Drosophila</i>	84
2.1.5 Aims: potassium channels in <i>Drosophila</i> hearing organ	85
2.2 Results	85
2.2.1 Homologous genes of K ⁺ channels in <i>Drosophila</i>	85
2.2.2 Distribution of K ⁺ channels in 2 nd segment of antenna	86
2.2.3 Effects of mutations in K ⁺ channels in fly hearing.....	88
2.2.4 Requirements of <i>Shaker</i> or <i>Shab</i> channel for <i>Drosophila</i> hearing?.....	93
2.2.5 Expression of potassium channels in JO.....	95
2.3 Discussion.....	99
2.3.1 Genetic parallels of K ⁺ channels in <i>Drosophila</i> and Vertebrate ears.....	99
2.3.2 Expression of K ⁺ channels in <i>Drosophila</i> ear	99
2.3.3 Role of Kv2 in mammals hearing and <i>Shab</i> in <i>Drosophila</i>	99
2.3.4 Achievements and questions to be answered?	100
List of references.....	101
List of abbreviations.....	107
List of Figures.....	108
List of Tables	110
Acknowledgment... ..	111

Preface

I. Nature of sound

I. I Generation of sound

Humans can perceive external stimuli from the surrounding environment by different senses, five of which were distinguished already by Aristoteles, including vision, smell, taste, hearing, and touch. Each sense is mediated by specialized sensory organs, including eyes, nose, tongue, ear, and skin, harbouring sensory receptor cells to receive external stimuli (Scanes, 2018). For instance, eyes harbour photoreceptors to receive light or photons. Nose or tongue contains olfactory or gustatory receptors to be activated by the chemical molecules, while ear and skin contain mechanosensory organs/receptors to detect mechanical stimuli, like sound or pressure. Hearing, as the main topic in this thesis, refers to the ability to sense sound, playing an important role to connect with the environment and maintain an interspecies connection through acoustic communication (Plack, 2018; Green, 2021). Before dwelling into the biophysics or molecular mechanisms that animals employ to hear, it is essential to understand the stimuli that the hearing organ detects. Therefore, the initial questions should be: What is sound? How is the sound generated and perceived?

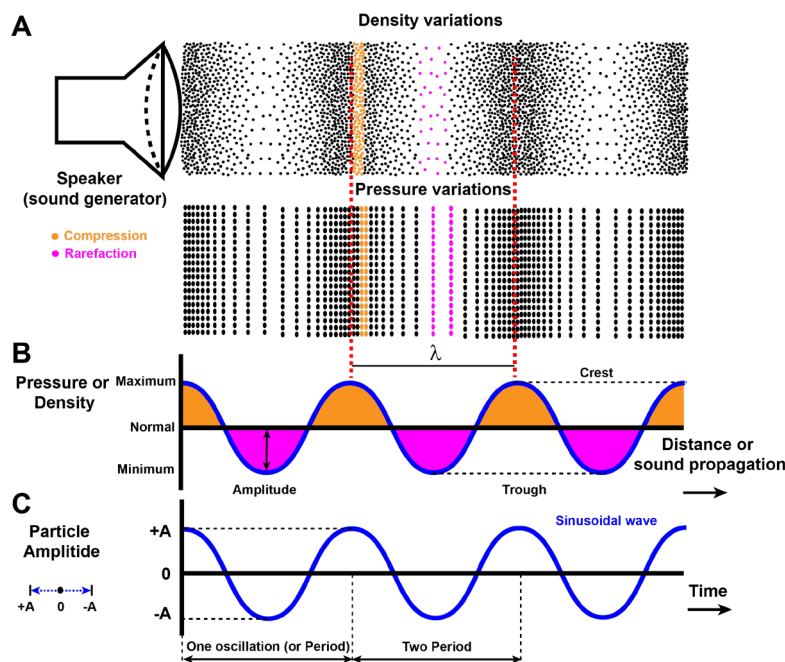


Fig. 1 Diagram of sound generation and two types of sinusoidal waves. (A) Illustration of sound generation. The sound is generated by the vibration of speaker's diaphragm, which leads to the periodic oscillation of air particles surrounding the diaphragm. The oscillating particles carrying the energy will continue to bombard adjacent downstream particles to do the same periodic movement, leading to the periodic change of particles and pressure and forming a so-called compression and rarefaction regions. (B) In physics, the changes of pressure or density can be shown as sine waves. The distance between two consecutive compressions or rarefaction is called wavelength. (C) The oscillation of single particle can also be illustrated by a sine wave. A period is defined as the time that the particle completes one oscillation. And the division of one oscillation to

period refers to sound frequency. Amplitude refers to the distance that oscillating particles move. The picture was modified from (Berg Richard *et al.*, 2016).

Sound is a mechanical wave (also called acoustic wave) that propagates through mediums such as water, gas, or solid, and carries mechanical energy to be perceived by the acoustic sensory organ. Sound is generated by the successive vibration of objects, which results in an oscillating motion of particles in surrounding media at the same rate. As the object continues to vibrate the neighboring particles as shown in Fig. 1A, sound propagates to a distance. The pressure and density of medium particles exhibit periodic changes when compression and rarefaction regions are formed, which is called sound wave or pressure wave (Fig. 1B). Sound waves possess two features: one is the disturbance travelling with velocity within the medium, which depends on the properties of the mediums such as particle density, temperature, or viscosity, etc; the other one is the kinetic energy of oscillating particles, regarding sound as a mechanical stimulus for auditory sensation.

Sound consists of two main components: pressure waves transmitting energy through mediums (Fig. 1B) and particles with periodic oscillations over time (Fig. 1C). In physics, the pressure wave and oscillation track of each particle can be described as sinusoidal plane waves and characterized by the following generic parameters that are assembled in a so-called sound wave, including wavelength (λ), amplitude, intensity (decibels; dB), frequency (or pitch, f), velocity (v), phase (related to the starting point of vibration), and time-period (or duration) (Berg & Stork, 2005; Sataloff & Sataloff, 2005; Kruth & Stobart, 2007; Bennet-Clark, 2019).

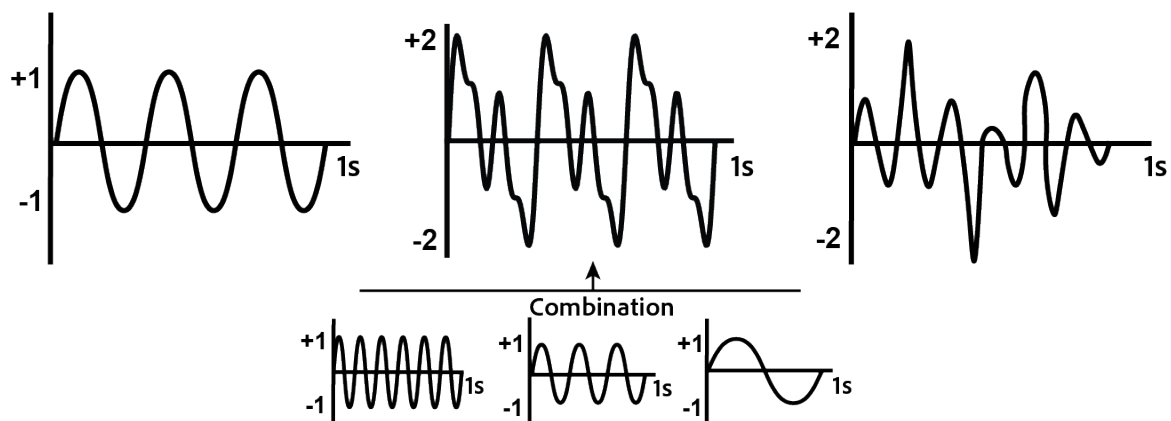


Fig. 2 Diagram of different sound waveforms. Left: a sinusoidal wave that contains only a single frequency. Middle: a complex periodic wave that contains three individual frequency components. It is repetitive. Right: irregular wave. The picture was modified from (Berg Richard *et al.*, 2016).

I. II Sound waveform and frequency filter

According to the acoustic components, the sound wave can be classified into (1) sinusoids which refer to the simple periodic signal, which consists of only one frequency, also known as pure tone; (2) complex periodic waves that are a repetitive non-sinusoidal pattern, containing more than one frequency components and differs across objects; (3) aperiodic waves that show an irregular pattern and are more

complicated, like noise (Fig. 2). With respect to complex sound waves, the Fourier analysis based on a mathematical analysis can be used to not only discriminate and decode them into single frequency components, but also compute amplitude and phase spectra. Animals have the ability to use various methods to decompose sounds into frequency components (Berg & Stork, 2005; Freegarde, 2012).

Besides being able to discriminate sound frequencies, animals have to distinguish biologically relevant sounds from noise. Irrelevant sound frequencies can be rejected by frequency filtering, allowing to isolate complex sound at relevant frequencies. Examples for such simple filters are lowpass filters allowing only low frequencies to pass through, highpass filters that suppress low frequency signals, and bandpass filters that isolate a frequency band by attenuating frequency components outside this band (Fig. 3). Frequency filters are also widely applied technically, with examples being filter circuits used to eliminate background noise, radio programs at given frequencies, tone control in the audio system, and auditory signal processing. The auditory systems of animals also make wide use of frequency filtering, whereby filtering takes place during neuronal signal processing and, prior to that, inside the ear (Pollack, 1948; Berg & Stork, 2005).

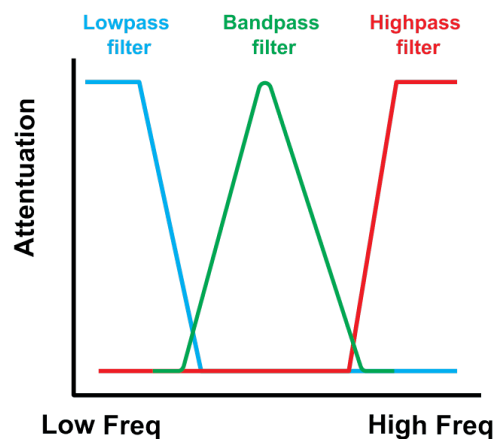


Fig. 3 Frequency response curve from different filters. The lowpass filter (blue) blocks the high frequency. The highpass filter (red) attenuates the low-frequency components and only enhances the high-frequency signals. Then bandpass filter (green) allows a particular frequency range in the center of the spectrum to pass through while attenuating the remaining frequency (low and high frequency components). The picture was modified from (Berg Richard *et al.*, 2016).

I.III Harmonic oscillation and resonance in acoustics

Sound can be viewed as a simple harmonic motion (SHM). SHM is one type of periodic oscillating movement in that the linear restoring force of the vibrating object is proportional to the magnitude of the displacement of the object towards the equilibrium position where the object remains at rest. The vibrating object can be referred to harmonic oscillator. Mathematically, the motion trajectory is a repetitive sinusoidal variation over time in case without any dissipation of energy and obeys Hooke's law (Fig. 4 left image). In this situation, the restoring force is calculated by an equation:

$$F = -\kappa \cdot X$$

where F refers to the restoring force, k represents spring constant that is related to the inherent properties of an object, and X is the displacement from the equilibrium position. If an additional force is added when the displacement of the object reaches the maximum at each cycle, this causes an increase in the amplitude of the movement as shown in Fig. 4 right image, which is called driven harmonic motion. However, considering the energy loss due to frictional force, such as air resistance, the amplitude of the vibrating object continuously decreases, until completely keeps still. This process is called damped harmonic motion (Fig. 4 middle image), in which quality Q (or Q factor) is introduced to describe the system energy and how underdamped an oscillator is, with the stored energy definition: $Q=2\pi*\text{energy stored}/\text{energy dissipated per cycle}$. The higher Q factor value is, the lower the rate of oscillator energy loss, and the slower of the oscillator eliminates. Additionally, it is notable that only the amplitude of the oscillator changes, whereas the period remains constant either in driven or damped harmonic motion (Fig. 4). With respect to the principle of sound generation, harmonic motion can apply to sound both physically and mathematically (Berg & Stork, 2005; Getachew, 2018; Hauko & Repnik, 2019).

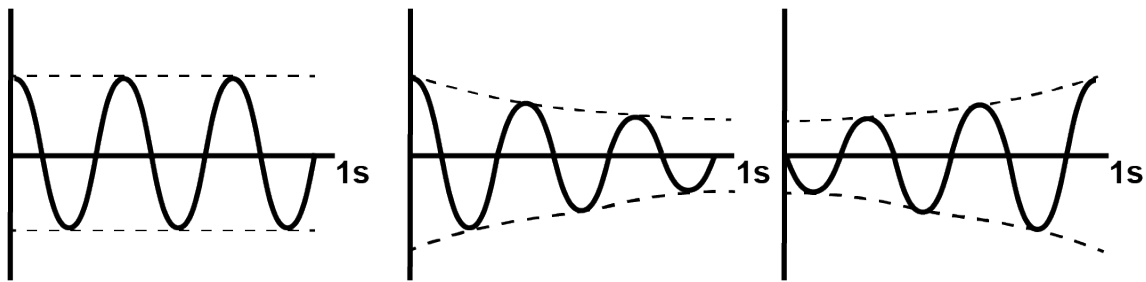


Fig. 4 Three harmonic motion. Left: simple harmonic motion with one vibrating frequency in the absence of energy loss. Middle: damped harmonic motion with the continuous decreasing amplitude because of the dissipation of energy. Right: driven harmonic motion with continuous increasing amplitude when the additional force is added. The period in damped and driven harmonic motion is constant. The picture was modified from (Berg Richard *et al.*, 2016).

Apart from SHM, the other concept is resonance. Resonance is defined as the phenomenon that a periodic force from one oscillating object is applied to another object, leading to increased amplitude and equal frequency that matched its natural frequency by the applied force. The occurrence of resonance behaviour needs to meet two conditions: one is the forced vibration that needs an external vibrating energy source, and the other is that the excitation frequency from applied force matched the resonant object's natural vibrating frequencies (or resonance frequency), causing the maximum response amplitude. The forced vibrating object refers to the resonator. In acoustic, the amplitude of the resonator is amplified only when the inherent resonance frequency is picked up to match the coming sound frequency. Meanwhile, the harmonic motion and its vibrating properties also apply to the resonance behaviour. In the context of hearing, the sound receiver in *Drosophila* and mammalian cochlea can be viewed as resonator in the presence of sound stimuli. The resonance of cochlear hair cells can be either mechanical or electrical to discriminate frequency components and generate resonance frequencies from coming sound (Yamanaka *et al.*, 2001; Göpfert & Robert, 2002; Berg & Stork, 2005).

II. Sound perception

II. I Sound propagation and perception in human ear

Sound propagation needs media. It is the mechanical energy originating from a vibrating object that the sound wave propagates, not the vibrating particles. During the propagation, sound waves can also be reflected, refracted, interfered, and diffracted when passing through the mediums (Berg & Stork, 2005). The medium properties can affect the characteristics of sound, like density, constitution, motion of media, or viscosity.

The ability of sound detection and perception is only widespread in vertebrates and insects, which are endowed with the auditory sensory organs called hearing organs or ears (Grinnell, 1969; Fritzsche & Beisel, 2001; Göpfert & Hennig, 2016). With respect to the sound component they detect, ears can be categorized into sound pressure and sound particle velocity sensitive ones. Both types of ears can be found within insects, which can present pressure-sensitive tympanal ears and particle velocity-sensitive bristles and antennal ears (Nadrowski *et al.*, 2011; Albert & Kozlov, 2016). Furthermore, sound perception is a complex processing that includes these following steps: (1) the ear receives the external sound signal through medium and the tympanic membrane or antenna's vibration is activated; (2) the mechanical auditory signal from ear is converted into electrical signals by auditory sensory neurons; (3) then the electrical signals are processed in the brain where the acoustic information is further decoded and ultimately initiate behaviours (Albert & Kozlov, 2016; Oxenham, 2018). The ear not only works as an astounding transducer involving signal conversion, but also serves as an analyser to decode the sound components like sound frequency, amplitude, and timbre to further downstream analysis.

The human ear, as one type of tympanal ear, is used as an example to explain how sound is perceived and transmitted during the hearing process (Fig. 5). The human ear consists of three main parts: the outer ear, middle ear, and inner ear (Alberti, 2001). Firstly, the outer ear constitutes a pinna to perceive and collect external sound pressure and an ear canal to channel sound waves downstream to trigger the vibration of eardrum in the middle ear, where the vibrating eardrum converts the acoustic energy into vibrating mechanical energy. The middle ear is like an air-filled cavity, consisting of a tympanal membrane, called eardrum, and three interconnected bones called ossicles: the hammer, anvil, and stirrup. The vibration of the eardrum synchronously sets the ossicles into mechanical motion at the same frequency as the sound wave. Moreover, because the vibrating displacement of stirrup is higher than the displacement of eardrum, the amplified signals can enable the ear to detect the faintest sound. The inner ear, which is connected to the middle ear through the oval window, consists of a coiled cochlea and the auditory nerve. The cochlea is a fluid-filled semicircular canal, where the mechanical movement is transmitted from vibrating ossicles to the motion of fluid through the oval window. Then the stereocilia of hair cells located within the organ of Corti in the canals is bent to activate the

mechanotransduction channel (MTC), leading to the conversion from mechanical signals to electrical nerve impulses that are signalled to brain afterward through connected auditory nerve (Rosowski, 2013; Ekdale, 2016; Mason, 2016). Meanwhile, it is the cochlear that can decode the pitch, amplitude, and timbre of complex sounds based on the tonotopic organization of hair cells along the basilar membrane (Alberti, 2001; Fettiplace, 2017).

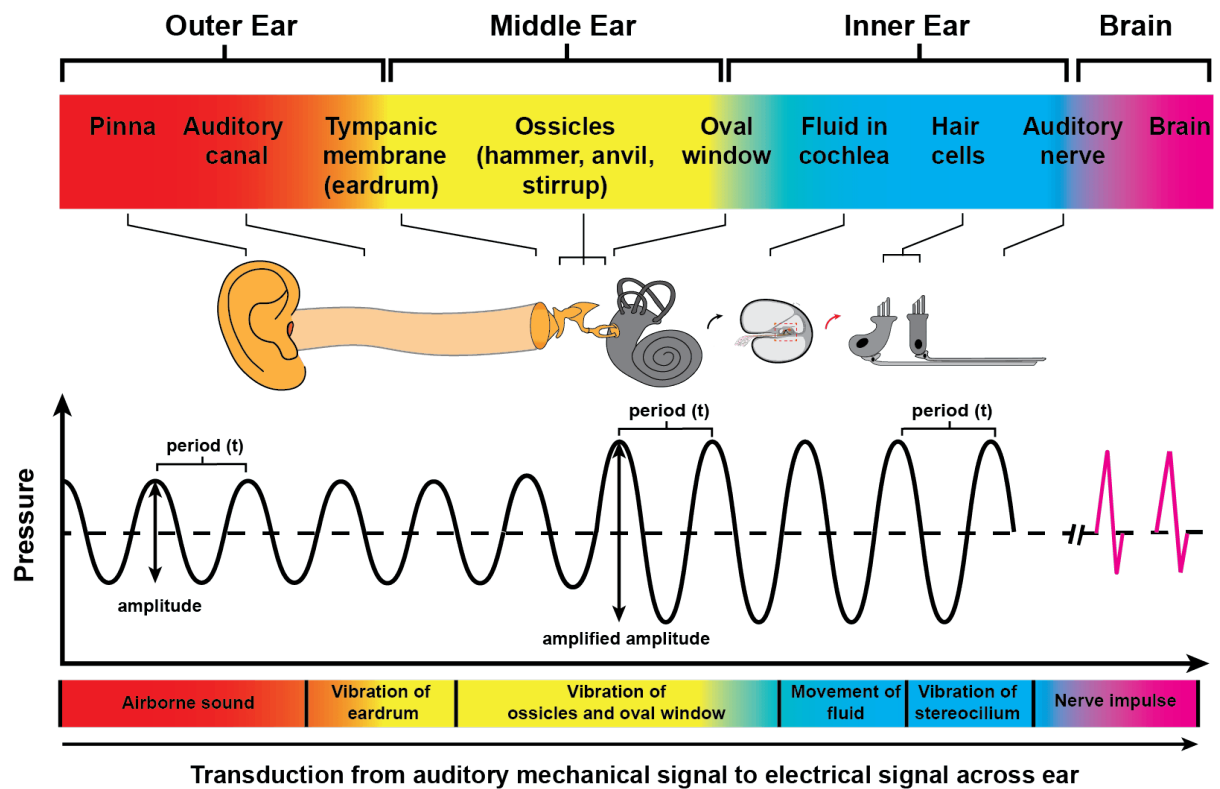


Fig. 5 Illustration of hearing process in human ear. The human ear consists of three parts: outer ear containing pinna and auditory canal to perceive sound pressure; middle ear containing a tympanic membrane to receive the sound stimuli and transmit sound energy into mechanical vibration, and ossicles to not only pass through the vibration from eardrum to cochlea by oval window but also enhance the auditory amplitude.; inner ear containing a fluid-filled canal and sensory hair cells to convert the mechanical movement of fluid into electrical impulses, which are processed to brain through auditory nerve. During propagation, the frequency of mechanical movement from eardrum, ossicles, fluid in cochlear, and hair cell are constant, but the amplitude is amplified by the cochlear amplifier. The image was obtained and modified from the free online websites: <https://ib.bioninja.com.au/>.

Abstract

Since the first confirmed evidence of potassium ions crossing the membrane to the first cloned and identified potassium channel from *Drosophila melanogaster*, the studies of potassium channels have extensively broadened our understanding of physiological activities in living organisms over the past few decades. Identifying the type of potassium channels from its numerous superfamilies in given cells or organs and their corresponding physiological properties is an indispensable step towards clarifying their cellular functions and the mechanism of their regulation. Hearing, as one aspect of basic sensory modalities, plays an essential role in receiving information from the environment and maintaining interspecies communication. Functions of potassium channels in hearing research have also been widely studied, including secretion of K⁺ ions from stria vascularis of the cochlea, efflux of K⁺ ions from hair cells for recycling, and electrical tuning modulation of turtle hair cells. In this dissertation, I used *Drosophila melanogaster* as a study model to further investigate the effects of potassium channels on hearing. Electrical tuning, as the main mechanism to discriminate frequency components from complex sound at frequency < 1 kHz in non-mammalian vertebrates, is a phenomenon with the involvement of multiple voltage-gated K⁺ channels. To test whether electrical tuning occurs in *Drosophila*'s ear or not, I recorded the compound action potential response from antenna nerve in *wild-type* flies and in flies carrying mutated K⁺ channel alleles. Additionally, the effects of voltage-gated calcium channels (Cav), inward-rectifier potassium channels (*Irk1*), and motor protein (*prestin*) were also measured. I found that the chordotonal neurons in the fly's ear can show an electrical resonance behavior over the tested frequency range, which is modulated by the *slo* or *Shaker* channel. It showed that *slo* or *Shaker* channel modulates hearing sensation to certain low-frequency ranges. Furthermore, I screened the homologs of potassium channels in Johnston's Organ (JO) and found that almost all types of potassium channels are present in JO, but with different expression abundance. Meanwhile, some of the tested K⁺ channels are expressed partly in different sub-population of JO neurons and partly show different subcellular localizations. Judging from the functional studies, none of the twelve tested K⁺ channels affected electrical signal transduction, but mutant defects were observed in the mechanical amplification that, based on the severeness of the amplification defects, can be categorized into three groups according to the influenced amplification gain value: no effect (*SK*, *Irk2*, *Shaw*, and *Shal* channels), mildly impaired (*slo*, *Irk1*, *Shaker*, and *KCNQ*), and severely impaired (*Shab*). This thesis provides insight into how the K⁺ channels perform and the molecular mechanisms of frequency discrimination in *Drosophila* hearing.

Keywords: Potassium channels; *Drosophila melanogaster*; Hearing; Johnston's Organ; Frequency discrimination; Electrical resonance

Chapter 1.

Molecular Mechanisms of Sound Frequency Discrimination in the *Drosophila* Ear

1.1 Introduction

1.1.1 The model organism *Drosophila melanogaster*

Apart from vertebrates, the ability to perceive sound is also widespread in insects with similar functions that convert acoustic information into electrical signals and ultimately initiate corresponding behaviours in brain, but with distinct ear structures (Albert & Kozlov, 2016). Hearing in insects can serve two fundamental functions: acoustic communication and acoustic detection of predators. The implementation of sound perception differs by using highly specialized structures between vertebrates and insects, therefore the biophysical principle can differ. The sound-receiving structures (also called the ear) in insects can be sorted into two varieties: tympanal and antennal ear (Hoy & Robert, 1996; Windmill & Jackson, 2016). A tympanal ear possesses an eardrum-like structure, the tympanum, that vibrates in response to sound pressure and acts as the sound receiver (Fig. 6A). In an antennal ear, the sound receiver vibrates in response to the sound particle velocity and is formed by the antenna's distal part, e.g., in *Drosophila*, the third antennal segment with its feather-like arista (Fig. 6B). Based on the differences of sound receiver, the pressure-sensitive tympanal ear can not only sense frequencies up to 300 kHz, but also enable long-distance sound communication. In contrast, the antennal ears typically allow to detect sounds at only low frequencies below 1 kHz are used for short-range sound-communication (Göpfert & Hennig, 2016). *Drosophila melanogaster* possesses antennal ears (Göpfert & Robert, 2002).

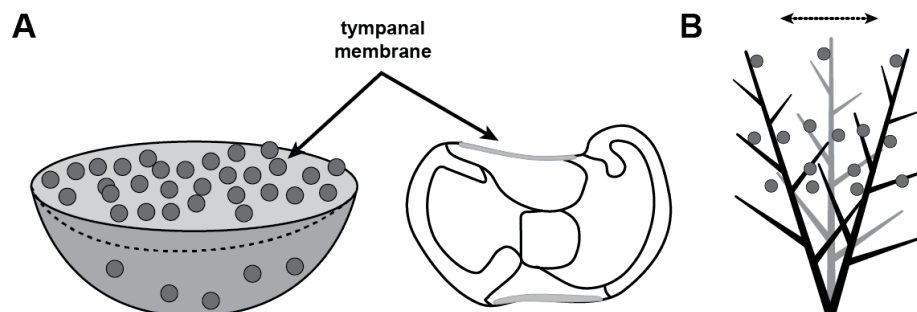


Fig. 6 Two types of ears in insects. (A) Tympanal ear: In the presence of external sound stimuli, the tympanal membrane was deformed to vibrate by mechanical force generated by sound-induced change in pressure. Left picture illustrates how the sound pressure changes. Right picture is an anatomical example of tympanal ear from crickets. (B) Antennal ear: the vibrating of antenna with a feather-like arista is caused by the oscillation of particles from sound. Images were modified from (Windmill & Jackson, 2016)

Drosophila melanogaster, also known as fruit fly, is a powerful and widespread used model organism in biological research benefiting from: (1) a completely sequenced genome to provide the possibility to address each gene's function; (2) high homology with human genome for over 60% and 75% homologous pathogenic genes discovered in human; (3) handy manipulations, the accessibility and diversification of genetic technologies, and short life cycle (Adams *et al.*, 2000; Hales *et al.*, 2015; Yamaguchi & Yoshida, 2018; Mirzoyan *et al.*, 2019). The study of *Drosophila* hearing began with the discovery of male-made courtship song to induce the female fly's copulation behavior in 1950's (Spieth, 1952). During courtship, the male flies vibrate one of their wings to generate two types of acoustic signals, called sine and pulse song, which are dominated by frequencies between 150 and 200 Hz (von Schilcher, 1976). The acoustic signals induce vibrations of the female's antenna, these vibrations are transduced into electrical signals, and these signals are processed in the brain to drive female mating decisions (Shorey, 1962; Narda, 1966).

1.1.2 Parallels between vertebrate and *Drosophila* ear

To better understand why *Drosophila* might be useful for dissecting fundamental processes in hearing, it might be helpful to compare hearing mechanisms between vertebrates and flies. Sound perception in vertebrates has been extensively studied and established over the past decades in aspect of biophysics, physiology, and genetics. Despite structural differences in morphology of auditory organ between vertebrates and fly, it is now clear that the antennal ear in the fly shows many genetic and physiological similarities (Lu *et al.*, 2009; Senthilan *et al.*, 2012). For example, in the vertebrate ears, an active process, the cochlear amplifier, actively augments sound-induced vibrations. The source of this amplifier resides in the motility of auditory hair cells. An equivalent mechanical amplification exists in the fly's antennal ear, where this amplification is driven by motile properties of JO neurons. Mechanical amplification in flies and vertebrates is associated with equivalent phenomena: compressive nonlinearity, active amplification/power gain, and self-sustained oscillations (Göpfert & Robert, 2003; Boekhoff - Falk, 2005; Ashmore *et al.*, 2010; Riabinina *et al.*, 2011). Moreover, the generation of active force is also similar: specialized stretched auditory cells as prerequisites and mechanosensitive channels to change ionic concentration gradients, leading to the change of membrane potential to generate action potential. In *Drosophila*, a transient receptor potential (TRP) channel, TRPN1 (also known as *NompC*), might serve as a mechanotransduction channel (MTC) which is localized in the distal cilium region of Johnston's organ neurons (JON) (Lee *et al.*, 2010; Effertz *et al.*, 2011). The functionality and localization of theoretical MTC in the JO neurons is equivalent to the MTC in the apical membrane of stereocilia in hair cells (Fig. 8) (Beurg *et al.*, 2009; Fettiplace, 2011).

With respect to genetic parallels in hearing, the functions of some genes are evolutionarily conserved (Lu *et al.*, 2009). The *Drosophila* transcription factor *atonal* (*ato*) in fly, as an example, is a morphogen that is indispensable for the morphogenesis of chordotonal organ. Its homologous gene in

the mouse is *Atoh1*. Loss of the protein *ato* or *Atoh1* in fly or mouse respectively both leads to the loss of auditory sensory cells (Bermingham *et al.*, 1999; Göpfert *et al.*, 2002). Moreover, Na⁺/K⁺ ATPases subunits are expressed in scolopale cells that enwrap the cilia of auditory neurons in Johnston's Organ (JO) and are important to maintain the ionic composition at high endolymph-like potential of scolopale space (Daniel F. Eberl *et al.*, 2012; Andrew P, 2014). Although the alteration of ionic composition cannot be measured currently in JO, dysfunction of Na⁺/K⁺ ATPases activities results in deafness, which is comparable with the disruption of endolymph potential (EP) by an imbalance of potassium homeostasis, which can cause deafness in vertebrates (Erichsen *et al.*, 1996; Weber *et al.*, 2001; Roy *et al.*, 2013). Additionally, the genetic screen for JO genes conducted by Senthilan *et al.* (2012) provided identified many genes whose disruption impairs fly hearing. Of 274 genes there were found to be expressed in JO, 20% have cognate genes that are implicated in human hearing disorders (Senthilan *et al.*, 2012). Apparently, the fly can be used to delineate deafness genes.

1.1.3 Mechanism basis of *Drosophila* hearing

1.1.3.1 Mechanics of sound perception and anatomy of JO

Drosophila uses antenna to detect sound, it is to say that the antenna is the fly's hearing organ. The paired antennas are symmetrically located between two eyes and each consist of three basal segments: scape (a1, 1st antennal segment), pedicel (a2, 2nd antennal segment), and funiculus (a3, 3rd antennal segment). Two small segments (a4 and a5) are coupled with the funiculus, along with a feather-like arista (a6) elongating from a5 (Göpfert & Robert, 2001; Göpfert & Robert, 2002). The scape holds muscles to modulate the movement of entire antenna. The pedicel harbours the auditory sensory organ, Johnston's organ (JO), which comprises ca. 500 sensory neurons to convert the mechanical stimuli into electrical signals (Yack & technique, 2004; Boekhoff - Falk, 2005). The funiculus not only serves as humidity and olfactory detector, but also is rigidly coupled with a4–a6 as an integral mechanical entity, which responds to sound stimuli and functions as sound receiver (Fig. 7A) (Stocker *et al.*, 1994; Göpfert & Robert, 2002).

Sound detection within the fly's antennal ear happens in two fundamental steps: (1) the sound receiver is displaced by particle velocity component from sound waves; (2) the sensory neurons in JO convert mechanical movement originating from sound receiver into electrical signals, subsequently transmitting them to brain. In the presence of sound, the distal antenna segment (arista) vibrates, inducing a rotation of the a3 to a6 about its longitudinal axis, relative to a2 to which this sound receiver is connected by an a2/a3-joint (Fig. 7B left). This rotational receiver vibrations alternately stretches and compresses the JO neurons, activating MTC channels. Ensuing electrical signals are converted into action potentials that the axons of the neurons propagate via the antennal nerve to the brain and signal

conversion from mechanical force to auditory electrical signals (Göpfert & Robert, 2002). Then, the generated electrical signals transmit along with the JO neurons and antennal nerves to the brain.

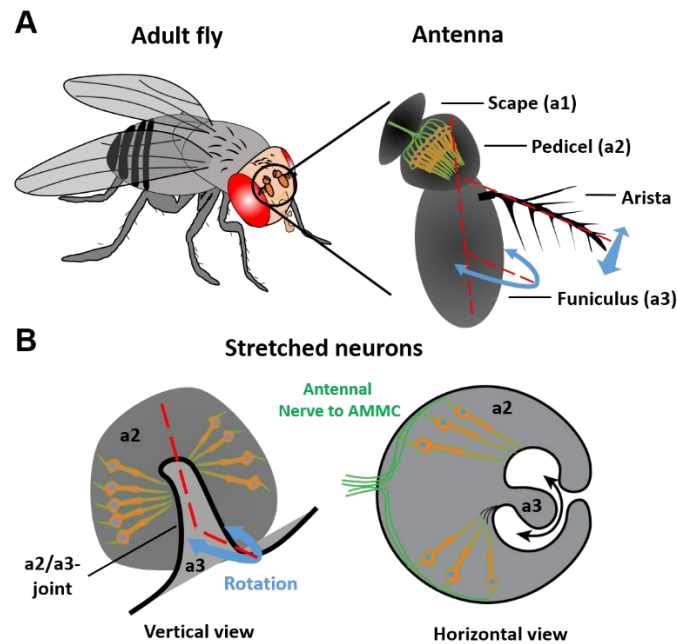


Fig. 7 The mechanics of hearing in *Drosophila* ear. (A) The hearing organ, antenna, locates between two eyes as shown in circle. The antenna contains three main segments: a1 scape; a2 pedicel; a3 funiculus, and a feather-like arista stiffly connected with a3 segment by a4 and a5. The scape is muscled to control the movement of entire antenna. A3 to a6 formed a mechanical entity, functioning as sound receiver. The rotational movement of sound receiver along longitudinal axis (red dash line) in response to sound stimuli can fire the sensory neuron in JO. (B) A joint connecting a2 and a3 segment (a2/a3-joint) is necessary to transmit the rotational movement of sound receiver into stretch activity of sensory neurons, opening or closing channels within neurons to modulate the generation of auditory electrical signals.

1.1.3.2 Transduction of sound signals and chordotonal organ

The generation of electrical signals from sound stimuli relies on the stretched sensory neurons housed in JO or chordotonal organ. The JO is multicellular, containing ca. 500 sensory neurons and surrounding accessory cells that are clustered into ca. 230 chordotonal sensilla, called scolopidia (Caldwell & Eberl, 2002; Todi *et al.*, 2004). Each scolopidium consists of two to three primary sensory neurons, and three types of supporting cells, including ligament cells anchored to the cuticle on its proximal end, cap cells attaching to the a2/a3-joint with its apical tip, and two scolopale cells (Fig. 8 A). The existence of scolopale cells is indispensable to wrap around the dendritic cilium of sensory neurons to form a liquid-filled environment, scolopale space, filling with K^+ - enriched extracellular lymph to presumably maintain a high membrane potential which is equivalent to EP in the vertebrate cochlea and essential for the occurrence of mechanotransduction in the fly ear (Fig. 8 A) (Roy *et al.*, 2013). Moreover, the sensory neurons can be subdivided into different cellular sub-compartments (from top to bottom in picture), including basal tip prolonged from axon and projecting to the brain, dendrite, and dendritic cilium, which can further be divided into proximal cilium and distal cilium (Fig. 8 A green color). These compartments can be recognized by typical proteins or channels localization. For instance, axons

contain the *elav* protein which is distributed in the nucleus. The *Iav/Nan*, which is required for signals transduction, are located at proximal cilium as a heteromer (Changsoo Kim, 2004), and *nompC* as the first discovered MTC in JO is located in the distal cilium and is required for electrical signal generation (Yun D. Chung., 2010; T Effertz & Göpfert, 2011). The mechanical forces originating from cap cells and dendritic cap (distal) are converted into electrical signals at distal cilium, then the nerve signals are propagated along the sensory neurons and antenna nerve to the brain for decoding.

The scolopidia unit spans across the a2 antennal segment and the a2/a3-joint. The rotational vibration from the joint carries the mechanical forces onto chordotonal neurons to modulate the open-close state of MTC. The accessory cells or structures also contribute to the auditory signal transduction. For instance, the scolopale cells are enriched with actin rods and house Na^+/K^+ ATPases that presumably are important for the initial tension of cilium and potassium homeostasis in scolopale space. Moreover, the disruption of dendritic cap enriched with *nompA* can cause the detachment of sensory neurons from dendritic cap and scolopidia from a2/a3-joint (Chung et al., 2001; Göpfert & Robert, 2003)). Taken together, the dysfunction of *nompA*, *nompC*, *iav*, or *nan* cause deafness in fly hearing. JO or chordotonal neurons belong to monodendritic type I sensory neurons that are settled in stretched receptors in *Drosophila* peripheral nervous system. Beside the chordotonal organ in leg or wing, the biggest chordotonal organ in the adult fly is the JO, responding to sound, gravity, and wind. Chordotonal neurons are also present in *Drosophila* larva and sorted into four groups: lateral pentascolopidial organ (lch5), single lateral organ (lch1), ventral organ A (vchA), and ventral organ B (vchB). Studies shows that the larvae are indicated to sense sound using the lch5 organ (Yuh Nung et al., 2013). Irrespective of whether lch5 organ might be sound-responsive, the Ich5 organ with five individual neuron as an integral closely resemble JO neurons anatomically as shown in Fig. 8 B (Field & Matheson, 1998).

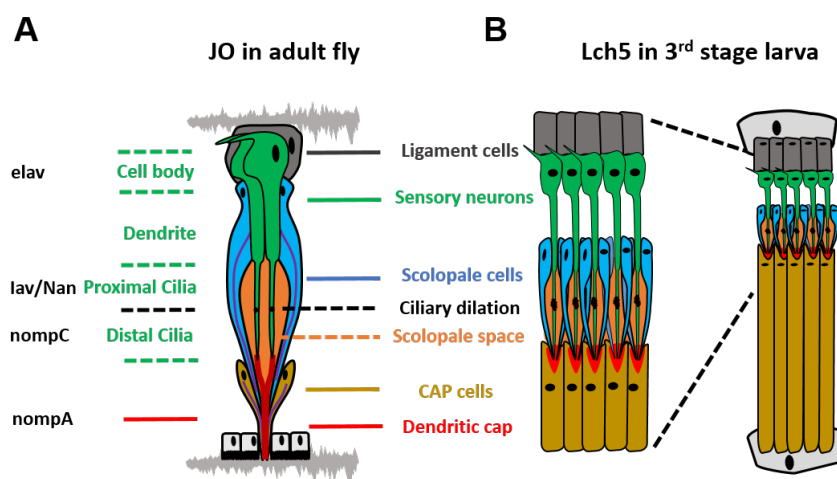


Fig. 8 Chordotonal neurons in JO and 3rd stage larva. (A) The constituent unit of scolopidia for all chordotonal neurons in JO, including sensory neurons (green), scolopale cells (blue), cap cells (yellow) and ligaments (gray), and dendritic cap (red) attached to the a2/a3-joint. Moreover, the sensory neurons can be divided into different areas (green dash line) endowed with the specialized gene expressions (text in black, beside the partition of neurons). The auditory mechanical forces from cap cells and dendritic cap (distal) are converted into electrical signals at distal cilia, then processing along the cilium, dendrite, and cell

body (proximal) to the brain. (B) The morphology of lch5 organ in 3rd stage larva displays a similar structure with adult JO. The distal well a long-elongated CAP cells and proximal are all attached with attachment cells, not cuticle.

1.1.3.3 Auditory signal processing in brain

To attain the sensory functions and reveal how the information from outside is present in the brain, not only studying the primary receptor neurons for stimuli is a prerequisite, but also knowing which brain areas and neurons encode particular sensory signals, how the electrical signals are transmitted throughout the brain, and their sensory pathways are indispensable. In anatomy, the auditory organ, JO, houses axons elongated from the proximal cell body to form a cluster of antennal nerves, passing through the a1 antennal segment, and projecting to antennal mechanosensory and motor center (AMMC), the primary auditory primary sensory center (Fig. 9 A and B). The AMMC is a neuropil and located at the posteroventral side of the Antennal Lobe (AL) in the brain (Matsuo *et al.*, 2016). According to the sensory neurons from JO, the AMMC can be classified into five distinct zones (Fig. 9 C), named from zone A to E with two distinct functional types: zone C and E comprise the primary center which responds to static deflection, such as gravity and wind, whereas zone A, B, and D form the primary auditory center which responds to sound vibration (Kamikouchi *et al.*, 2009). Downstream of auditory processing after the AMMC, the auditory pathway continuously elongates to the wedge (WED), then to the ventrolateral protocerebrum (VLP) and to the lateral protocerebral complex (LPC) (Pacheco *et al.*, 2021), in which the detailed structures and neural circuits are still unresolved (Fig. 9 B). However, there are still some established features of the auditory activity in brain: (1) It originates from the auditory sensory neurons in JO; (2) It is widespread in most of the central brain with utilization either specific auditory neurons or other type of sensory neurons; (3) The diversification of respons is temporal and spatial; (4) Its signal convention is from stereotyped at primary sensory organ to variable at higher-order brain centers (Lai *et al.*, 2012; Matsuo *et al.*, 2016; Pacheco *et al.*, 2021).

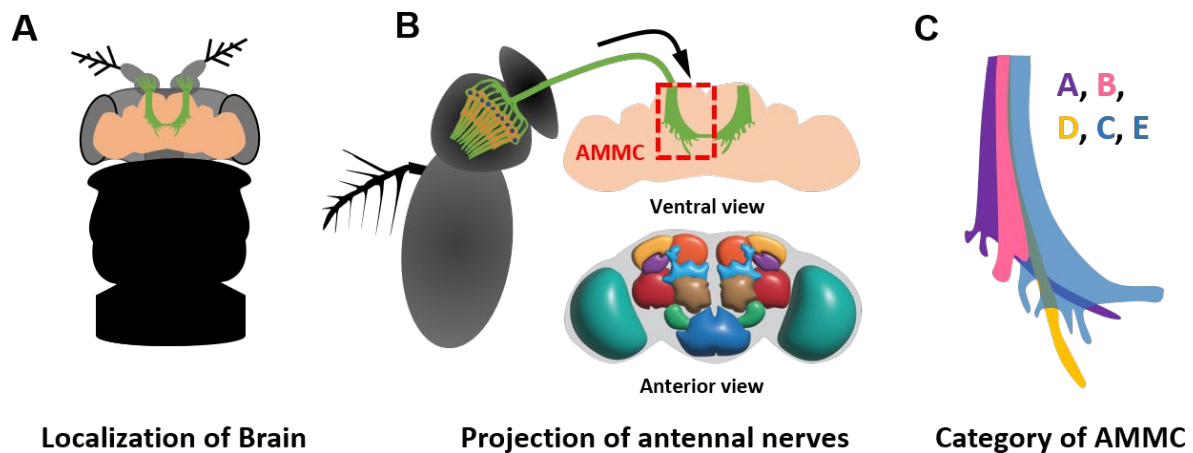


Fig. 9 Auditory circuit in *Drosophila* brain. (A) Diagram of the location of fly's antenna and brain. (B) Projection of JO neurons from the 2nd antennal segment to the brain. The antennal nerves shown in green color from axons of JO neurons project and terminate in the primary AMMC area. Each antenna corresponds to an AMMC in brain. The morphology of brain is displayed by two views: ventral and anterior view. The anterior view shows the distinct area in brain: Medulla (MED, cyan),

Antennal Lobe (AL, brown), Subesophageal Ganglion (SOG, dark blue), Antennal Mechanosensory and Motor Center (AMMC, green), Ventrolateral Protocerebrum, Dorsal part (VLP-D, red), Mushroom Body (MB, blue), Optic Tubercle (OPTU, purple), Dorsolateral Protocerebrum (DLP, yellow), Superior Dorsofrontal Protocerebrum (SDFP, orange). (C) The classification of AMMC zones according to the projection of JO neurons. Zone C and E (blue) is primary gravity/wind center and response to the deflection, and Zone A (purple), B (pink), and D (yellow) forms the primary auditory center in brain.

1.1.4 Sound frequency dependent of JO neurons

1.1.4.1 Classification of JO neurons and their localization

The antennal nerves from JO terminate at the primary center zone, AMMC, with five distinct locations from A to E. Each zone represents a specific subgroup of JO neurons, from class A to E accordingly (Kamikouchi *et al.*, 2009). Each subgroup of JO neurons possesses specialized neuron populations and functions, which responds to particular mechanical stimuli. Subgroups A and B respond to acoustic vibration and comprise ca. 250 JO neurons. Subgroups C and E contain ca. 200 neurons and are sensitive to maintained antennal deflections imposed by wind or gravity. In contrast to class A, B, C, and E, subgroup D includes the smallest number of neurons, ca. 40, that are both vibration- and deflection-sensitive (Fig. 10 A) (Kamikouchi *et al.*, 2006; Matsuo *et al.*, 2014). Each scolopidia unit consists of two or three sensory JO neurons belonging to two distinct functional classes (Ishikawa *et al.*, 2019). By labelling the cell bodies of neurons with *elav* antibody, imaging the whole antenna, the spatial structure of JO can be visualized in a 3-dimensional space (Fig. 10 B). The distribution of JO neurons shows a bowl-shape arrangement, in which the neurons lie vertically, with the cell body aligned alongside the outer cuticle and distal cilia centrally converging at the a2/a3-joint (Fig. 10 B), like a cone, and leaving a non-sensory neurons space in the middle area (Kamikouchi *et al.*, 2006). Using subgroup-specific reporter genes, it was shown that the subgroup A and B neurons located at the medial region of this bowl-shape arrangement surrounding the empty middle area, whereas the C, D, and E are organized at the periphery (Jonathan *et al.*, 2014).

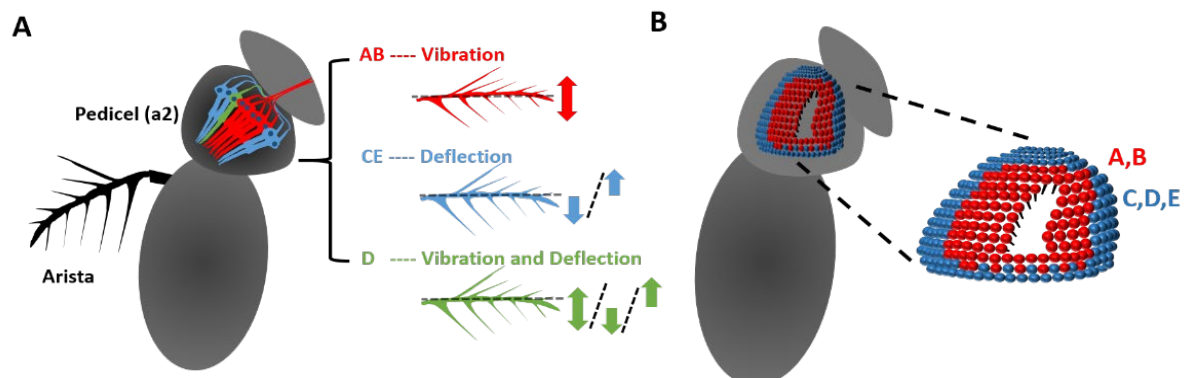


Fig. 10 Category of JO neurons. (A) The diagram of cross-section of JO neurons. These neurons can be classified into three groups according to their response to external stimuli: Class A and B neurons are sensitive to vibration (red); Class C and E neurons response to static deflection, such as wind or gravity (blue); Class D can be activated either by vibration or deflection (green). The neurons population of each functionality is also different. (B) The illustration of 3D array for JO neurons cell body. The vibration-sensitive AB neurons are located in the medial side of the bowl shape structure (red), and the other neurons (C, D, E; blue) are arranged at the periphery surrounding the AB neurons.

1.1.4.2 Classification of auditory JO neurons

Because subgroups C and E are deflection-sensitive and respond to wind and gravity, which are not the focus of my thesis topic, there is no further discussion about C and E neurons. The subgroup A, B, and D can sense airborne sound and are defined as auditory sensory neurons, targeting the primary auditory center in fly's brain.

Although it is still unclear whether the fly can hear sound at frequencies above 1 kHz, it is clear that the JO neurons respond to sounds up to some 800 Hz, covering the frequency range of courtship songs (Hu *et al.*, 2021). Vibration-sensitive chordotonal neuron subgroups differ in their frequency-characteristics. Calcium imaging in the AMMC with series of sound frequencies stimuli, revealed that that the subgroup A is preferentially activated by high frequency (400 Hz), subgroup B is preferentially activated by low frequency (lower than 100 Hz), and subgroup D is preferentially activated by middle range frequency (ca. 200 Hz) (Yorozu *et al.*, 2009; Matsuo *et al.*, 2014). The response of subgroups A/B/D over the frequency range displays an overlapping pattern (Fig. 11) (Yorozu *et al.*, 2009; Matsuo *et al.*, 2014). Moreover, Eriko Matsuo demonstrated that the signals from subgroup B showed a continuously decreasing trend ranging from maximum response at 40 Hz to minimum response at 800 Hz, whereas the response from subgroup A or D JO neurons displayed an inverted V shape trend, in which the maximum responses (apex) was at 400 Hz and 200 Hz respectively.

The different frequency selectivity of JO neuron subgroups implies that sound frequencies are decomposed in the fly's hearing organ. Because all the ca. 300 auditory sensory neurons connect to the same sound receiver that displays a single mechanical resonance and cell intrinsic tuning mechanism, this frequency discrimination must take place in JO neurons. However, addressing how the auditory JO neurons respond to sound frequencies at single JO neuron level is not accessible yet. Identifying particular genes that contribute to the discrimination within JO neurons is an alternative method. Therefore, in this chapter, I tested for genetic defects in frequency tuning to gain insights into the tuning mechanism in *Drosophila*. The *Drosophila* larva can perceive widely range of sound frequency, which can be selectively discriminated by the five individual chordotonal neurons in lch5 organ, providing additional evidence that chordotonal neurons can be tuned intrinsically (Hu *et al.*, 2021).

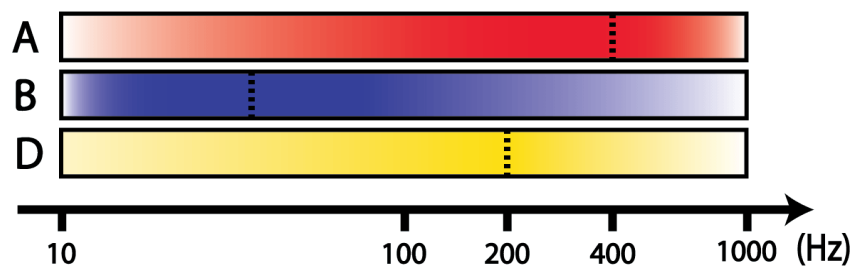


Fig. 11 Frequency preference of auditory JO neurons. The class A, B, and D are acoustic vibration-sensitive. The class A are preferentially activated by higher frequency sound (red). The class B is below than 100 Hz (blue), and class D is preferentially activated by middle frequency (yellow). The gradient color represents the change of signals from calcium imaging. The picture was made according to the published work from (Yorozu *et al.*, 2009; Matsuo *et al.*, 2014).

Up to here, the fundamental information of fly's hearing has been introduced, including the anatomy of hearing organ, mechanics of fly's sound receiver, auditory signal transduction, categories of JO neurons with particular functions, and frequency-characteristics of auditory JO neurons. Apart from transducing mechanical stimuli into electrical signals, another essential role of hearing organs is to decode sound into frequency components for further processing in brain. The sound frequency discrimination occurs in the vertebrate cochlea, but it is still yet elusive in *Drosophila* ear. My main tasks throughout my PhD project are to explore the occurrence of frequency discrimination by recording the mechanical and electrical response in the adult fly's ear, as written in this chapter, and the molecular basis for this modulation. Before I present my work and results in the fly model, I would like to introduce the background of frequency discrimination in the cochlea to answer the following questions: (1) what is frequency discrimination and why it is important? (2) how come the discrimination happen in the vertebrate cochlea; (3) the mechanisms for this modulation.

1.1.5 Frequency discrimination in the cochlea

1.1.5.1 What is frequency discrimination and why it is important?

Sound frequency or pitch is defined as the number of periodic oscillations of vibrating sound particles per second with the equation: $f=1/T$ (Hz) (T: stands for one complete oscillation cycle). The acoustic frequency can be divided into three different ranges according to the auditory perception range, including audible range, ultrasonics, and infrasonics (Berg & Stork, 2005). The audible range refers to the range of sound frequency that can be detected by vertebrate and insect ears and the ranges can vary significantly between species. For instance, humans can perceive sound from ca. 20 to 20.000 Hz, bats can hear the frequency ranging from 1000 to 150.000 Hz, and turtles can hear only a small frequency range, ca. 30 to 600 Hz (Berg Richard *et al.*, 2016). In line with the human audible frequency range, ultrasonics refers to the range whose frequencies lie above the audible range, ranging from 20 kHz to higher frequencies, while infrasonics refers to the ranges whose frequencies lie below the audible range, lower than 20 Hz (Berg & Stork, 2005).

In physics, pure tone with single frequency stimuli can be described as a sinusoidal wave with the variable amplitude, phase, and frequency (Fig. 1). The sinusoidal waves can interact and interfere with each other, involving in wave phase summing and cancelling to form an overall complex sound waveform, which is a time-dependent mixture that contains all the individual frequency components (Fig. 12 first two images). In real world, the majority of perceived sound is complex, because each sound generator has its own inherent frequency range. During the vibration of an object, these inherent frequencies are simultaneously generated, and the actual frequency waveform derives from a combination of every single frequency and can differs across various sound generators (Fig. 12). Frequency discrimination refers to the ability to perceive and decode the relative amplitude and

frequency compositions from a complex sound into individual ones through Fourier analysis (Xu *et al.*, 2019). Based on the particular waveform constituted by the intrinsic frequency range, the sound sources can be accurately recognized, classified, and labelled. Perceiving and decoding the sound frequency make-up as information sources is crucial in real life. For examples, people can distinguish the friend's voice in a crowded and noisy circumstance. People can receive the sound as a dangerous sign, like booming, screaming, or earthquake. Not only accurate classification, but also spatial positioning and localization of sound also rely on the frequency constitutions. In animal world, animals can distinguish companions, foe, or prey by receiving the sound waves constituted of specific frequencies, then determine their spatial position and make timely responses (Grothe *et al.*, 2010; Yin *et al.*, 2019; Fettiplace, 2020). In the vertebrate ear, it is the cochlea that houses different subset of hair cells to discriminate frequency components and generate corresponding electrical signals (Fig. 12) (Fettiplace, 2017).

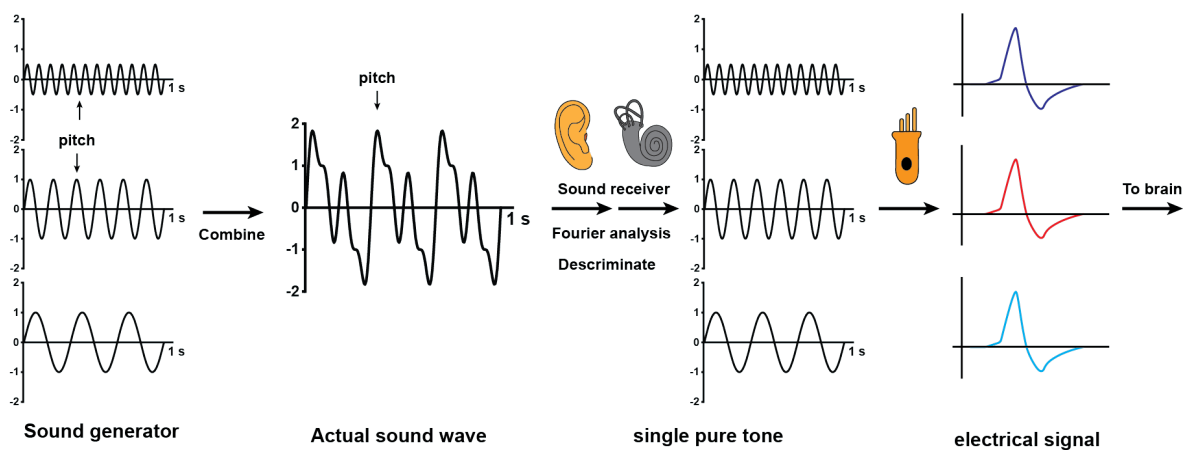


Fig. 12 Sound generation and frequency discrimination. (From left to right sequentially) The object assumedly contains three inherent frequencies (first image). During the sound generation, the object vibrates at all three simple frequencies simultaneously and these frequency waves combine into a complex sound waveform (second image) that actually propagate. The combined sound wave propagates through media and is collected by human ear or sound receiver, then process to cochlea or sound analytical instruments. Subsequently, the complex soundwave is discriminated into three single frequency again through Fourier analysis (third image). In cochlea, the discriminated frequency is assigned to the different position on basilar membrane. The mechanical signal from each frequency is converted into electrical signals by particular hair cells, which process to center nerve system in brain afterwards.

1.1.5.2 Cochlea frequency selectivity

The mammalian cochlea is a spiral semicircular canal that receives vibrations via the oval window and is innervated by spiral ganglion neurons that synapse onto hair cells (Yin *et al.*, 2019). The organ of Corti, as the core component, is located in the scala media between the vestibular duct and the tympanic duct, and supported by the basilar membrane (BM), it houses two types of mechanosensory hair cells (outer hair cell and inner hair cell) and is the place where the signal conversion and frequency discrimination occurs (Hudspeth *et al.*, 2014). The BM is like an elastic band running along the cochlea, grading in mass and stiffness along its length from cochlear base to apex. In the presence of sound, the sound vibration is converted into movement of fluid in the cochlea that contains all acoustic frequency

components. The frequencies are mechanically filtered to the different locations along the BM during the movement of fluid that propagates in form of a traveling wave. The traveling wave propagating along the basilar membrane provides a spatial frequency map, with the lowest frequencies being mapped to the cochlear base and high frequencies to the cochlear apex (Fig. 13). Each position is endowed with specialized hair cells that can filter a certain frequency range (or characteristic frequency, CF). In this way, the frequency components from complex sound waves are discriminated and positioned along the length of BM in a gradient tonotopic map pattern. Depending on their position in the cochlea, hair cells thus experience different frequency inputs and, accordingly, assume different characteristic frequencies, and signalled to the brain for downstream analysis (Fig. 13) (de Boer & Nuttall, 2000; Grothe *et al.*, 2010; Fettiplace, 2020).

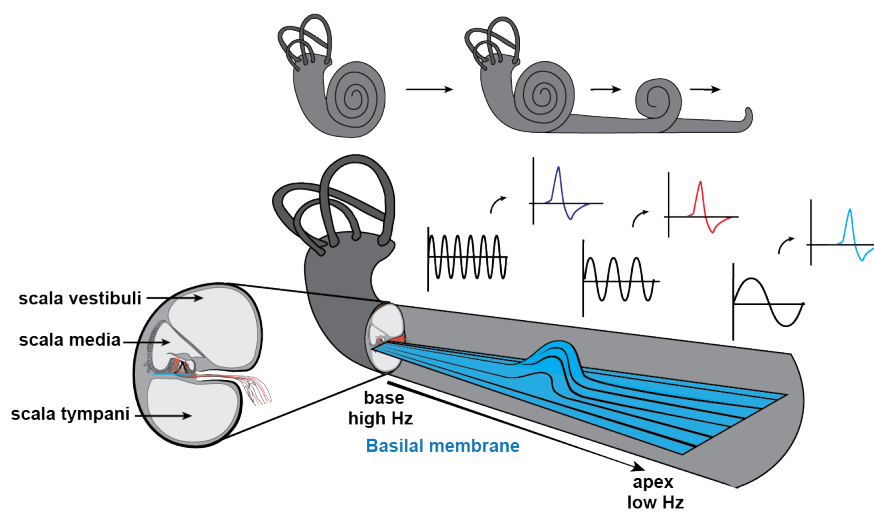


Fig. 13 Frequency discrimination on basilar membrane of a coiled cochlea. Illustration of how the different frequencies distribute along the human cochlea. In physiological state, the human cochlea is a spiral, hollow, conical cavity. The cross-section of cochlea shows that it consists of three different chambers: scala vestibuli, scala media, and scala tympani. From the uncoiled cochlea, the basilar membrane can run through the length of cochlea from the base to apex, where the high frequencies are arranged at base, whereas the low frequencies gradient are located at the cochlear apex. Each discriminated frequency corresponds to respective electrical signal, which are downstream progressed to brain.

1.1.5.3 The mechanisms of frequency discrimination in cochlea

The vertebrate cochlea contains an array of filters to isolate sound frequency components by sensory hair cells, performing a similar function as a Fourier analysis on the complex sound. During the propagation of the traveling wave in the cochlea, the hair bundles, a cluster of stereocilia of hair cell, are triggered to vibrate together with the vibration of BM, displaying a resonant behavior. The audible frequency range differs between the vertebrate species with their particular cochlea structure and tonotopic map (Fig. 14 A). For instance, the rat cochlea, similar to the human cochlea, is a spiralled, hollow, conical cavity. The highest audible frequency is up to 60 kHz at the cochlear base. In contrast with rat, the chicken and turtle can sense a lower tonal range with a more simplified cochlea (Fig. 14 A). Because of the difference of tonal ranges across vertebrate species, two distinct mechanisms,

including mechanical resonance and electrical resonance, are identified in the frequency discrimination (Fettiplace, 2020). In mammals, such as rats or humans, the tonal range is higher than 1 kHz and the hair cells utilize the mechanical resonance to filter the frequency components, originating from the stiffness and mass of basilar membrane. By contrast, the mechanism of electrical resonance is ubiquitous in all non-mammals in which the tonal range is defined less than 1 kHz (Fettiplace, 1987; Fettiplace & Fuchs, 1999).

In electrical resonance, the frequency components are filtered and sharpened by multiple voltage-gated ion channels, originating from negative feedback between hair cell membrane potential and the current (Fettiplace, 1987). This process involves the combined action of voltage-gated Ca^{2+} channels and large-conductance Ca^{2+} activated K^+ (BK_{Ca}) channels (Fig. 14 B). Firstly, when the hair cells are stimulated, the depolarization of hair cells allow for Ca^{2+} influx through Ca_v channels, then the adjacent BK_{Ca} channels are activated by intra-cellular Ca^{2+} . Secondly, the generated K^+ current closes the Ca_v channels because of the membrane hyperpolarization, leading to dissipate of intracellular Ca^{2+} and the first electrical oscillation. Subsequently, the existence of extrinsic current continuously initiates Ca^{2+} influx to activate a smaller fraction of BK channels, which are deactivated from first oscillation, for the second oscillation with a decreased amplitude, generating a damped oscillatory electrical resonance due to the delayed feedback of this activation. Moreover, the resonant frequency of hair cells is related to the density of BK/Ca_v channels (Fettiplace & Fuchs, 1999). The lower frequency hair cells tune, the lower density of BK/Ca_v channels hair cells have. Additionally, other types of voltage-gated K^+ channels or inward rectifiers (Kir) channels involvement may contribute to reduce the oscillating frequency to dozens of hertz (Navaratnam DS, 1995; Goodman M, 1996).

Moreover, the upper resonance frequency is also limited by the kinetics of channels originating from different channel isoforms due to alternative splicing. The faster kinetics of BK_{Ca} and Ca^{2+} are, the higher resonance frequency oscillation is tuned (Lagrutta A, 1994). The distribution of electrical resonance differs between species. At tonal range < 1 kHz, like turtles, electrical tuning is dominant. If the tonal range spans the 1 kHz, like frog and lizards, mechanical and electrical resonance both exist. When lower limit of frequency is higher than 1 kHz or upper limit is beyond 5 kHz in higher animals, the mechanic resonance is dominant (Fettiplace & Fuchs, 1999; Tan *et al.*, 2013; Fettiplace, 2020).

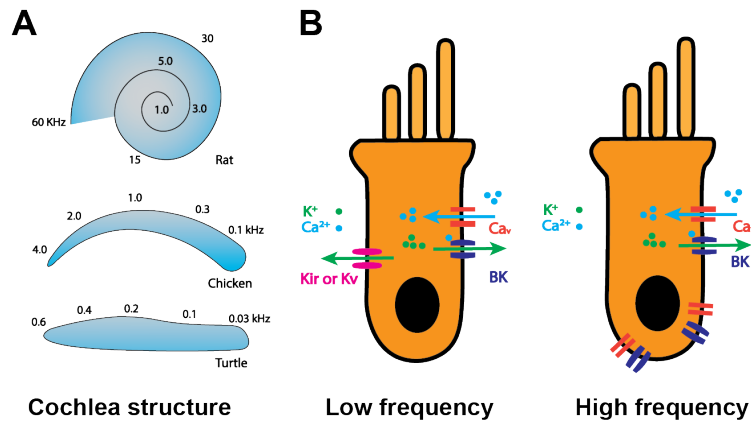


Fig. 14 Different cochlea structure and mechanism of electrical tuning. (A) Illustration of different cochlea structure in various species (rat, chicken, and turtle) with their particular tonal range distribution. (B) Mechanism of electrical resonance if the resonance frequency is upper limited to 1 kHz (turtle hair cells as an example). The resonance fliting is depended on the density of BK_{Ca} and Ca_v. The resonance frequency arises along with the increasing of density of these two channels. Some other types of Kv and Kir channels many also involve in the modulation at low frequency. Pictures were modified from (Fettiplace, 2019).

1.1.6 The comparison between hair cells and JO neurons

As outlined above, vertebrates and fly ears can discriminate sound frequencies. In vertebrate, hair cells select out sound frequencies using mechanical (mammals) and electrical (non-mammals) tuning mechanisms according to the vertebrate species and tonal range (Fig. 15). By contrast, the ca. 250 auditory JO neurons attain the frequency tuning functions at the cellular level based on the classification of JO neurons. Also, JO neurons can select out sound frequencies, possibly using electrical tuning as well as they sense sub-kilohertz sound frequencies. However, some questions, such as how the frequency is tuned, how the fly's ear responds to different frequency stimuli, and the mechanism at the genetic level, are still little understood. A fruit fly can sense sound at hundreds of Hertz (Hz), which hypothetically may utilize a similar electrical tuning mechanism to filter the frequency components. To test this assumption, this chapter mainly focuses on: whether the JO neurons possess electrical resonance behavior, and what the molecular mechanism is (Fig. 15).

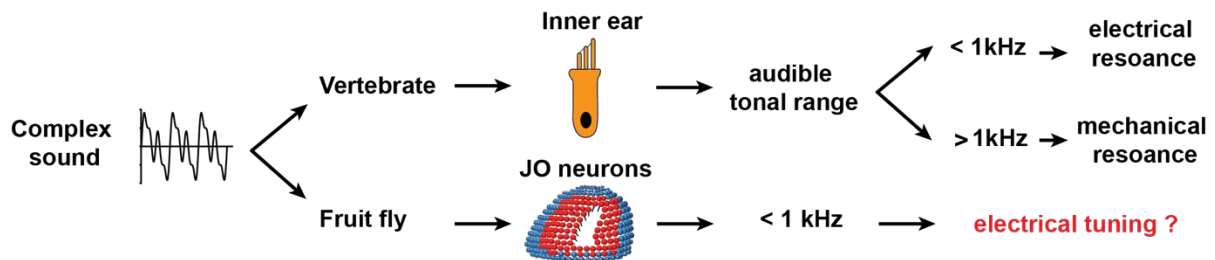


Fig. 15 Comparison of auditory frequency components processing in vertebrate and fly ear.

1.2 Materials & Methods

1.2.1 Genetic approaches for the studies of genetics in *Drosophila*

Drosophila melanogaster is a powerful and well-studied model organism due to the entirely sequenced genome and various genetic engineering approaches, such as conventional genetic screens by ethyl methanesulfonate (EMS) or X-rays, transposon elements insertion, targeted mutagenesis by homologous recombination, and site-specific mutagenesis by CRISPR/Cas9 systems, etc. These gene-manipulating methods assist the accessibility to interesting genes in *Drosophila*, such as functional analysis, physiological and underlying molecular mechanisms.

1.2.1.1 Transposable Elements

Transposable elements (TEs), also referred to as Transposons or “Jumping genes”, are pieces of DNA segments that can change their genomic position within the genome (Rebollo *et al.*, 2012). Mobilization of TEs not only benefits to the evolution, but also potentially turns into mutagens that may be harmful or beneficial. With the development of bioengineering and genetic technology, several transposons systems have been manipulated and, then provided powerful and flexible tools for genetics and genomic research, including *P-elements*, *piggybacks* and *Minos* (Metaxakis *et al.*, 2005; Laptev *et al.*, 2018). Those tools are used to 1) screen for tissue/cell specific enhancers or expression patterns, 2) disruption of gene function, 3) generation of deficiencies, and 4) targeted deletion or silencing of interesting genes (Ryder & Russell, 2003). Further information on TEs functions and structures can be addressed by the Reviews of Edward Ryder, Tabitha J. McCullers, Chih-Chiang Chan, and Gene Disruption Project Database (GDP) website (https://fruitfly.org/p_disrupt/index.html).

1.2.1.2 GAL4 / UAS system

The GAL4/UAS system is a widely used method to study gene expression and function in tissue- and/or cell-specific patterns in organisms since the finding of the transcriptional activation factor, Gal4 protein, and enhancer Upstream Activation Sequence (UAS) motif. Gal4 can specifically bind to the UAS motif and trigger the downstream interested genes expression. These expression system from yeast are introduced into the genome of *Drosophila* by P-element, in which the Gal4 gene is placed downstream under the control of targeted gene promoter and the UAS motif is placed upstream of interest genes that are transcribed, such reporter genes, and RNAi sequence, respectively. In the parental generation, the Gal4 proteins and UAS motif are present in different strains, therefore the switch to control the expression of interested gene is off. However, in the F1 generation from GAL4/UAS parental crossing, the Gal4 homodimers protein controlled can bind to UAS motifs and facilitate the gene expression in cell- or tissue- specific pattern once Gal4 protein and UAS motif are present in the fly synchronously (Fig. 16) (Keegan *et al.*, 1986; Fischer *et al.*, 1988).

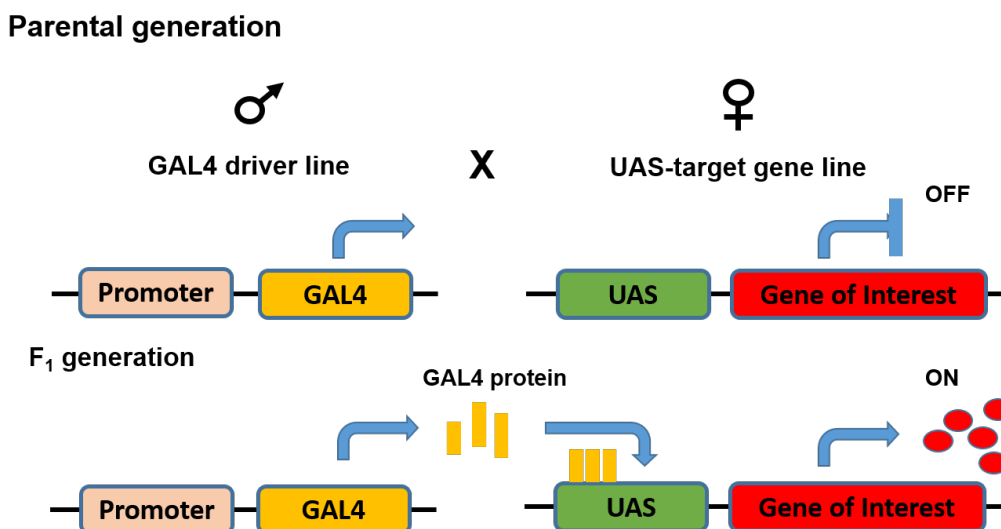


Fig. 16 Schematic of Gal4/UAS system in *Drosophila*. The female and male flies carrying on the Gal4 and UAS genes respectively are crossed to mating. The progenies inheriting both Gal4 and UAS motif in same genome from F₁ generation are collected for downstream experiments such as gene expression assay, gene knockdown, or overexpression.

1.2.2 Immunohistochemistry

1.2.2.1 Johnston's organ staining in adult flies

The flies aged between five and seven days are collected to check the protein expression pattern in the adult JO. The harvested flies were anesthetized with CO₂. The heads were dissected with suitable forceps and immersed in 4 % paraformaldehyde (PFA) solution (4% PFA and 0.3% Triton-X-100 in PBS solution, pH 7.4) around 1 hr for fixation on a rotating disc at room temperature (RT). Then, the heads were oriented upwards and embedded in albumin-gelatine. After complete solidification of gelatin solution, the samples were incubated in 6 % PFA, overnight at 4 °C. The second day, the samples were sequentially dehydrated in 100% methanol for 15 min and rehydrated in PBS solution for 5 min before ready to slices preparation.

The tissue sections were manipulated in a PBS-filled groove assembled on a Leica Ultracut S microtome device. Embedded head/antenna samples were sectioned into a 40 µm thick slices, washed one time for 10 min with 1X PBS before incubation in blocking solution (5 % Normal Goat Serum, 2 % Bovine Serum Albumin, and 1 % PBST) for 1 hr at RT. Subsequently, the samples were incubated with the desired primary antibody diluted in blocking solution at a ratio of 1:1000 for overnight. The following day, after washing three times with 0.05% PBST (0.05% Triton X-100 in 1X PBS) and 20 min per time, the sections were incubated with designated secondary antibodies at a diluted ratio of 1:300 for 2 hr. Afterwards, the slices were washed three times with 0.05% PBST and mounted on a glass slide immersed in DABCO solution and stored at 4 °C until further use. The

immunohistochemistry images were acquired using a Leica TCS SP8 Laser Scanning Confocal Microscope assembled with 63x oil aperture lens and subjected to Image J software for further analysis.

1.2.2.2 Larva *lch5* organ staining

The third-stage larvae were collected and dorsal-upwardly immobilized with stainless steel insect pins at the anterior and posterior ends in a petri dish filled with 1X PBS solution (pH 7.4). Then, the larvae were cut longitudinally along the middle of two dorsal trunk tracheal tubes and the unwanted internal organs or tissues were removed except the body wall. The dissected larvae were washed two times with PBS and fixed in 4 % PFA solution for 40 min at RT. After rinsing 3 times with PBS and two times with 0.3% PBST, the larvae filets were incubated in blocking solution for 1 hr at RT. Then the primary antibody was added for overnight at 4 °C incubator. Subsequently, the samples were rinsed with 0.1 % PBST for 30 min and stained with secondary antibody for 3 hr at RT. After the larvae filets were washed with 0.1 % PBST for 30 min, PBS for 20 min, it was mounted in DABCO and stored at 4 °C for imaging.

1.2.2.3 The whole antenna and brain staining

Adult flies aged five to seven days were used for staining. For whole antenna staining, the antennae were dissected directly from the heads and immersed in 4 % PFA in PBST solution for fixation. The brains were dissected in 1X PBS with two INOX 5 forceps and fixed in 4 % PFA solution for 90 min. Then, these samples were rinsed with 0.3% PBST three times, incubated with blocking solution overnight at 4 °C, and incubated with respective primary antibodies for two days. Afterwards, the secondary antibodies were added for another two days incubation following the washing step with 0.3% PBST. After removing the 2nd antibody and rinsing with 0.3% PBST and 1X PBS three times respectively, the samples were incubated in DABCO overnight and mounted on glass slides for image acquisition.

The details on how to mount the *Drosophila* brain can be found in JOVE website, referring to Mounting Adult *Drosophila* Brains: A Method to Prepare Slides for Confocal Imaging. Serial optical section images were obtained at 0.84 μm intervals by using Leica TCS SP8 Laser Scanning Confocal Microscope equipped with 63x oil aperture lens. Subsequently, for three-dimensional image reconstruction to visualize the whole antennal neurons and brain, confocal images datasets were reconstructed and analyzed with FluoRender, an open-source 3D reconstruction software. To enhance the signal of DsRed in JO neurons and trace the antennal neurons projection in AMMC area, UAS-DsRed-S197Y (label the nuclei of JO neurons) and UAS-mCD8::GFP were used. Anti-DsRed stained with DsRed-S197Y and anti-nc82 stained with brain areas as background.

1.2.3 Polymerase Chain Reaction (PCR)

1.2.3.1 Reverse Transcription (RT) – PCR

The RT-PCR assay in this thesis included three steps: total RNA extraction, cDNA synthesis, and PCR amplification. Total RNA isolated from *Drosophila* heads or 2nd segment of antennas was carried out by using Zymo RNA extraction kit according to the commercial manufacture protocol. The concentration of total RNA was measured by using a Nanodrop spectrophotometer. After that, the sample is either proceeded to downstream applications or stored at -80 °C freezer.

For cDNA synthesis, 500 ng total RNA as input template was used to synthesis complementary DNA by using Luna® Universal RT-PCR Master Mix kit. The ratio of reaction mix and condition can be addressed on the NEB product website. To determine whether the genes exist in heads or 2nd segment of antenna, after generation of cDNA, 1 µl cDNA as input was added to the PCR reaction mix according to the GoTaq® G2 Green Master Mix protocol and the PCR product was amplified for 35 cycles by using designed gene specific primers respectively, as shown in the primer list, then loaded on a 1 % agarose gel containing 0.005 % Roti®-Gel Stain dye for visualization of nucleic acids afterwards. The images of amplified PCR in the electrophoresis gel were obtained using iBrightCL1000 gel documentation system and analysed in Image J software to adjust the brightness and contrast.

Table 1. PCR primer list for K⁺ channels screen

Gene name	Orientation	Sequence (5'-3')
<i>slowpoke</i>	Forward	TAGAAGACTGCATACTGGATC
	Reverse	AGAGTTCTGTATCTGGATCATC
<i>Irk1</i>	Forward	GTAACACAGGTCTCCAATATG
	Reverse	TTGTTGAATAGCGTGTAGTC
<i>Irk2</i>	Forward	GTAAATATAGCTGGATCTGGC
	Reverse	CTCAGCTTTATCCTGTCTTG
<i>Irk3</i>	Forward	CGATAACAGATCACCGCC
	Reverse	CGCTGATGGAAGCTGGAG
<i>Ork1</i>	Forward	CCGAGTGATAAATGTCATGATC
	Reverse	CTTCTACATATCCTACCTGATG

<i>eag</i>	Forward	CAATTTGGCGCATATGATGTCC
	Reverse	CTGTATTGGATCCCATTATCCG
<i>sei</i>	Forward	TCCCAATGACATGATTACTTCC
	Reverse	ACATAAGAGATCCAACGAGC
<i>elk</i>	Forward	GCGCTCTTCATTGTAGATATTC
	Reverse	CGTAGCGTCTCGTATATATC
<i>KCNQ</i>	Forward	ATGACGCCCGTGAAGCTG
	Reverse	GAATGTCACTCCTAGGAAAG
<i>Shaker</i>	Forward	AGGTACAGGTAAGGCGATGAC
	Reverse	GGGAGTTCTTCTACGACG
<i>Shab</i>	Forward	CCCGGGTTATCGCAGTGA
	Reverse	GCGTCGGTTGTGCAGGTT
<i>Shaw</i>	Forward	CCTACACACAGCATCGCG
	Reverse	GCGCACCAATATTTCAAAGG
<i>Shal</i>	Forward	CCGGTCAATGTCCCTTTAGAC
	Reverse	CGGCTTGCGAACTTTC
<i>SK</i>	Forward	TGTCTACACAAAGGCATCG
	Reverse	GCATTTTTTCAGCCGTTTCG
<i>cac</i>	Forward	CGTCGTATGGGATTGGTTG
	Reverse	CGGAATTTCTGTACTATGCTG
<i>Ca-αD</i>	Forward	CTAGATAACTTCCAGGAGTACA
	Reverse	GGACTIONTGTACTTTTTCTGAG
<i>Ca-αT</i>	Forward	GCCTCCTCATTACAGACC
	Reverse	CCTTCAGATCTTCGACGA
	Forward	TCCAATACGTCTCCAAGTAC

<i>Ca-β</i>	Reverse	TCTTCAAGAAACAGGAGACG
-------------	---------	----------------------

1.2.3.2 Rapid amplification of cDNA ends – PCR

Rapid amplification of cDNA ends (RACE) – PCR is a powerful method in molecular biology to identify the full-length sequence of an RNA transcript by using gene specific primer (GSP) within cells or organs, and discover novel RNA transcript isoforms as well. RACE-PCR contains the following experimental steps: poly A⁺ or total RNA isolation, cDNA synthesis (RT-reaction), PCR amplification with GSP (RACE amplification), PCR product purification and cloning, transformation, and sequencing.

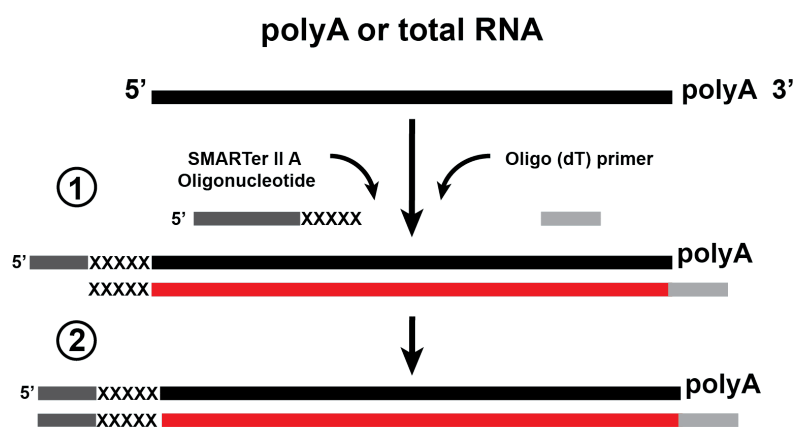


Fig. 17 SMARTer (RACE-PCR) cDNA synthesis. Either total RNA or polyA⁺ can be used for RACE-PCR cDNA synthesis. For 3' RACE cDNA synthesis, modified oligo (dT) primer binds to the poly A tail of RNA and reverse transcription occurs when the SMARTScribe Reverse Transcriptase presents. For 5' RACE cDNA synthesis, the additional SMARTer II A Oligonucleotide was needed to anneals to the tails of cDNA at 5' position and amplified for cDNA.

Total RNA for cDNA synthesis was isolated from the second segments of antennae with Zymo RNA extraction kit according to the manufacturer's instructions. RNA integrity was determined by running a 1% agarose gel with a single band around 1000 base pairs. The amount input of total RNA for cDNA synthesis was at least 1 µg. Comparing with conventional cDNA synthesis described in section 2.1.4.1, the SMARTer cDNA for RACE is synthesized by using a modified oligo(dT) primer and adding additional several nontemplated residues at 5' position that the SMARTer II A Oligonucleotide anneals to and amplify as a template for SMARTScript RT according to the user manual (Fig. 2). In detail, the reaction mix for 5' RACE cDNA contains 4.0 µl Master mix, 5.5 µl denatured total RNA sample mix, and 0.5 µl SMARTer II A Oligonucleotide in total 10 µl volume, whereas the 3' RACE cDNA reaction mix contains 4.0 µl Master mix and 6.0 µl denatured total RNA sample mix in the identical volume.

To denature total RNA, the reaction contents were mixed into a fresh 1.5 ml microcentrifuge tube according to the ratio from table 2. After gently pipetting and centrifuging the mixtures, the tubes were

put into a pre-warmed thermal cycler for RNA denaturation (reaction temperature 72 °C for 3 min and 42 °C for 2 min). Afterwards, the tubes were spun at 14.000 xg for 10 sec to collect the content at the bottom. Additionally, another 0.5 µl SMARTer II A Oligonucleotide was added into 5' RACE denatured RNA tube. For the preparation of Master Mix, firstly the Buffer Mix solution was prepared as the following reagents and ratio: 2 µl 5X First-Stand Buffer, 0.25 µl 100 mM DTT, and 0.5 µl 20 mM dNTPs pre reaction supplying from the kit; then the Master Mix solution was made by adding buffer mix solution, RNase inhibitor, and SMARTScribe Reverse Transcriptase (RT) into a new microcentrifuge tube at the ratio of 2.75:0.25:1 µl per reaction respectively (Table. 3). The 5' or 3' RACE cDNA synthesis was carried out by mixing 6 µl denatured RNA solution and 4 µl Master mix solution at a total 10 µl reaction volume in tube, as shown the detailed compounds in Table 4. After pipetting and centrifugation, the tube was transferred to a pre-heated thermal cycler for incubation at 42 °C for 90 minutes and 70 °C for 10 minutes. Till now the cDNA synthesis was accomplished, and the stock solution was diluted by adding 90 µl Tricine-EDTA into the tube, aliquot the dilution and stored at - 80 °C freezer for further use.

Table 2. Denatured total RNA reaction mix

Name	Total RNA (µl)	CDS primer A (µl)	Sterile H ₂ O (µl)	Oligonucleotide (µl)
5' RACE	3.5	(5') 1.0	1.0	0.5
3' RACE	3.0	(3') 1.0	2.0	

Table 3. Buffer mix and Master mix

Buffer mix	5X First-Stand Buffer	100 mM DTT	20 mM dNTPs	volume
1 reaction	2 µl	0.25 µl	0.5 µl	2.75 µl
Master mix	Buffer mix	RNase inhibitor	RT	volume
2 reactions	5.5 µl	0.5 µl	2 µl	8 µl

Table 4. 5' or 3' RACE cDNA synthesis Mix

Name	Denatured total RNA	Master Mix	volume
5' RACE	6 µl (contain SMARTer II A Oligonucleotide)	4 µl	10 µl
3' RACE	6 µl	4 µl	10 µl

The gene-specific primers (GSPs) were designed according to the manual's instruction for Rapid Amplification of cDNA Ends. According to the length of amplified mRNA products, the 5' or 3' RACE were both utilized in this thesis. The strategies for PCR reaction mix and amplification conditions was set up according to the Table 5. To avoid non-specific amplification and obtain high output PCR products, the ratio of PCR reaction and setup needed to be optimized. After generating the RACE amplified product, the solution was loaded and isolated by gel-electrophoresis in 1% agarose gel. The fragments of interest at desired size were extracted from the gel with the NucleoSpin® Gel and the PCR Clean-up kit from Machery-Nagel according to the user manual. Afterwards, purified PCR products were cloned into the pCR® 2.1 vector by using the TA Cloning™ Kit Dual Promoter. The reaction mix was maintained at 4 °C for overnight to increase the rate of successful cloning. Subsequently, the chemically competent *Escherichia coli DH5α* bacteria were transformed with the cloning and at least five clones were randomly picked up from LB-Agar plate for further purification. The plasmid DNA containing gene fragments from clones was isolated using NucleoSpin® Plasmid kit from Machery-Nagel, and further tested by restriction digest with EcoRV enzymes in case of pCR® 2.1 vector. The plasmid DNAs with cloned gene fragments were send for sequencing. The sequencing data were subjected to Geneious Prime software for final analysis.

Table 5. RACE PCR reaction mix and PCR program

Component	5' RACE (μl)	3' RACE (μl)	PCR program
5' RACE cDNA	1	-	Initial step: 94 °C 2 min
3' RACE cDNA	-	1	5 cycles 94 °C 30 sec
10X advantage 2 SA PCR buffer	5	5	72 °C 5 min
10X UPM T3	5	5	10 cycles 94 °C 30 sec
5' GSP (10 μM)	2	-	72 °C 30 sec
3' GSP (10 μM)	-	2	72 °C 5 min
dNTPs (10 mM)	1	1	25 cycles 94 °C 30 sec
H ₂ O	35	35	68 °C 30 sec
50X Advantage 2 polymerase	1	1	72 °C 5 min
Total volume	50	50	Final step: 72 °C 10 min

Table 6. Primer list for identification of *slowpoke* transcript isoforms

Gene name	Sequence (5'-3')
UPM	Combination of long (2 mM) and short (10 mM)
UPM long T3	ATT AAC CCT CAC TAA AGG GAA AGC AGT GGT ATC AAC GCA GAG T
UPM short T3	ATT AAC CCT CAC TAA AGG GA
T7	GTA ATA CGA CTC ACT ATA GGG CGA AT
T7-Sp6	TA ATA CGA CTC ACT ATA GGG ATT TAG GTG ACA CTA TAG AAT ACT CAA GC
GSP (<i>slo</i>) 5' RACE	GGTTGCGATCCAGTATGCAGTCTTCTAAGC
GSP (<i>slo</i>) 3' RACE	CAGTACCACAATAAGGCATACTTGCTG
M13 forward	GTA AAA CGA CGG CCA G
M13 reverse	CAG GAA ACA GCT ATG AC
<i>slo</i> reverse	CGAATACCTGATCTGTTGGCA
<i>slo</i> forward	CAGTACCACAATAAGGCATACTTGCTG

1.2.4 Cell- or tissue-specific ablation and eyFLP

In genetics, the FLP/FRT recombination is a widely used technology to manipulate mosaic gene expression under controlled conditions. The recombinase flippase (FLP) originating from *Saccharomyces cerevisiae* yeast is capable to recognize a specific 34 long base pair sequence (5' GAAGTTCCTATT*Cttagaaa*GTATAGGAACTTC 3'; also called flippase recognition target, FRT). The recombination happens when two identical FRP sites align in the same plasmid with correct reverse orientation. In the presence of FLP and FRP in same genome, the FLP binds to the first 13 base pairs, then FRT-mediated cleavage occurs to expose the asymmetric single strand 8 base pair sequence region from double strand DNA. The cleaved DNA segment with two exposure 8 bp regain can self-assemble to form a circular DNA containing one FRT site. The other cleaved DNA either can assemble together with one FRT site or connect to an insertion DNA segment which also has two FRT site. For example, in Fig. 3, the gene expression is terminated when a stop codon is present between two FRP sites. After the FLP cleavage, the stop codon can be excised to allow the translation of downstream genes. Because the FLP is temperature sensitive, the FLP expression level and efficiency of FRT-mediated cleavage is controlled by heat shock and time durations. Only with appropriate timing and intensity of

heating stimulation, the expression and cleavage of FLP could be efficient (Phelps & Brand, 1998; Theodosiou & Xu, 1998; Newsome *et al.*, 2000).

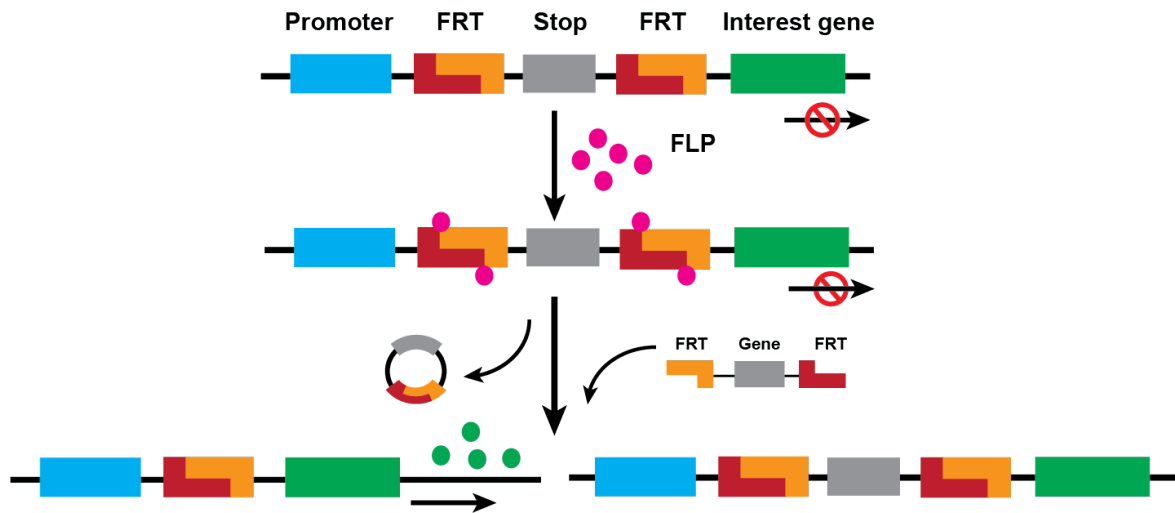


Fig. 18 Scheme of FLP/FRT system. The gene can express in a controlled condition. As an example, no expression occurs when a stop codon presents between two FRTs upstream of interested genes. In the presence of FLP, the FLP can particularly bind to the 34 bp DNA sequence in FRP and cleaves it asymmetrical. Subsequently, the cleaved ends containing the stop codon can assemble together to form a circular DNA strand. The other two cleaved end in the genome can either join to form an integral FRT site to trigger the gene expression, or fuse to another circular DNA strand containing one FRT site into genome.

To ablate the cells in specific tissues or organs (in this thesis, interested subgroup of JO neurons were ablated, including class AB neurons, class CE neurons, and class D neurons), several systems were utilized: (1) The Gal4/UAS system – the Gal4 strains contain the cell-specific enhancer in targeted organ (*Drosophila* JO), for instance JO15 in class AB neurons, NP6250 for class CE neurons, NP1064 for class B neurons, NP5035 for class D neurons, and NP0761 for all JO neurons; (2) A modified UAS strain which contains a ricin toxic A subunit sequence and two FRT sites was used, additionally a miniwhite cassette is inserted between these two FRT site. The ricin belongs to one type of holotoxics, is a lectin protein sourcing from seeds of *Ricinus communis*, and consisted of two active subunits, A and B. The ricin displays cytotoxicity activity by letting active A chain cleave the glycosidic bound within rRNA to failure the gene translation. In the modified UAS construct, a miniwhite cassette is inserted between two FRTs, then this sequence segments were fused upstream of ricin A subunit cDNA. Only when the Gal4 and FLP are present in one genome as the integral key, the expression of ricin can be unlocked; (3) Moreover, to limit the expression of ricin in desired cells or organs (in JO), the FLP should be present in interested cells to cleave the FRT. To do that, an eye-specific enhancer fragment sourcing from *ey* gene and restrictedly expressed in eye and antenna is fused upstream of FLP sequence to guarantee FLP activity and ricin toxic in interested cells, which are also called eyFLP. In summary, JO neurons ablation occurs only when the above three conditions are achieved. For instance, in the parental generation, one strain containing eyFlp and particular JO neurons driver crossed to the strain containing UAS-FRT-mini white-FRP-ricin. Then, the progenies having all three eyFLP, UAS, and

Gal4 are considered to be desired strains and used for downstream experiments (Phelps & Brand, 1998; Theodosiou & Xu, 1998; Newsome *et al.*, 2000).

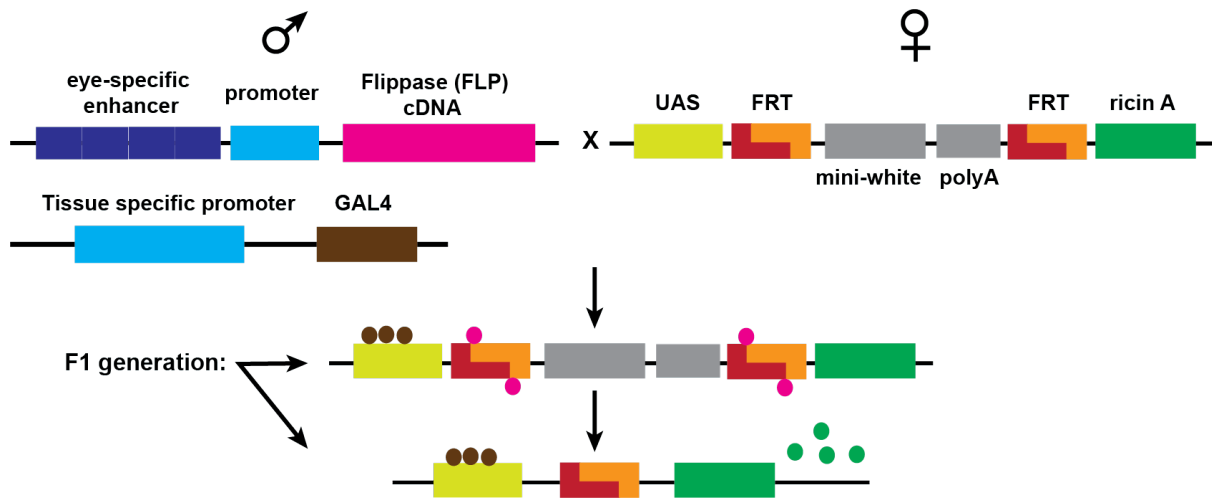


Fig. 19 Parental generation crossing for cell specific ablation. A 258 bp eye-specific enhancer fragment sourcing from the *Drosophila ey* gene are extracted and used for eye-specific expression. Its expression is defined only in eye and antennal neurons in JO. Four copies of this eye-specific enhancer and hsp70 promoter fragment is fused upstream of a FLP cDNA to define the FLP expression in eye and antenna (called eyFLP or eyeless-FLP). The cell- or tissue- specific promoters are fused to upstream Gal4 cDNA to restrict the Gal4 protein in targeted cells. A UAS construct is modified by inseting two FRTs (a mini-white cassette between FRTs) between UAS and ricin cDNA. JO neuron ablation experiment is achieved by crossing maternal strain containing eyFLP and Gal4 to parental strain containing modified UAS-FRT-mini white-FRP-ricin, and the offspring simultaneously having eyFLP, Gal4, and UAS were harvested for experiment from F1 generation.

1.2.5 Maintenance of fly stocks

All *Drosophila melanogaster* were raised on standard *Drosophila* yeast-based food (1 kg dry yeast, 1kg sugar, 40 g salt, 120 g agar, 500 g flour, 2 L apple juice, and 60 mL propionic acid in 14L total volume) at either 18 °C or 25 °C with 60% humidity in 12/12 hr light/dark cycles. The flies used in this thesis were either purchased from commercial fly stock centers, Bloomington Drosophila Stock Center (BDSC) and Vienna Drosophila Resource Center (VDRC), or kindly gifted from other labs.

Table 7. Fly strains in this thesis

Genotype	Description	Types	Reference
<i>w</i> ¹¹¹⁸	<i>w</i> ¹¹¹⁸	control fly	Lab stock
<i>Canton-S</i>	<i>Canton-S</i>	Wild type	Lab stock
<i>w;eyFLP/eyFLP;JO15/TM3</i>	<i>JO15</i>	Class AB Gal4 line	Lab stock
<i>w;NP6250/NP6250;eyFLP/eyFLP</i>	<i>NP6250</i>	Class AB Gal4 line	Lab stock

<i>w;eyFLP/eyFLP;NP0761/NP0761</i>	<i>NP0761</i>	Class ABCDE Gal4 line	Lab stock
<i>NP1046;FM7c;;eyFLP/TM3</i>	<i>NP1046</i>	Class B Gal4 line	Lab stock
<i>NP5035;FM7c;;eyFLP/TM3</i>	<i>NP5035</i>	Class D Gal4 line	Lab stock
<i>w * ;; Dnai2-Gal4</i>	<i>Dnai2-Gal4</i>	Dnai2 driver line	Lab stock
<i>w[1118] TI{GT-GAL4}Ca-α1T[Gal4];;</i>	<i>Ca-α1T[Gal4]</i>	Gal4 line in X	BDSC:68201
<i>w[1118] PBac{w[+mC]=WHR}Ca-α1T[del];;</i>	<i>Ca-α1T[del]</i>	Null allele in X	BDSC:51994
<i>y[1] w[*]; TI{GFP[3xP3.cLa]=CRIMIC.TG4.1}Ca-β[CR01554-TG4.1];</i>	<i>Ca-β[CR01554-TG4.1]</i>	Gal4 line in II	BDSC:86444
<i>w[1118] PBac{w[+mC]=WHR}Ca-β[del];;</i>	<i>Ca-β[del]</i>	Null allele in II	Gift from Prof. Kazuo Emoto
<i>b[1] Ca-α1D[X10] pr[1] cn[1] wx[wxt] bw[1]/CyO</i>	<i>Ca-α1D[X10]</i>	Null allele in ii	BDSC:25141
<i>y[1] w[*] Mi{Trojan-GAL4.0}cac[MI02836-TG4.0]</i>	<i>cac[MI02836-TG4.0]</i>	Gal4 line in X	BDSC:67444
<i>w[1118];;PBac{w[+mC]=IT.GAL4}Irk1[0034-G4]</i>	<i>Irk1-Gal4</i>	Gal4 lime in III	BDSC:62587
<i>y[1] w[*];;Mi{y[+mDint2]=MIC}Irk1[MI08404]</i>	<i>Irk1[MI08404]</i>	Mutant in III	BDSC:51080
<i>w[1118];; P{w[+mC]=EP}Irk2[G8696]</i>	<i>Irk2[G8696]</i>	Mutant in III	BDSC:33278
<i>y[1] w[*] Mi{Trojan-GAL4.0}Ork1[MI09481TG4.0]/FM7c;;</i>	<i>Ork1[MI09481-TG4.0]</i>	Gal4 in X	BDSC:77903

<i>w[1118] eag[del];;</i>	<i>eag[del]</i>	Null allele in X	Gift from Dr. Griffith
<i>y[1] w[*]; Ti{GFP[3xP3.cLa]=CRIMIC.TG4.1}sei[CR02410-TG4.1]/SM6a;</i>	<i>sei[CR02410-TG4.1]</i>	Gal4 line in II	BDSC:92255
<i>y[1] w[*]; Ti{GFP[3xP3.cLa]=CRIMIC.TG4.1}eag[CR01421-TG4.1];;</i>	<i>eag[CR01421-TG4.1]</i>	Gal4 line in X	BDSC:86374
<i>w[1118]; P{w[+mC]=EPg}sei[HP21840]</i>	<i>sei[HP21840]</i>	Mutant in II	BDSC:21935
<i>y[1] w[*]; Mi{y[+mDint2]=MIC}Elk[MI01110]</i>	<i>Elk[MI01110]</i>	Mutant in II	BDSC:30186
<i>w[1118] Mi{GFP[E.3xP3]=ET1}SK[MB03486];;</i>	<i>SK[MB03486]</i>	Mutant in X	BDSC:24653
<i>w[1118]; ;Mi{GFP[E.3xP3]=ET1}slo[MB04469]</i>	<i>slo[MB04469]</i>	Mutant in III	BDSC:24811
<i>y[1] w[*]; Mi{y[+mDint2]=MIC}slo[M113492]/TM3, Sb[1] Ser[1]</i>	<i>slo[M113492]</i>	Mutant in III	BDSC:59344
<i>y[1] w[*]; Mi{PT-GFSTF.2}slo[MI04413-GFSTF.2]/TM6C, Sb[1] Tb[1]</i>	<i>slo[MI04413-GFSTF.2]</i>	Fusion EGFP tag	BDSC:60542
<i>w[1118]; Mi{GFP[E.3xP3]=ET1}slo[MB11481]</i>	<i>slo[MB11481]</i>	Mutant in III	BDSC:29918
<i>w[1118];;Shab[3]</i>	<i>Shab[3]</i>	Null allele in III	Gift from Prof. Wu, C.F
<i>y[1] w[*]; Mi{PT-GFSTF.1}Shab[MI00848-GFSTF.1]/TM6C, Sb[1] Tb[1]</i>	<i>Shab[MI00848-GFSTF.1]</i>	Fusion EGFP tag	BDSC:60514
<i>w[1118]Shaker[133]</i>	<i>Shaker[133]</i>	Null allele in X	Gift from Prof. Wu, C.F
<i>w[*]; P{w[+mC]=UAS-Shaw.tr.FLAG}332</i>	UAS-Shaw [DN]	Dominant negative	BDSC:55748

1.2.6 *Drosophila* hearing assessment by Laser Doppler Vibrometry

1.2.6.1 Fly mounting

The preparation of a fly for hearing measurements has been established previously with minor modifications (Göpfert & Robert, 2002). In detail, the arista and funiculus (3rd segment of antenna) together constitute a mechanical entity, the sound receiver, to sense sound stimuli and vibrate. Therefore, to minimize unrelated movement effects from other parts of fly's body, firstly the flies' legs were thoroughly fixed on the top of a plastic rod with eicosane, then the movements from abdomen, thorax, and wings were prevented by fixation using wax or dental glue. The movement of head and mouth movement was eliminated by adding dental glue between the head and thorax under UV exposure. The left-side whole antenna was fixed with dental glue or eicosane. At last, dental glue was added to junction between JO and head capsule to guarantee and stabilize the rotation of only sound receiver along its longitudinal axis (Fig. 20 A). Hearing measurements were performed on an air-filled table to reduce external unwanted vibrations (Fig. 20 B).

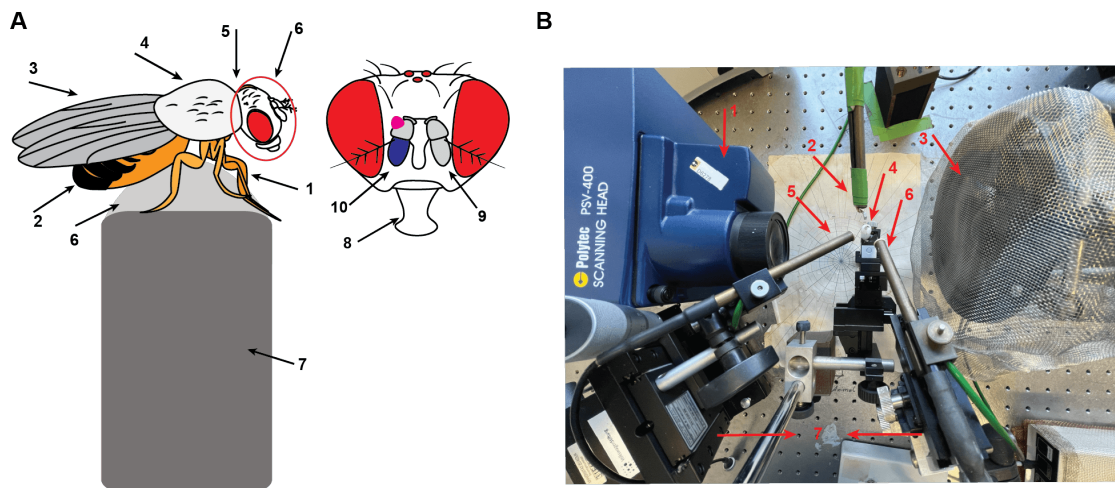


Fig. 20 Fixation of fly and LDV measurement setup. (A) The flies aged between 5 to 7 days after eclosure were collected for fixation and hearing measurement. Flies were narcotized with CO₂ on a panel. Then they were fixed on the top of a plastic rod (7) with wax using good forceps (6). Later on, the thorax (4), wing (3), abdomen (2), and legs (1) were stabilized with more wax. Then the dental glue was added into the position (4) between head (6) and thorax to fix the head. The proboscis (8) and the unused antenna (9) were fixed to the head with dental glue, and lastly little drop of glue (color in purple) was added to fix the pedicels to head on the other antenna (10). After the fixation, only the sound receiver (color in blue) can freely vibrate. (B) Illustration of LDV hearing measurement setup. All devices are placed on an optical table, including Polytec PSV-400 Scanning head (1), microphone (2), loudspeaker or sound source (3), rod with fixed flies (4), leading electrode (5), reference electrode (6), and micromanipulators (7) for movement control of two electrodes.

1.2.6.2 Mechanical measurement

The recording of *Drosophila* sound receiver consists of two measurements: one is free fluctuation of arista in the absence of sound stimuli; the other one is to measure the neuronal response in the presence of pure tone. The differences can be found in Fig. 21.

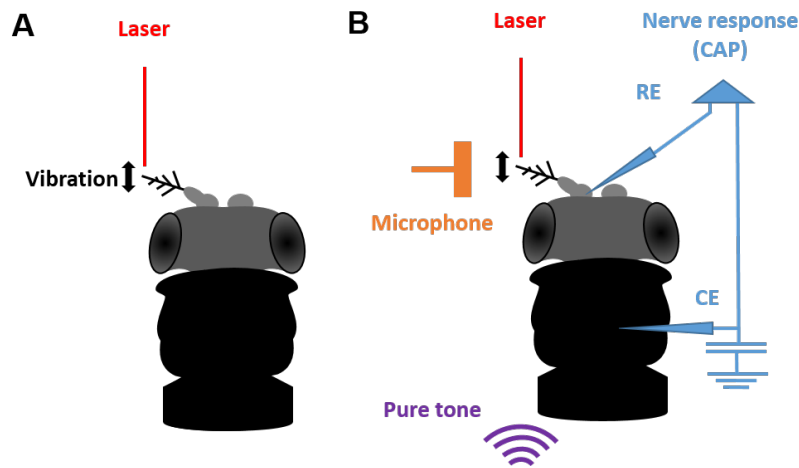


Fig. 21 Illustration of two recordings for *Drosophila* sound receiver. (A) Free fluctuation recording of sound receiver without sound stimuli. The laser points on the tip of vibrating arista to obtain the highest amplitude. The performance of vibrating arista and time trace for 100 second was collected by PSV-VID 9.0 software. The integral of power spectral density (PSD) was acquired from 1 Hz to 3200 Hz. (B) Sound-induced intensity recording with pure tone stimuli (color in purple). The laser was to record the precise displacement of arista. A microphone was used to record the loudspeaker voltage for sound particle velocity (SPV), and two electrodes were inserted to record the extra-cellular antennal nerve response (also called compound action potential response, CAP response). Before the initiation of sound stimuli, the tip of leading electrode was inserted into the scape or the junctions between scape and head, and the reference electrode was placed into the thorax. Images were modified from Thomas Effertz dissertation.

1.2.6.3 Free fluctuation recording of sound receiver

Any objects have their own set of natural frequency spectrum that they fluctuate according to (Riabinina *et al.*, 2011a). The free fluctuation properties of the fly's sound receiver are affected by two factors: its intrinsic properties and the thermal energy from surrounding air particles. The Laser Doppler Vibrometer (LDV, Polytec PSV-400) was used to monitor the free fluctuation of the sound receiver-arista, by positioning and focusing the laser beam on the apex of the arista in the absence of sound stimuli (Fig. 21 A). It can measure the velocity of sound receiver at precise resolution (nm/s). During the free fluctuation measurement, the velocity time trace was recorded for 100s by the LDV and a Fast Fourier Transform (FFT) was conducted aside to convert velocity-time trace into displacement-time trace by LDV software, from which frequency dependent velocity characteristic of fluctuation and power spectral (nm²) were obtained as well. The power spectral density (PSD, nm²/Hz) of the fluctuations was calculated by integrating power spectral of frequency ranging from 1 Hz to 3200 Hz, but the ranges restricted between 100 and 1500 Hz were considered as the systems power (or system energy, nm²). Individual best frequency (iBF) is selected as the frequency at which the PSD of free fluctuation recording is maximum (peak) in the FFT-spectrum. The iBF and power value may vary because of individual differences or loss of gene functions.

1.2.6.4 Sound-induced intensity measurement at iBF

To assess the performance of the fly's sound receiver with the external sound stimuli, the measurement consists two parts: mechanical response and antennal electrical response (Göpfert & Robert, 2003). In

the presence of sound, the mechanical response was recorded from the arista displacement and sound particle velocity (SPV), whereas the electrical response was recorded as compound action potential (CAP) response (Fig. 21 B). The integral experimental method has already been established and described previously (Göpfert & Robert, 2003).

Briefly, all flies were measured at their individual best frequency identified in the free fluctuation recording. The pure tone at iBF was generated by a loudspeaker/HiFi-system. Different sound intensities were set in controlled steps ranging from 6 to 96 decibel (dB) by an attenuator in 6 dB-steps. An Emkay NR 3158 pressure-gradient microphone was used to assess the stimulus sound particle velocity (SPV) caused by loudspeaker. The arista displacement was monitored by pointing the laser beam on the apex of the arista. The CAP was monitored with two etched tungsten electrodes, one recording electrode inserted between 1st antennal segment and the head capsule and one reference electrode placed into thorax. The SPV, arista displacement, and CAP amplitude were analyzed by Spike 2 software and subjected to Fast Fourier transforms windows (FFT) in Polytec 9.0 software to obtain the values for individual sound stimuli. The value were the average data from at least ten times continuous measurements. It is noted that the values of SPV and displacement were collected at single stimulus frequency, whereas the CAP amplitude was collected at doubled iBF.

Several parameters are defined to evaluate the sound-induced intensity characteristics, including mechanical sensitivity (gain), amplification gain, threshold, and maximum CAP amplitude. The mechanical sensitivity is defined as the division of antennal displacement versus SPV, and amplification gain is calculated according to the formula: Maximum gain / Minimum gain. The amplification gain values are not only essential to assess the mechanical responses of sound receiver, but also, more importantly, provide a good way to estimate the impacts of auditory integrity among different mutant phenotypes. The maximum CAP amplitude is the highest absolute value of nerve responses obtained from series intensities stimuli in iBF and may differ individually. The value or elimination of CAP amplitude can be used to describe the electrical nerve transduction along antennal chordotonal neurons, which may be normal, undermined, or completely abolished. To eliminate value difference from different animals, the individual CAP responses were normalized based on the formula: $V - V_{\min} / V_{\max} - V_{\min}$ and plotted against corresponding either SPV or antennal displacement. Subsequently each CAP/SPV or CAP/Displacement plotting was fitted with Hill-Fit equation ($f(x) = y_{\min} + ((y_{\max} - y_{\min}) / (1 + |x/ml|^n))$) to make electrical responding curve. The SPV or antennal displacement amplitude attained 10% of maximum CAP amplitude from Hill fit is defined as SPV or antennal displacement threshold. Data acquisition and initial analysis were done using PSV-VIB 9.0 (Polytec) and Spike 2. Figure plotting, Hill-Fitting, and statistical evaluation were accomplished in Excel, OriginLab, and Prism-GraphPad software.

1.2.6.5 Sound-induced intensity measurement at different frequencies

The measurements of a fly's hearing at other frequencies (from 50 to 850 Hz) were performed as the same as described in section 1.2.6.4. The displacement, SPV, and CAP responses were recorded for various frequencies. The range of utilized frequencies were located between 50 Hz to around 850 Hz, which is based on two factors: (1) when the input sound frequency is less than 50 Hz, the noise signals coming from the systems such as vibration of instruments and environment data lead to high imprecision and inaccuracy of output data; (2) The CAP amplitude (also the maximum CAP) continuously decreased with the increasing frequency and is not detectable when the frequency is higher than 850 Hz in control flies (*w¹¹¹⁸* and *Canton-S*). The data set from all frequencies were plotted in identical graphs to compare differences. To evaluate the mechanical responses at difference frequencies, the mechanical sensitivities were calculated and plotted against SPV, then the curves were fitted with Electrophysiology/ExpDec3 function respectively according to the equation: $y = A1*\exp(-x/t1) + A2*\exp(-x/t2) + A3*\exp(-x/t3) + y0$.

To examine the gain variation with frequencies, the gain value was calculated from the above equation at explicit intensities ranging from $2*10^{-5}$ m/s to $2*10^{-2}$ m/s and plotted against frequencies. Subsequently, each individual curve was fitted with a simple harmonic oscillator model. The resonance frequency, f_0 (iBF at individual intensity), and quality factor, Q (the sharpness of tuning), were extracted to describe how the gain changed. In the aspect of electrical response, the data set of the CAP response at frequencies were plotted against corresponding either SPV or Displacement and the curves were fitted with Hill-fit equation ($f(x) = y_{min} + ((y_{max}-y_{min}) / (1+1x/ml^n))$). CAP values were calculated at defined intensities (also called Iso-intensity) from the fit ranging from $2*10^{-5}$ m/s to $2*10^{-2}$ m/s and defined displacements (also called Iso-displacement) ranging from 50 nm to 500 nm respectively.

The CAP response at Iso-intensity or Iso-displacement were plotted against input frequencies and the curves were also fitted with simple harmonic oscillator model, from which resonance frequency (f_0) and Q factor were utilized to show the fitting trend. The graphs and fitting functions were all prepared using Origin software.

1.2.7 Image analysis and statistical data analysis

The images obtained from PCR gel electrophoresis and immunohistochemistry staining of JO and larva were subjected to Image J software to adjust the brightness and contrast. The series data set from whole antenna and brain projection staining were analyzed and reconstructed in 3D visualization in FluoRender. Data from fly hearing measurements were analyzed and plotted by utilizing multiple software, including Microsoft Excel, Origin, Sigma-Plot, and GraphPad Prism. The data were displayed as mean \pm standard deviation (1SD). Scientific statistical significances analysis from different groups was calculated with Two-Tailed Mann-Whitney-U tests, and shown in different P value: $P > 0.05$, no difference; $* P \leq 0.05$;

** P ≤ 0.01; *** P ≤ 0.001. The final data arrangement and diagrams were done in Adobe Illustrator 2021.

1.2.8 Additional information for antibody

Table 8. Antibody used in this thesis

Antigen	house	Concentration	Catalog NO/Supplier
Anti-GFP	chicken	1:1000	GTX13970 /GeneTex, Irvine, CA, USA
Anti-RFP	rat	1:1000	5F8 /ChromoTek, Germany
Anti-nc82	mouse	1:50	AB_2314866 /DSHB
Anti-Shaker	rabbit	1:50	20095731/BIOZOL
Anti-22C10	mouse	1:50	AB_528403 /DSHB
Anti-elav	rat	1:50	AB_528218 /DSHB
Cy3-conjugated goat anti-HRP	goat	1:300	123165021/Jackson ImmunoResearch
Alexa Fluor 633 Phalloidin	mouse	1:300	A22284 / Thermo Fisher Scientific
488-conjugated goat anti-HRP	goat	1:300	123545021 / Jackson ImmunoResearch
Alexa Fluor 488 anti-chicken	rat	1:300	A21316 / Thermo Fisher Scientific
Alexa Fluor 546 anti-rat	goat	1:300	A-11030 / Thermo Fisher Scientific

1.3 Results

To assess how the fly's ear responds to sound stimulation at different frequencies, I started with wild-type fly strains (*Canton-S* and *w¹¹¹⁸*), and tested the effects of different subgroups of JO neurons by performing specific JO neurons ablation assay (see section 1.2.4), lastly screened the genes, including BK, Cav, Kir, Kv, and piezo channels, to further explore the potential molecular mechanisms of frequency tuning in fly's ear as shown in Fig. 22.

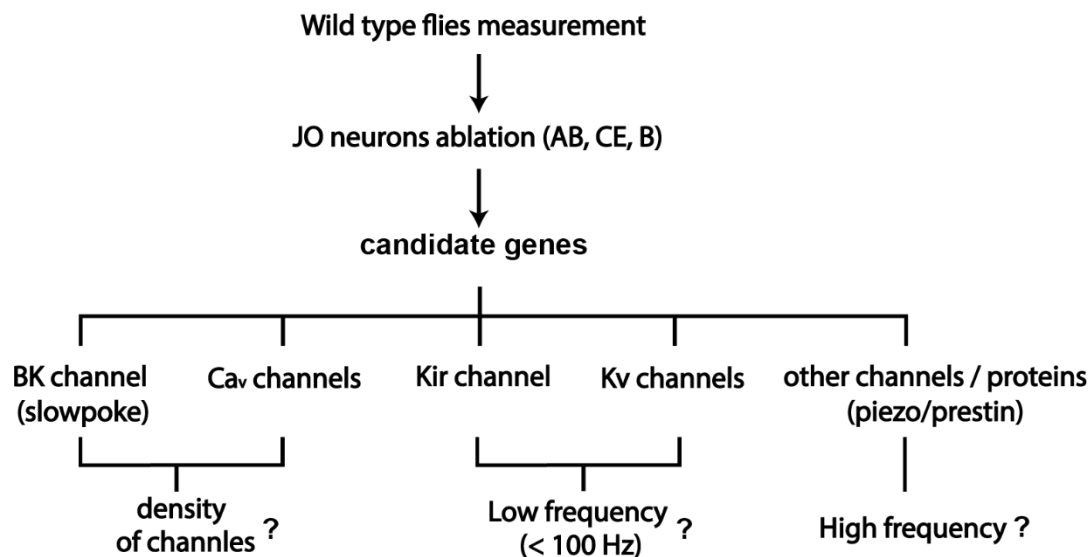


Fig. 22 Workflow for fly hearing performance measurement. The performance of fly's ear with various frequencies was firstly established. Then the ablation of different JO neurons and genes screen were carried out sequentially to investigate the molecular mechanism.

1.3.1 Auditory performance of fly's ear in wild-type strains

1.3.1.1 Anatomical analysis of JO neurons

Drosophila hears sound with antennal ears. The JO houses not only the chordotonal neurons which function as a signal converter (mechanical vibration → electrical nerve impulses), but also multiple supporting cells (Fig. 8). Fig. 23 (left) shows the location of antenna on the head. Moreover, the anatomical analysis of the JO illustrates that the sector-shaped cross-section displayed the bowl-shaped 2nd segment of antenna (Fig. 23 middle): the portion of cilium converges at and connected with a2/a3-joint and the dendrite along with the chordotonal neuron cell bodies display a divergent arrangement (stained with HRP and *elav* respectively) as shown in Fig. 23 (right).

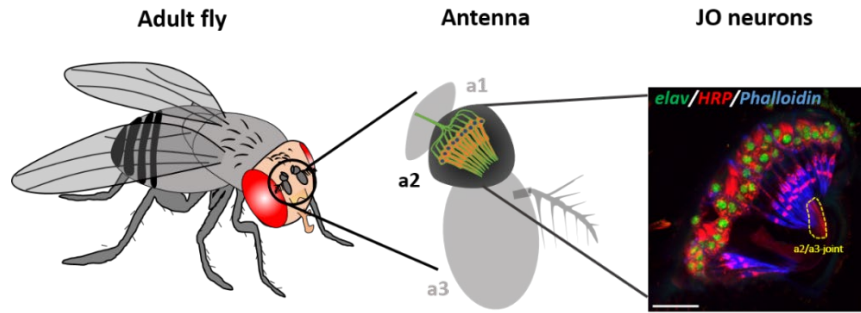


Fig. 23 Anatomy of JO in fly's ear. Left and middle: illustration of JO location on fly's head. Right: anatomical analysis of cross-section slices from JO, staining with HRP, *elav*, and Phalloidin. HRP (red) can label the contour of JO neurons' cell body and dendrite. Cell body was labelled with *elav* antibody (blue). Phalloidin (blue) showed the actin rod in scolopale cells. The scale bar is 20 μm .

1.3.1.2 Hearing performance at individual best frequency (iBF)

In the absence of sound stimulation, the fly's antennal sound receiver (the entity of arista and funiculus) can freely fluctuate, which is affected by two motions: active motion caused by JO neuron motility and passive motion caused by the thermal energy from adjacent air particles' bombardment (Jorg. Albert, 2011; Göpfert, 2008; Göpfert, 2005). To figure out how the antenna responds at natural physiological conditions without sound, I used *Canton-S* and *w¹¹¹⁸* as control strains in my study. A laser Doppler vibrometer was employed to record the mechanical free fluctuations of the antennal sound receiver and Fast Fourier Transforms (FFT) were utilized to analyse and export the power spectra of the receiver's mechanical free fluctuation for frequencies between 100 and 1500 Hz. The maximum power spectral density (peak) across the frequency range was considered as the individual best frequency (iBF) or resonance frequency (f_0) derived from fits with the simple harmonic oscillator model.

In active motion (awake control flies), the fluctuation power of wild type flies was $1612 \pm 607 \text{ nm}^2/\text{Hz}$ (*w¹¹¹⁸*) and $1191 \pm 264 \text{ nm}^2/\text{Hz}$ (*Canton-S*) respectively. The iBF was located at $226 \pm 30 \text{ Hz}$ (*w¹¹¹⁸*) and $296 \pm 39 \text{ Hz}$ (*Canton-S*), within the fly's courtship song frequencies (Fig. 24). Moreover, the free fluctuations of the antenna can also be described by a simple harmonic oscillator model, fitting the SHO formula with a calculated quality Q value at ca. 2.2 in active motion (Fig. 24 black and red fitting lines). By contrast, in antennal passive motion, such as flies with ablated class AB neurons, the power of antennal free fluctuation decreases accompanying with the shift of iBF to higher frequency (T. Effertz & Göpfert, 2011). Comparing to the sharp peak with a high Q factor in active motion, the trend is much blunter with a low Q factor value ca. 0.8 in passive motion of ablated JO class AB neurons in Fig. 53.

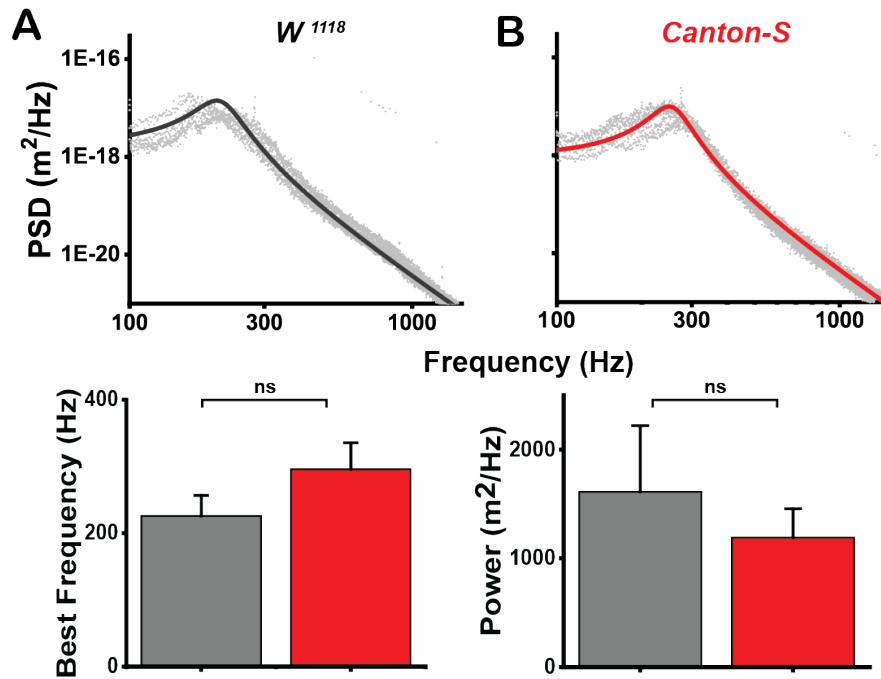


Fig. 24 Free fluctuation of antenna in wild type fly without sound. The *Canton-S* (black) and w^{1118} (red) were used as control strains and monitored to record the free fluctuation movement. The recording trace of active motion was displayed between 100 and 1500 Hz, which is considered as system energy range. The traces were fitted with simple harmonic oscillation model to calculate the Q factor and iBF (black and red line). Corresponding parameters, best frequency, and power were calculated from free fluctuation measurement. Data are shown as mean \pm 1SD (N=5 per strain). Two-tailed Mann Whitney U-test is used for statistically analysis. ns: not significant (N=5) $P > 0.05$.

To further analyze the hearing performance of the antennal ear, the flies were stimulated with pure tone at iBF with the different attenuations (intensities) ranging from 6 dB to 96 dB. The arista displacement, sound particle velocity (SPV), and antennal nerve response (also called compound action potential or CAP) were recorded (see details in Materials and Methods section). The data from sound-evoked measurements were displayed for two components: mechanical and electrical responses. In the mechanical response, the control flies' antennal ear shows a compressive nonlinearity, causing a higher amplitude of arista displacement at low sound intensity compared to the linearity of the passive system (Fig. 25 brown dash line). This nonlinear amplification along with the decreasing input sound intensity increases the mechanical sensitivity when sound is faint. In control flies, the maximum amplification gain was at 9.1 ± 2.6 (w^{1118}) and 12.3 ± 1.5 (*Canton-S*). Consistent with the passive motion in free fluctuation, the compressive nonlinearity was eliminated if sound-sensitive JO neurons were ablated, and mechanical response from this ablated strain was also passive (Fig. 54). Moreover, the mechanical sensitivity which is related to nonlinear amplification is defined by dividing the displacement to the corresponding SPV. In control flies, the sensitivity gain is higher when the sound is faint and decreases as the SPV increases (Fig. 25 middle images).

With respect to CAP response, it was measured by inserting tungsten electrodes into the antennal nerve. To eliminate the differences of absolute CAP value from each measurement, the CAP amplitudes

were normalized. Then the normalized CAP amplitudes were plotted against either corresponding SPV or arista displacement, displaying a sigmoidal curve that can be described with Hill-equation (Fig. 25). In control flies, the SPV threshold to evoke 10% of maximum CAP was ranging from 0.04 to 0.05 mm/s, whereas the minimal arista displacement threshold was ranging from 72 to 82 nm. The maximum CAP was $67 \pm 35 \mu\text{V}$ (w^{1118}) and $76 \pm 25 \mu\text{V}$ (*Canton-S*). Overall, these two curves (Fig. 25 A bottom) reflect the auditory sensitivity of the fly's ear: JO neurons sensitivity to antennal displacement and mechanical sensitivity of antenna to SPV. Shifts of these two curves illustrate the reduction of auditory sensitivity, either the increase stiffness of auditory system that required more input energy or less JO neurons (Fig. 55).

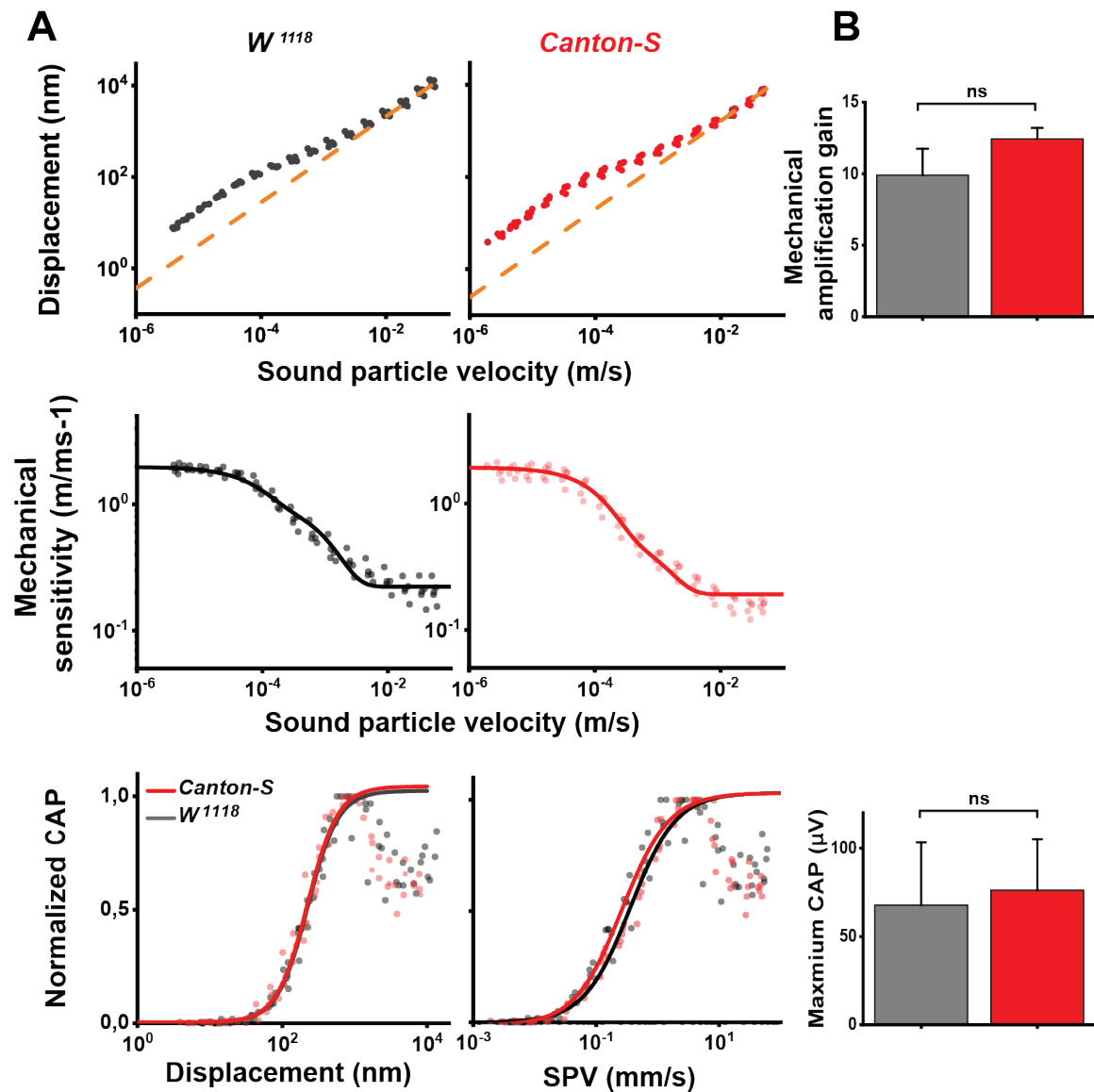


Fig. 25 Sound-evoked intensity measurement in *wild-type* fly at iBF. (A) Five to ten-days old control flies (w^{1118} and *Canton-S*) were measured with different sound attenuation ranging from 6 to 96 dB. A. (upper image) the control flies displayed a compressive nonlinearity comparing to the passive system (dash line). (middle) Mechanical sensitivity of the antennal receiver versus SPV. (bottom image) The normalized CAP amplitude to the corresponding SPV and Displacement for electrical response, fitting with Hill-equation. Maximum amplification gain and Maximum CAP were calculated from mechanical response and highest absolute CAP value respectively. *Canton-S* and w^{1118} , they both showed the similar sound-

evoked hearing performance. Data are shown as mean \pm 1SD (N=5 per strain). Two-tailed Mann Whitney U-test is used for statistically analysis. ns: not significant (N=5), P>0.05.

1.3.1.3 Hearing performance at different frequencies

1.3.1.3.1 Mechanical and electrical response at different frequencies

The performance of the fly's ear at different frequencies has been previously done by Thomas Effertz in his diploma, in which he recorded the frequency range from ca.150 Hz to 800 Hz by using *Oregon-R* fly strain. To further assess the mechanical and electrical responses of sound receiver at different frequencies in other wild type flies (*Canton-S* and *w¹¹¹⁸*), the recording was carried out as same as the measurement at iBF, but with series pure tones ranging from 50 to 800 Hz. Because when the pure tone was lower than 50 Hz or higher than 800 Hz, the absolute CAP value was either variable at lower frequency (< 50 Hz) or not detectable at higher frequency (> 800 Hz).

After plotting corresponding data from different frequencies into graphs, it was clear that the nonlinear amplification was gradually lost with the increasing frequencies, resulting in linear or passive system when applying with high frequencies (> ca. 500 Hz) (Fig. 26 A). When frequencies are lower than iBF, there was a partial reduction either in amplification or sensitivity gain, but not completely abolished (Fig. 26 A). The trend of calculated maximum sensitivity gain displayed an inverted “V” shape along the frequency range (Fig. 26 C). The data showed passive, linear behavior (linearity does not compress) of the fly's ear only occurs at high frequencies. For the electrical response, the CAP amplitude was highest at iBF. For the antennal electrical response, the CAP amplitude was highest at iBF. A gently decrease of the CAP amplitude from 62 μ v to 40 μ v was observed (Fig. 26 C), and then the amplitude remained constant at low frequencies, whereas at increasing frequencies from iBF, the reduction of CAP amplitude was continuous and sharp (from 62 μ V to barely 0 μ V) (Fig. 26 B and C).

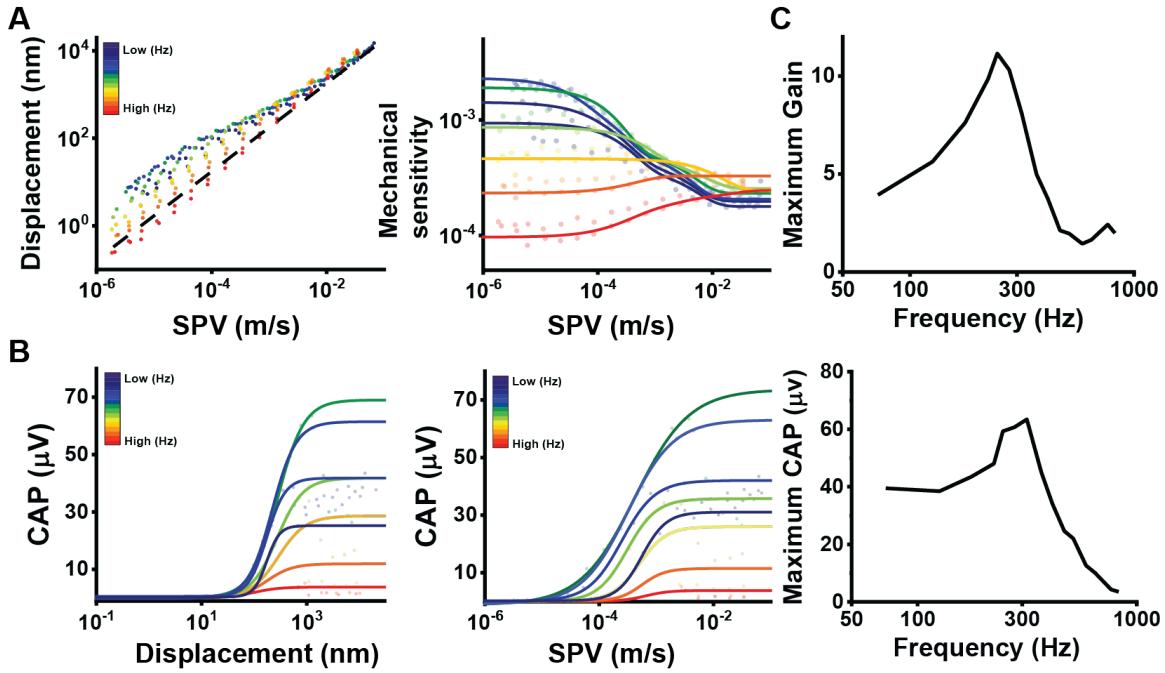


Fig. 26 Mechanical and electrical response in *wild-type* fly with series frequencies stimulation. The *Canton-S* flies were measured and stimulated with series frequencies ranging from 50 to 800 Hz. (A) Left: arista displacement versus SPV at series frequencies. Right: mechanical sensitivity of arista versus SPV at series frequencies. (B) Absolute CAP amplitude versus SPV (left) and displacement (right) at series frequencies. The color gradient was made by using Spectrum from Origin, showing the frequency range. (C) Maximum sensitivity gain and maximum CAP were obtained from applied single frequency and plotted against frequencies. A-C: Data of one representative animal of five examined flies (*Canton-S*).

1.3.1.3.2 Responses at Iso-Intensity and Iso-Displacement

To further evaluate the mechanical and electrical responses at given SPV and arista displacement, a total of 11 accurate equal sound intensities (iso-intensity) ranging from 2×10^{-5} to 2×10^{-3} m/s and 6 equal displacements (iso-displacement) ranging from 100 to 500 nm were chosen (Fig. 27A and Fig. 29A). To calculate the corresponding values (Gain and CAP) at iso-intensity and iso-displacement, the Gain/SPV, CAP/SPV, and CAP/Displacement curves were created and fitted with corresponding formulas respectively as shown in Materials and Methods section.

With respect to mechanical response in control flies, the sensitivity gain at individual iso-intensity was calculated and plotted against frequencies. Then the data at each iso-intensity was fitted with simple harmonic oscillation model (Fig. 27 B), meanwhile Q factor and iBF were obtained to describe the sharpness of fitting curves and peak shift respectively. As shown in Fig. 27, the iBF of the iso-intensity mechanical response shifted from from 280 Hz at the lowest intensity to 756 Hz at the highest intensity, however the Q factor showed an opposite trend, which reduced from 1.6 to 1.2 (Fig. 27 C).

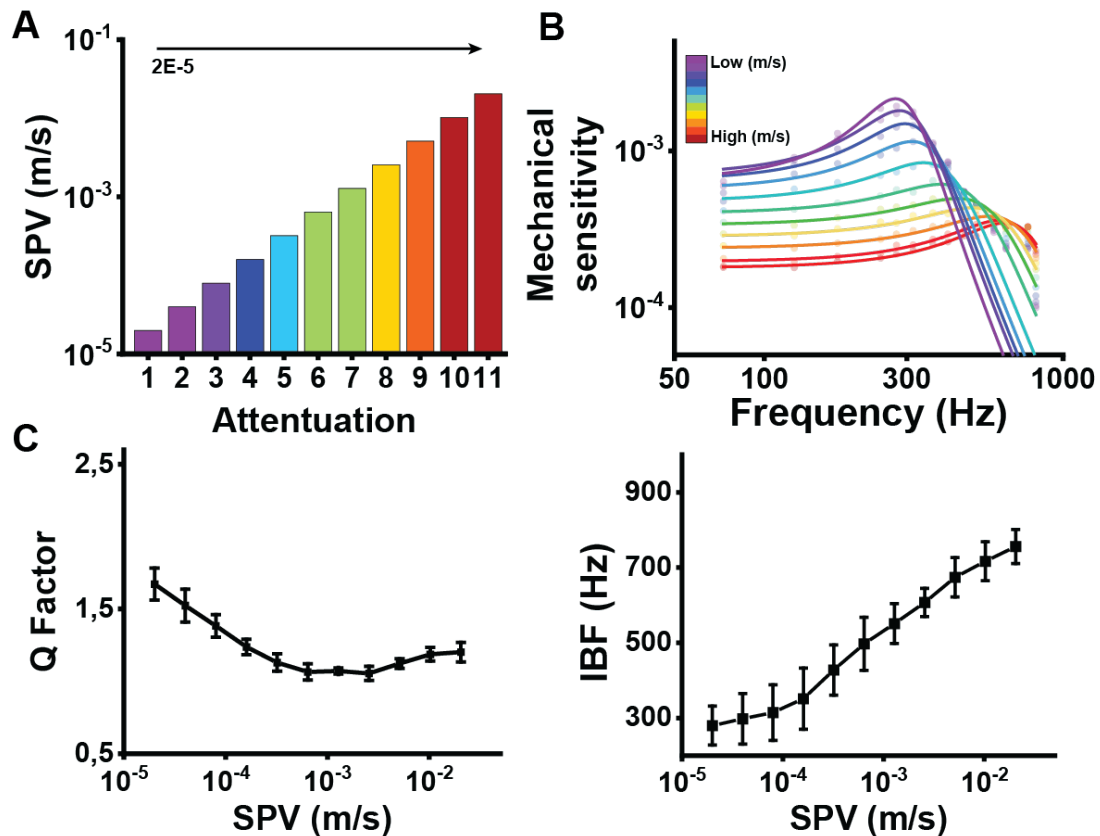


Fig. 27 Mechanical sensitivity in wild-type fly at iso-intensities. (A) The accurate linear value for iso-intensity which starts from $2E-5$ m/s with a continuous interval of $2E-5$ m/s. (B) The mechanical sensitivity of arista versus frequencies at iso-intensity and the fitting with SHO model. The data represents one of five measured flies with consistent output. (C) The Q factor and iBF were obtained from the simple harmonic oscillation model from (B). B: Data of one representative animal of five examined flies (*Canton-S*). C: Data are shown as mean \pm 1SD (N=5).

Because of the experimental limitations and differences of inherent properties of individual sound receivers, it is difficult to control and capture the exact CAP response at sound stimulation, such as particular arista displacement or SPV. To overcome the limitation and compare the CAP amplitude at given conditions, each accurate CAP was deduced at iso-displacement and iso-intensity from the CAP/Disp and CAP/SPV Hill-fit curves. Eleven intensities and six displacements were utilized (Fig. 27 A and Fig. 29 A). As shown in Fig. 28 A, the CAP amplitude at iso-intensity were plotted against frequencies, displacing an inverted “V” shape tread with a peak around iBF. Furthermore, to eliminate the variation, normalization is also introduced, displaying a superimposed trend from variable iso-displacement and iso-intensity.

The amplitude of CAP response increases from low frequency and reach a peak at iBF, then decrease as the frequency keep increase, till the CAP amplitude was undetectable, which is consistent with calcium imaging response that the maximum response occurs at the priority of different JO neurons. Then the intensity-gain or displacement-gain were defined as the division of corresponding CAP versus either SPV or displacement, then plotted against frequency and fitted with simple harmonic oscillation model (Fig. 28 B and Fig. 29 B)). Comparing to the Fig. 27 B at mechanical response, the

quality Q at iso-intensities decreased from 2.1 at lowest iso-intensity to 1.14 to highest iso-intensity, and a slightly shift ca. 70 Hz of iBF were observed. Whereas at iso-displacement, the Q factor hardly changed, assuming values between 0.9 and 1.2 with a little iBF shift ca. 50 Hz (Fig. 28 C). From these results, it showed that frequencies response can be toned at the location around iBF if ignoring the species-dependent frequent tuning.

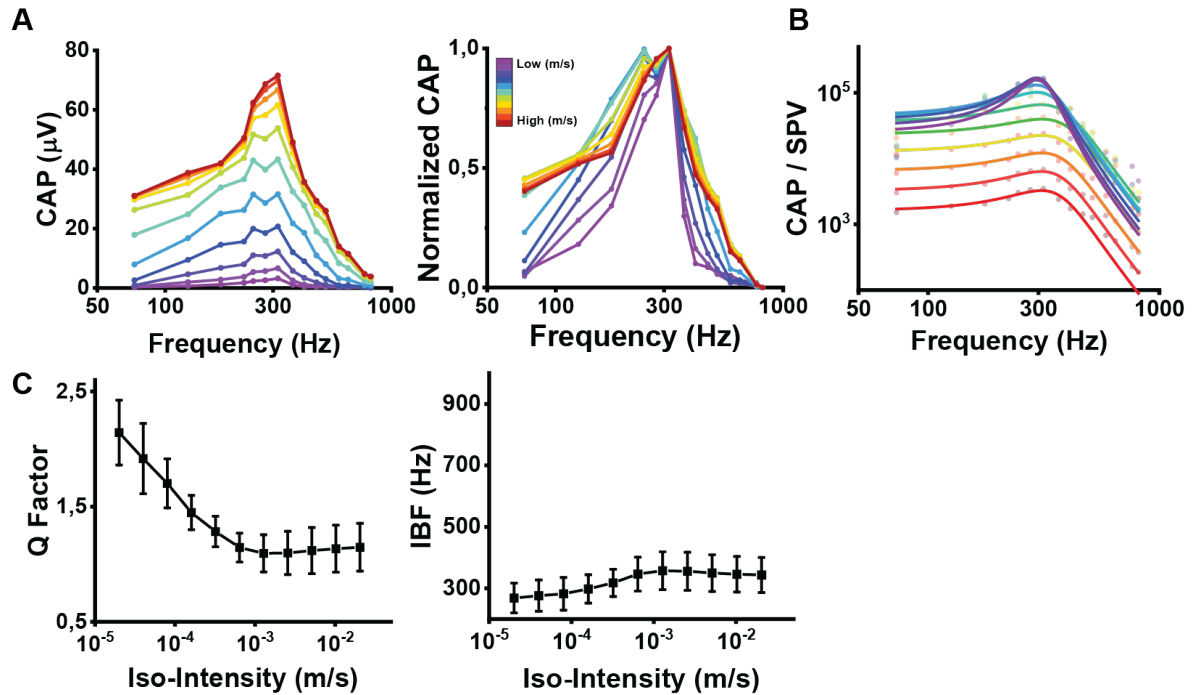


Fig. 28 Electrical response in *wild-type* fly at iso-intensity. (A) Left: The absolute CAP amplitudes versus frequencies at each iso-intensity. The data were calculated from Fig. 26 B, then plotted against frequencies. The gradient color showed the individuals of iso-intensity. Right: Normalization of CAP amplitude at iso-intensities from Fig. 28 A left. (B) The intensity gain was defined by the division of CAP/SPV, then plotted again frequencies and fitted with simple harmonic oscillation model. (C) The Q factor and iBF were obtained from the fitting in Fig. 28 B. The curves showed the change of Q factor and iBF along with iso-intensities. A-B: Data of one representative animal of five examined flies (*Canton-S*). C: Data are shown as mean \pm 1SD (N=5).

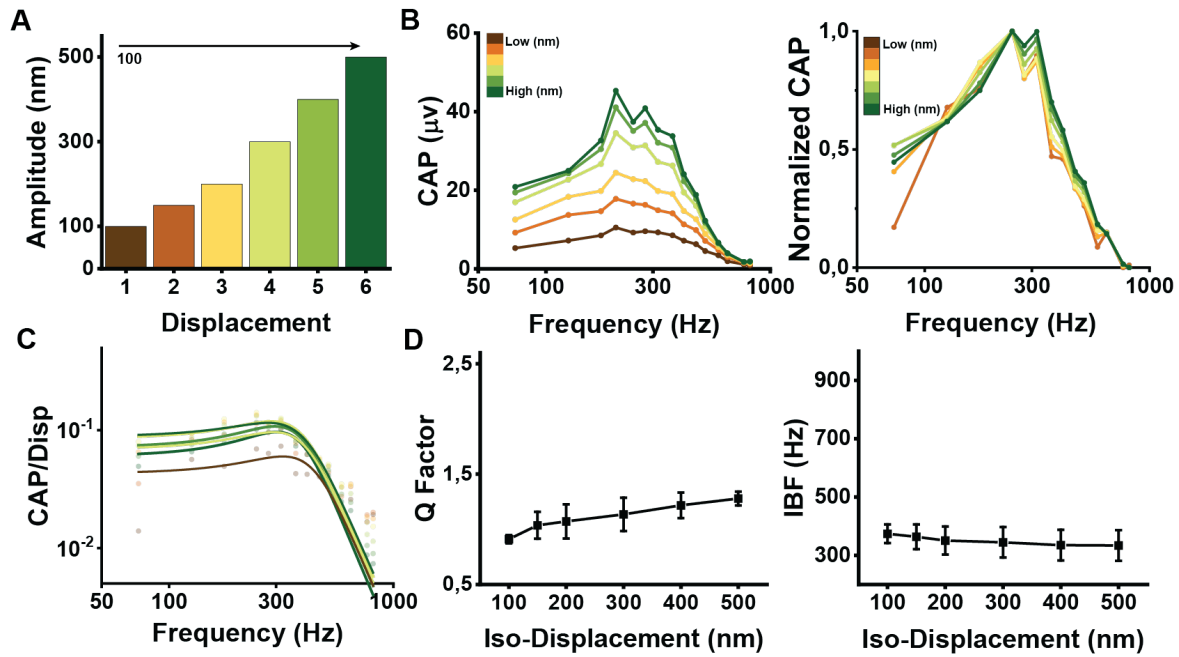


Fig. 29 Electrical response in *wild-type* fly at iso-displacement. (A) Six different displacements ranging from 100 to 500 nm were defined as iso-displacement at dynamic range to calculate the CAP amplitude respectively. (B) Left: The absolute CAP amplitude versus frequencies at the iso-displacement. The data were calculated from Fig. 26 B, then plotted against frequencies. The gradient color showed the different iso-displacements. Right: Normalization of CAP amplitude at iso-displacements. (C) The displacement gain was defined by the division of CAP/Displacement, then plotted against frequencies and fitted with simple harmonic oscillation model. (D) The Q factor and IBF was obtained from the fitting of simple harmonic oscillation model. The curves showed the change of Q factor and iBF along with iso-displacements. A-C: Data of one representative animal of five examined flies (*Canton-S*). D: Data are shown as a mean \pm 1SD (N=5).

1.3.2 Effects of ablated auditory JO neurons

Frequency preference occurs in fly auditory JO neurons, and it is a cell inherent mechanism recorded by the calcium imaging in AMMC zones (Yorozu *et al.*, 2009). To further test the frequency tuning by detecting the antennal electrical response, in this section, I selectively ablated the different subgroups of JO neurons to check the differences.

1.3.2.1 Distribution and localization of auditory JO neurons

Firstly, I checked the distribution and localization of different subgroup of JO neurons in adult flies by using particular Gal4 enhancer lines along with multiple staining methods. *Dnai2* and *NP0761* Gal4 fly strains contain non-selective promoters that can label all classes JO neurons, whereas *JO15*, *NP6250*, *NP1046*, and *NP5035* Gal4 strains only contain the promoters that selectively label class AB, CE, B, and D neurons respectively (Fig. 30). By staining the JO neurons with nuclear-RFP and reconstructing the JO neurons in 3D model, a bowl-shaped JO was present with a “open bowl” arrangement, meanwhile the AB neurons arranged on both sides of the array whereas the CE neurons were located on the peripheral of the bowl shape array, surrounding the AB neurons (Fig. 31). For the cross-sections staining of JO samples, it also proved a similar distribution of JO neurons (Fig. 30). *Dnai2*-expressing neurons are distributed in the whole JO, however, *JO15* only labelled sound-sensitive neurons, *NP6250*

labelled gravity/wind-sensitive neurons. It was notable that class D neurons were hardly detectable in cross-section staining because of low numbers and limitations of sectioning techniques.

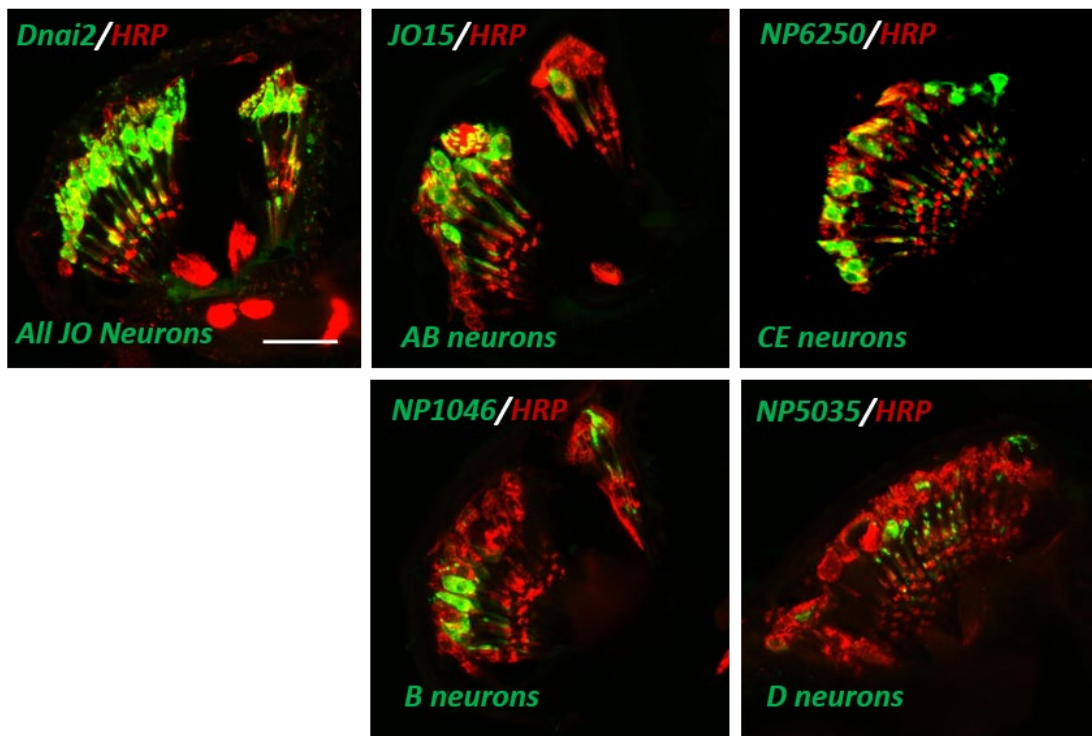


Fig. 30 Cross-section staining of JO neurons with different driver lines in adult flies. All flies for staining were harvested from the progenies that corresponding driver lines cross to UAS-GFP. *Dnai2* is an established protein that non-selectively expressed in all JO neurons. *JO15* can particularly label the auditory class AB neurons. *NP6250* labels class CE neurons. *NP1046* labels class B neurons and *NP5035* labels class D neurons. Scare bar is 20 μ m.

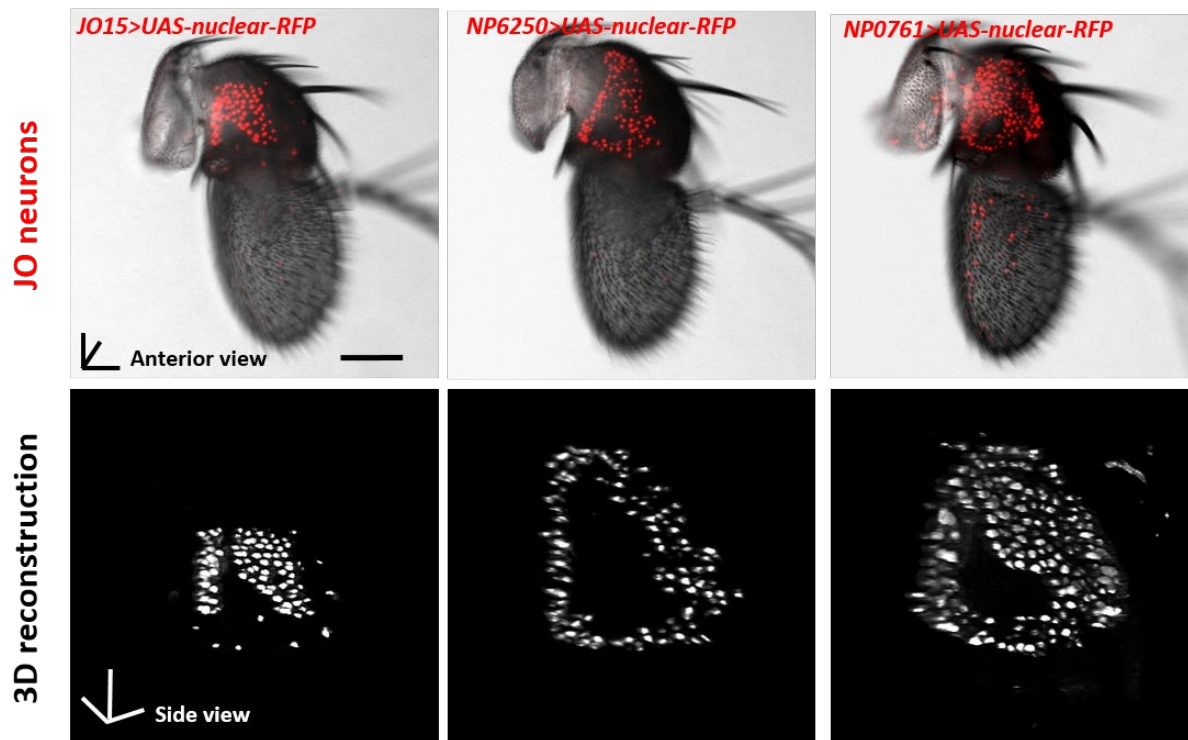


Fig. 31 Whole antenna mounting with nuclear-RFP staining and 3D reconstruction. The *JO15*, *NP6250*, and *NP0761* Gal4 fly strains were crossed with *UAS-DsRed* strain, then the progenies were collected for whole antenna mounting according to the methods described in Materials and Methods section. After the collection of images, the series slides were reconstructed and whole antenna was displayed in 3D model structure. Scare bar is 30 μm

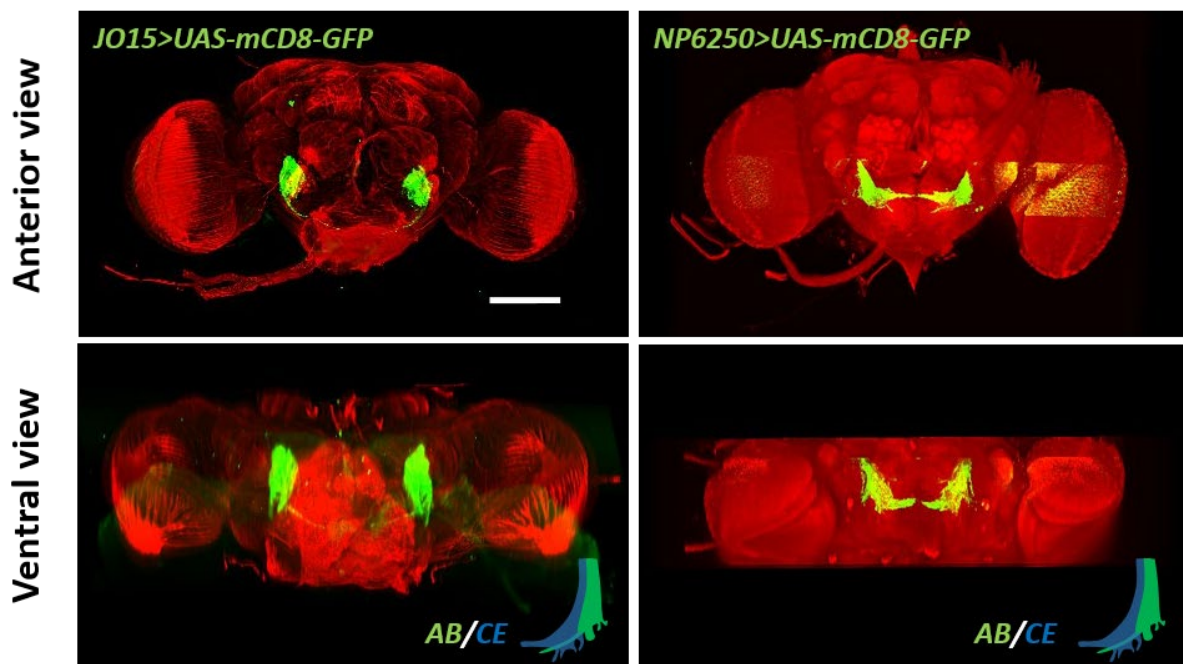


Fig. 32 Brain projection of JO neurons. The *JO15* and *NP6250* were crossed to *UAS-RFT-stop-RFP-mCD8-GFP*, the brain from F1 generation were collected and subjected to downstream brain staining process described in Material and Methods section. The series confocal images were scanned and collected, then reconstructed to build the whole fly brain. The projection of antennal AB and CE nerve were also showed in brain AMMC area. Green: antennal nerve. Red: HRP. Scare bar is 100 μm .

1.3.2.2 Auditory performance of JO neurons at different frequencies

To access the auditory performance of different subgroups in JO, the different class JO neurons were selectively ablated by introducing the *eyFLP* and *FLP/FRT* systems with the specific Gal4 enhancer in fly.

Previous studies have shown that the ablated AB neurons lead to complete deafness in the fly with elimination of mechanical amplification and scarcely CAP response at iBF (T Effetz *et al*, 2011). However, elimination of class CE neurons in the JO maintains normal hearing function. Here, I re-measured these two ablated strains, adding another other two groups, ablated class B and D JO neuron as comparison. Without sound, the power of the receiver's free fluctuation in flies with ablated class AB neurons significantly reduced to $72.8 \pm 40.7 \text{ nm}^2/\text{Hz}$, with a shift of iBF from ca. 250 Hz in control flies to $429 \pm 40 \text{ Hz}$. In flies with ablated class B neurons in JO, it displayed a similar phenotype as the strain with ablated class AB JO neurons (Fig. 33 A and Fig. 53). Moreover, the power was partly affected if only ablating class D neurons, and free fluctuation of sound receiver was not influenced with the absence of class CE JO neurons (Fig. 33 A).

During the stimulation with pure tone at iBF, the mechanical amplification was completely abolished in both ablated class AB and class B neurons with a decreased gain at 1.7 ± 0.2 and passive

sound receiver's system. With respect to ablated class D or CE group, the amplification gain was mildly impaired without class D neurons, but no effect occurred in the latter group at iBF (Fig. 33 B). With sequential frequencies stimulation, the displacement amplitude in both AB and B ablation groups lost non-linear compression. Whereas, in ablated class CE and D groups, non-linear compression was gradually lost to a linear passive system as the frequencies increased (Fig. 33 B). The sensitivity gain calculated from iso-intensities showed differently between strains. In class AB and class B neuron groups, the peak was located in the high frequency region > 700 Hz and scarcely no shift of iBF was observed comparing with control group. But in ablated class D neurons strain, the iBF shifted from 438 Hz to 702 Hz as the SPV increased and in ablated CE strain, the shift started at 290 Hz and ended at 754 Hz.

As for CAP response, it is severely impaired but still detectable when the sound is loud, for instance, stimulation at 12 or 6 dB in ablated AB neurons strain. When stimulated with series pure tones < 300 Hz, the maximum CAP in flies with ablated AB neurons gradually increased and reached peak at ca. 100 Hz as shown the superimposed curves in Fig. 33 D and E. But in flies with ablated B neurons, there was a sharp drop between 100 Hz to iBF, then CAP amplitude increased again when frequency was lower than 100 Hz. In ablated class CE and D group, iso-displacement and iso-intensity responses resembled those of control flies (*Canton-S*) (Fig. 33 D and E).

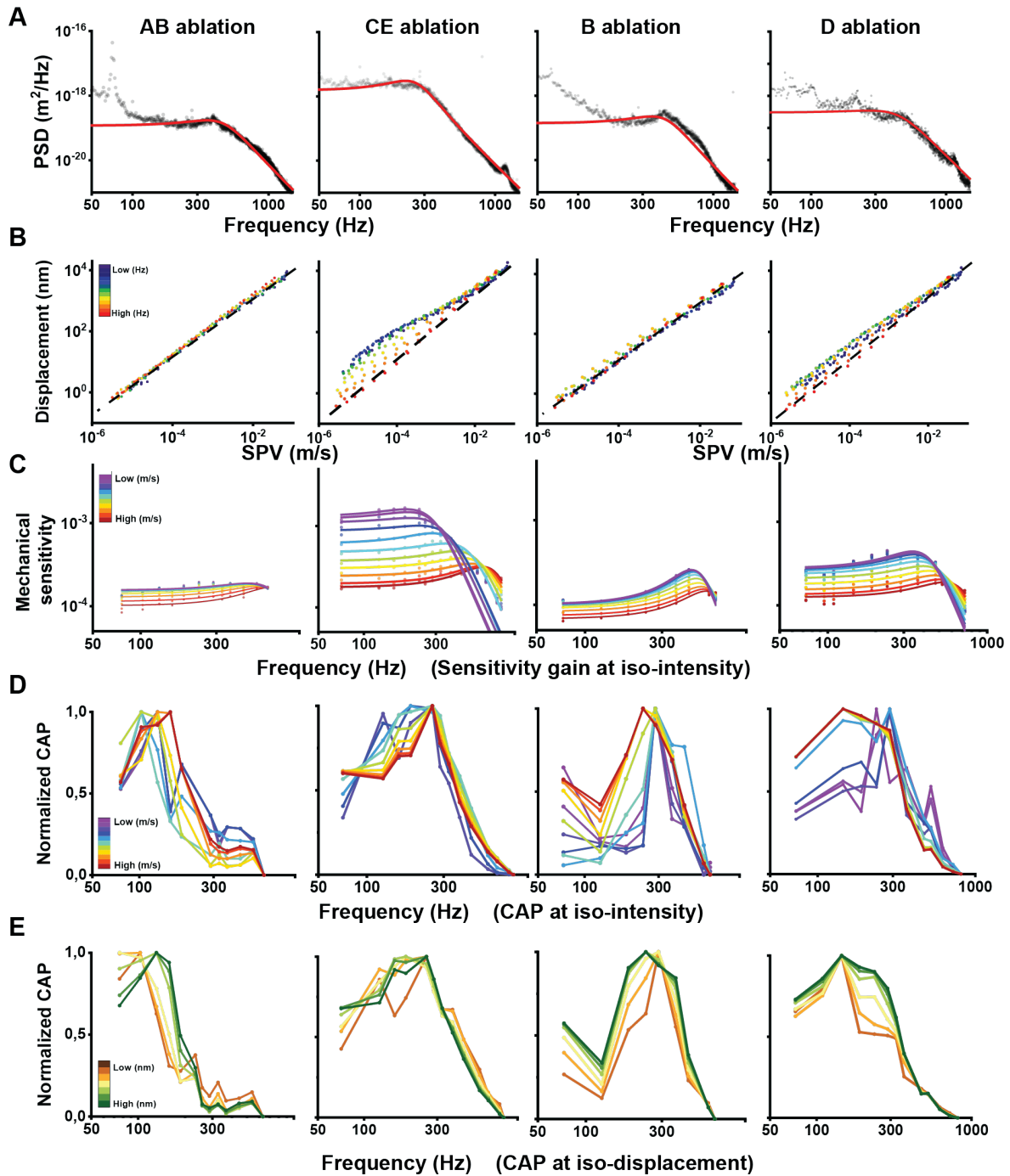


Fig. 33 Auditory performance in ablated JO neuron strains at different frequencies. (A) Free fluctuation measurements of arista from the ablated JO neuron populations: class AB (*JO15*), CE (*NO6250*), B (*NP1046*), D (*NP5035*). Black dots: PSD amplitude at each oscillating frequency. Red line: simple harmonic oscillation model fitting. (B) The arista displacement versus SPV at each frequency. Black dash line: linear system. (C) The mechanical sensitivity versus frequencies at iso-intensities. The iso-intensities were shown in gradient color and fitted with simple harmonic oscillation model. (D) and (E) The normalization of CAP amplitude at iso-intensities and iso-displacement over frequency range. Data is from one representative animal of three examined flies (N=3 per strain).

1.3.3 Candidate genes for regulating frequency tuning of JO neurons

In the vertebrate cochlea, the frequency components from complex sounds can be discriminated based on two mechanisms: mechanical tuning and electrical tuning. When frequency is lower than 1 kHz, the frequency can be electrically filtered and tuned, which is a poly-regulatory process regulated by voltage-dependent ion channels, involving in Cav, BK, Kir, and Kv channels (Hudspeth AJ, 1983; Hudspeth AJ, 1988). In this section, I tested the potential genes that are established in the cochlea to see whether these genes have similar regulatory functions by recording the mechanical and electrical response in the fly, and how these genes participate in the modulation. Additionally, the *piezo*, which has been proved to participate in the high sound frequency sensing in larva, are also included in this section (Zhang *et al.*, 2021).

1.3.3.1 The voltage-gated calcium channels in fly's hearing

1.3.3.1.1 The voltage-gated calcium channel expression in JO

In electrical tuning, the classic model for hair cells to filter and sharp the frequency components relays on the combination of two channels: voltage-gated calcium channel (Ca_v) and large-conductance Ca²⁺ activated K⁺ channels (BK channels). Several homologous Ca_v genes has been identified in flies that are essential to normal activities, such as modulation of action potential generation, muscle contraction, wing motoneurons, and calcium mediated signalling, etc (Kanamori *et al.*, 2013; Chorna & Hasan, 2012; Ly *et al.*, 2008). These Ca_v channels include Ca²⁺-channel protein *a*₁ subunit D (*Ca-a 1D*), Ca²⁺-channel protein *a*₁ subunit T (*Ca-a 1T*), Ca²⁺-channel protein *beta* subunit (*Ca-beta*), and cacophony (*cac*). Before testing their functions in fly's hearing, I firstly tested their expression patterns in the JO of adult flies.

For *Ca-a 1D*, because of the non-accessibility of proper Gal4 enhancer line or antibody against *Ca-a 1D*, the presence of *Ca-a 1D* expression in JO was detected by using RT-PCR with gene specific primers. A PCR product of *Ca-a 1D* mRNA at expected size was detectable (Fig. 34), indicating expression of *Ca-a 1D* in the JO. Furthermore, from the immunostaining with GFP-reporter assay, I showed that only *Ca-a 1T* and *Ca-beta* express in JO, not *cac* (Fig. 35).

mRNA in 2nd segment of antenna

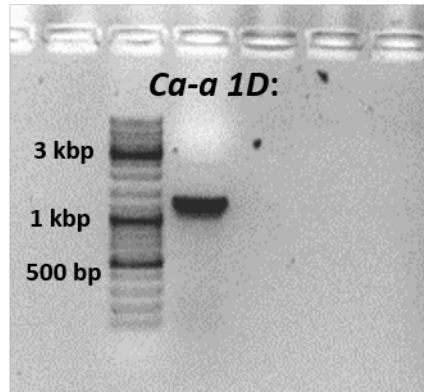


Fig. 34 RT-PCR result for *Ca a 1D* in the 2nd segment of antenna. Whether the presence of *Ca-a 1D* in JO was detected by using RT-PCR method with gene specific primers described in Method section. The 2nd antennal segment was used for total RNA extraction.

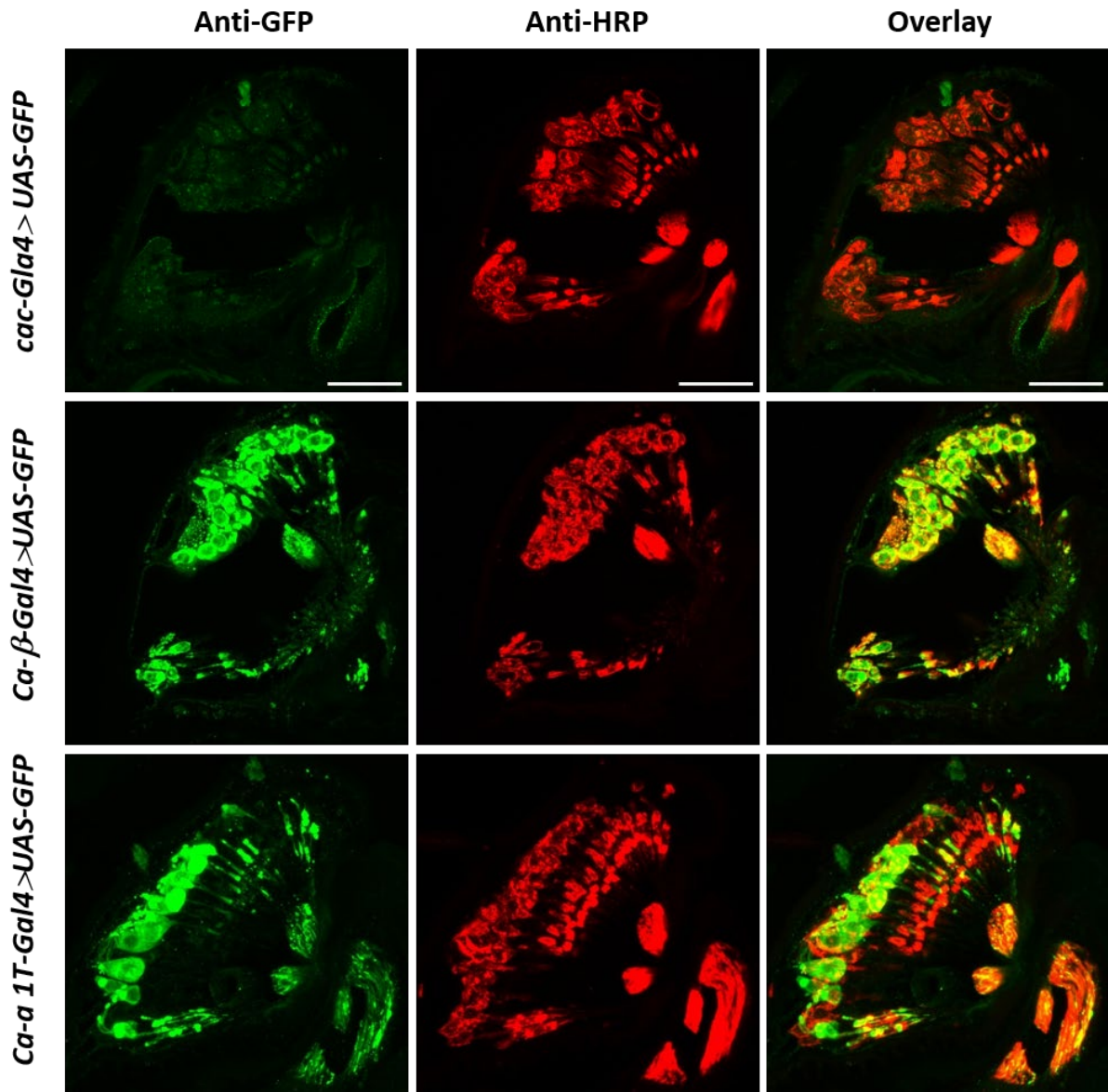


Fig. 35 Voltage-gated calcium channel expression in JO. Besides the *Ca-a 1D* was detected by RT-PCR, the other three Cav channels, including *Ca-a 1T*, *Ca-beta*, and *cac*, were investigated by using Gal4/UAS-GFP system. As shown, *cac* was not detectable in JO and no green GFP signal was observed. *Ca-beta* was expressed in all JO neurons, whereas *Ca-a 1T* was expressed in subset of JO neurons, not all. Green: GFP signal to show the expression of driver genes. Red: HRP signal to show the JO neural structure. Scale bar is 20 μm .

1.3.3.1.2 The voltage-gated calcium channels in fly's hearing

Next, the effects of these voltage-gated calcium channels (*Ca-a 1D*, *Ca-a 1T*, and *Ca-beta*) in fly hearing were measured by exposing the flies carrying the null allele at different frequencies. Because the *cac* is not detectable in JO, I would not talk about the *cac* gene further.

For auditory performance, three null alleles, *Ca-a 1D^{x10}*, *Ca-a 1T ^{Δ 135}*, and *Ca-beta ^{Δ full}*, were tested for a possible function in normal hearing and respective involvement in mechanical and electric tuning. Firstly, the power of receiver's free fluctuation revealed no significant difference compared to control flies. Moreover, no significant shifts of iBF were observed from flies carrying *Ca-a 1D^{x10}*, *Ca-a 1T ^{Δ 135}*, and *Ca-beta ^{Δ full}* (Fig. 36 A).

Consistent with the free fluctuation, the compressive non-linearity of tested Cav null alleles was not significantly altered compared to control groups in the presence of sound stimuli at iBF. Therefore *Ca-a 1D*, *Ca-a 1T*, and *Ca-beta*, may have no effects on fly's hearing, either in mechanical or electrical responses (Fig. 36 B). With the sequential frequencies stimuli, it was obvious that the non-linear amplification was gradually lost, and the auditory system changed to be passive from being active with the increasing frequencies in all these null strains, which behaved like wild type flies (Fig. 36B). As for the mechanical response, the change of gain at iso-intensities were no different when compared to control flies.

For *Ca-a 1D^{x10}*, the Q factor decreased from 1.8 at lowest intensity to 1.2 at highest intensity. The variation range was from 1.7 to 1.1 for *Ca-a 1T ^{Δ 135}*, and from 1.8 to 1.3 for *Ca-beta ^{Δ full}* respectively (Fig. 36 C). Neither in mechanical response nor antennal electrical nerve response, these null allele Cav channels displayed wild type-like auditory performances. The CAP amplitude was gradually reduced with the increasing frequencies. The normalization of CAP amplitude at iso-intensities and iso-displacement showed a similar trend with one peak at around iBF, along with a rise from low frequency to iBF and a drop from iBF to high frequency (Fig. 36 D and E). Taken together, the data provide no evidence that the tested Cav channels contribute to the frequency tuning alone.

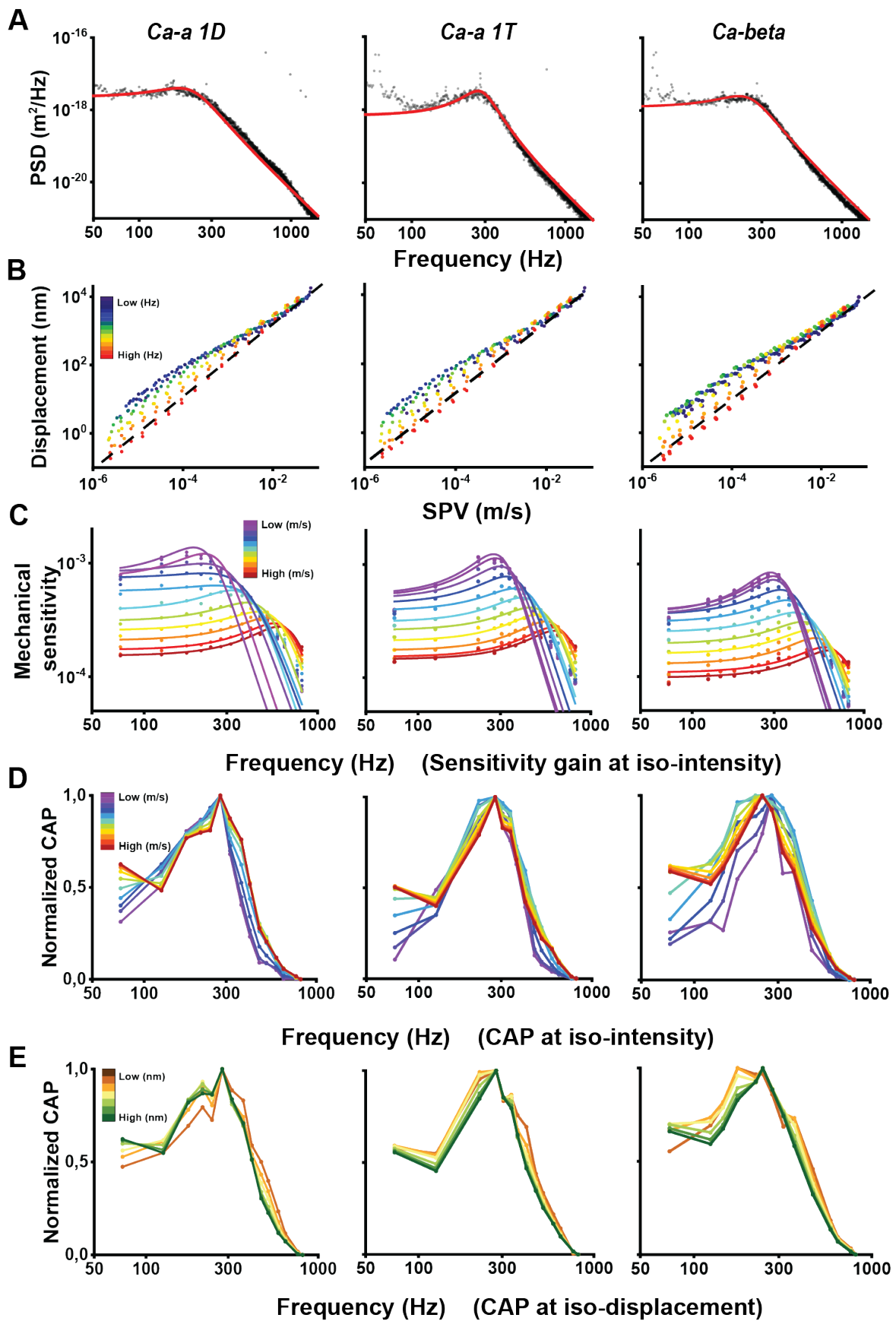


Fig. 36 Auditory performance in *Ca-a 1D*, *Ca-a 1T*, and *Ca-beta* mutants at different frequencies. (A) Free fluctuation measurement from three null Cav channels alleles, *Ca-a 1D*^{x10}, *Ca-a 1T*^{Δ135}, and *Ca-beta*^{Δfull}. Black dots: PSD amplitude at each oscillating frequency. Red line: simple harmonic oscillation model fitting. (B) The arista displacement versus SPV at

each frequency. Black dash line: linear system. (C) The mechanical sensitivity versus frequencies at iso-intensities. The iso-intensities were shown in gradient color and fitted with simple harmonic oscillation model. (D) and (E) The normalization of CAP amplitude at iso-intensities and iso-displacement over frequency range. Data is from one representative animal of three examined flies (N=3 per strain).

1.3.3.2 BK_{Ca} channel in fly's hearing

According to the published works, electrical tuning has been observed in many species, including chick, turtle, frog, and alligator (R Fettiplace, 1981; PA Fuchs, 1988; AJ Hudspeth 1988; RA Eatock, 1993). And the mechanism of electrical tuning regulation is conserved across these species, combining Cav and BK channels to generate oscillatory electrical response. Besides the Cav channel that allows the Ca²⁺ influx into hair cells, subsequently the nearby BK channel is activated by Ca²⁺ ions. Not only the frequency range below 1 kHz can be electrically tuned by these two channels, but also the frequency can be defined at a range from 100 to 600 Hz, which is modulated by the density of paired Cav/BK channels and kinetic properties of channels.

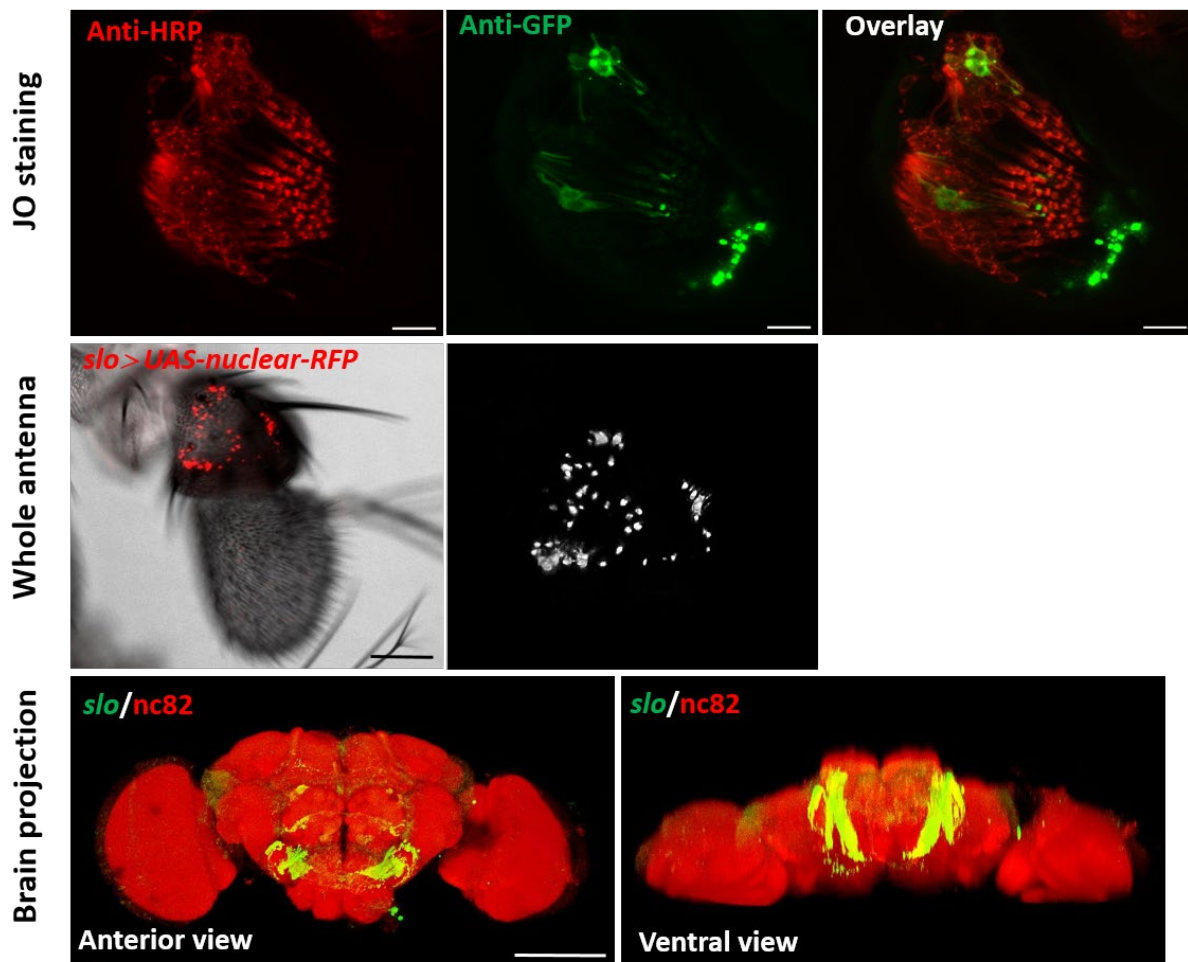


Fig. 37 Calcium-activated potassium channel (BK) expression in JO. A *slo-Gal4* enhancer line was utilized as driver line for all crossings: cross with UAS-GFP for JO staining; cross with UAS-nuclear-RFP for whole antenna mounting; cross with UAS-mCD8-GFP for brain staining. The procedure was described in Method section. Scare bar in JO staining is 10 μ m, in whole antenna mounting is 30 μ m, and in brain staining is 100 μ m.

In *Drosophila*, the homologous gene of BK_{Ca} channels is called *slowpoke* (or *slo*) which is essential to maintain electrical excitability in neurons and muscle cells (Atkinson *et al.*, 2000). In the fly's ear, a GFP reporter assay with a *slo-Gal4* enhancer line driving a *UAS-GFP* fluorescent reporter demonstrated that *slo* channel was present in JO, but only in subset of ca. 500 JO neurons. Furthermore, by doing the whole antenna mounting with nuclear RFP staining and 3D antennal reconstruction, there are ca. 60 to 70 JO neurons that contain *slo* channel. In antenna nerve projection in brain AMMC area, *slo* channel was further identified and distributed not only in primary auditory area, but also in primary gravity/wind sensitive area.

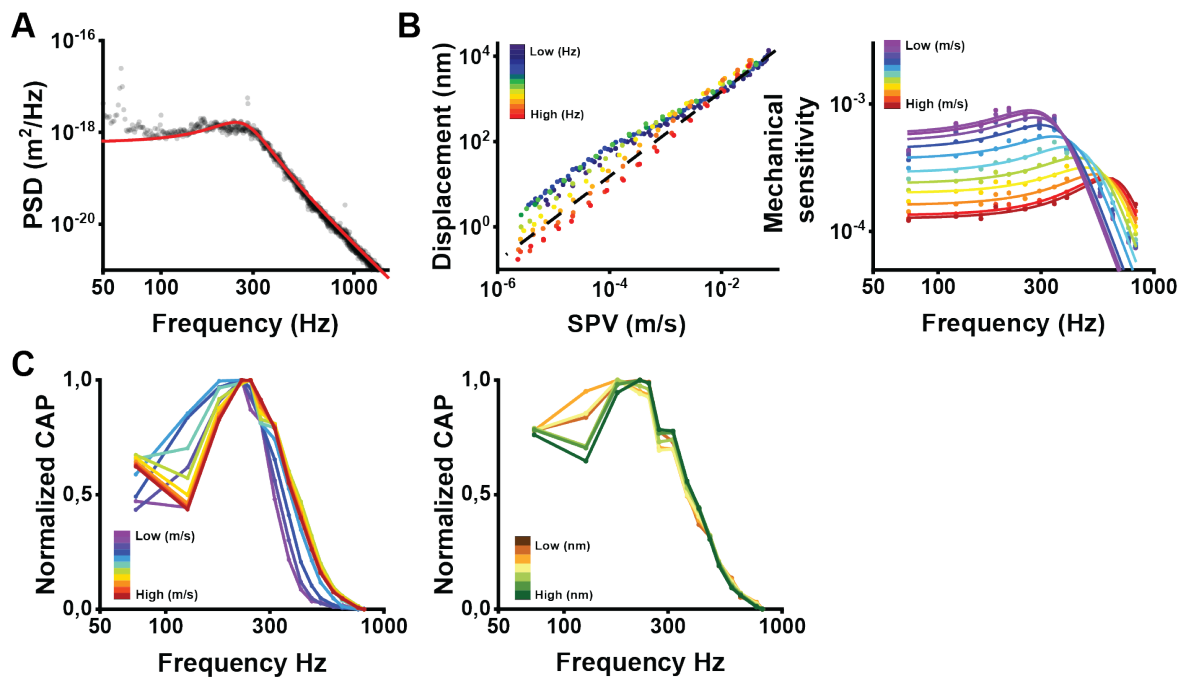


Fig. 38 Auditory performance in *slowpoke* channel mutant at different frequencies. (A) Free fluctuation measurement from *slo*^{MB11481/Df(3R)BSC397} mutant, that the null allele *slo*^{MB1148} was crossed to an deficiency strain to eliminate the effect of genetic background. Black dots: PSD amplitude at each oscillating frequency. Red line: simple harmonic oscillation model fitting. (B) Left: The arista displacement versus SPV at each frequency. Black dash line: linear system. Right: The mechanical sensitivity of arista versus frequencies at each iso-intensity. The various intensities were shown in gradient color and fitted with simple harmonic oscillation model. (C) The normalization of CAP amplitude at iso-intensities (left) and iso-displacement (right) over frequencies. Data is from one representative animal of five examined flies (N=5).

To measure the hearing performance of *slo* channel in fly's ear, a mutant, *slo*^{MB11481} without any gene products in fly's head (Jepson *et al.*, 2014), was utilized and crossed to corresponding deficiency strain to eliminate side effects from genetic background. The progenies with *slo*^{MB11481/Df(3R)BSC397} genotype were collected for measurement. With a limited expression of *slo* channel in JO (Fig. 37), it showed that the fly can still detect sound with a mild loss of mechanical amplification (5.5 ± 1.4) at iBF (Fig. 54), but the CAP response was not affected compared to control flies (Fig. 55). Meanwhile, in the absence of sound, the power from arista free fluctuation was slightly decreased to $286 \pm 40.1 \text{ nm}^2/\text{Hz}$ in comparison with control flies (Fig. 38 A and B and Fig. 53). With sequential frequencies stimulation, the amplification gain was completely lost at low intensities when the frequency was higher than ca. 500 Hz along with a decreasing of CAP amplitude (Fig. 38 B, left). As for the sensitivity gain at iso-

intensities across frequencies, the peak of SHM fitting curve shifted from 345 Hz at lowest intensity to 723 Hz at highest intensity (Fig. 38 B, right). In contrast with the undetectable difference at CAP response versus iso-intensities with wild-type, the distinctive CAP response at iso-displacement, especially at frequency < 100 Hz, was worth to take into account. Comparing with control flies in CAP/iso-displacement curve, the superimposed lines from isolated displacement amplitude declined more slowly when the frequency dropped from iBF (Fig. 38 C), which meaning that the neurons were more sensitive to fire at low frequency without *slo* channel.

1.3.3.3 Other Potassium channels in fly's hearing

Potassium channels, as the most widespread and distributed ion channels in living organisms, have been well studied and are essential to maintain biological functions, as well as their regulations in hearing. In the vertebrate cochlea, the frequency discrimination of hair cells not only depends on the density of Cav and BK channels, but also may involves other potassium channels, such as voltage-dependent K⁺ channels (Kv) and inward rectifiers (Kir) channels (Hudspeth AJ, 1983; Hudspeth AJ, 1988). In this section, I tested the effect of potassium channels in electrical tuning of fly's ear.

1.3.3.3.1 Voltage-gated channels expression in JO

In turtles and frogs, the molecular mechanism of electrical tuning is slightly different according to the frequency range. For instance, at the frequencies >100 Hz in turtle, the Cav/BK channels are dominant, whereas at low frequencies < 100 Hz, a calcium-independent delayed rectifier K channel is required to generate low frequency oscillation (Evans MG, 1990). Shaker cognate b (*Shab*) is the fly homolog encoding alpha subunit of delayed rectifier K channel 2 (Kv2). To further compare with other Kv channels in fly frequency tuning regulation, other Kv channels that include *Shaker* and *eag* are also measured and analysed.

From the immunostaining of JO, it shows that both *eag* and *Shab* channels were non-selectively expressed in all JO neurons. However, with the anti-*sh* antibody staining, *Shaker* channel only distributes in subset of JO neurons, mainly located on the auditory sensitive neurons compared to JO15 enhancer line expression pattern. Additionally, *Shaker* is also a channel that was identified and localized in dendrite of chordotonal neurons JO. Moreover, *Shaker* channel not only showed a selective expression in JO, but also only presents in four of total five *lch5* neurons of the dendrite of chordotonal neurons in 3rd stage larva (from number 2 to 5) (Fig. 39).

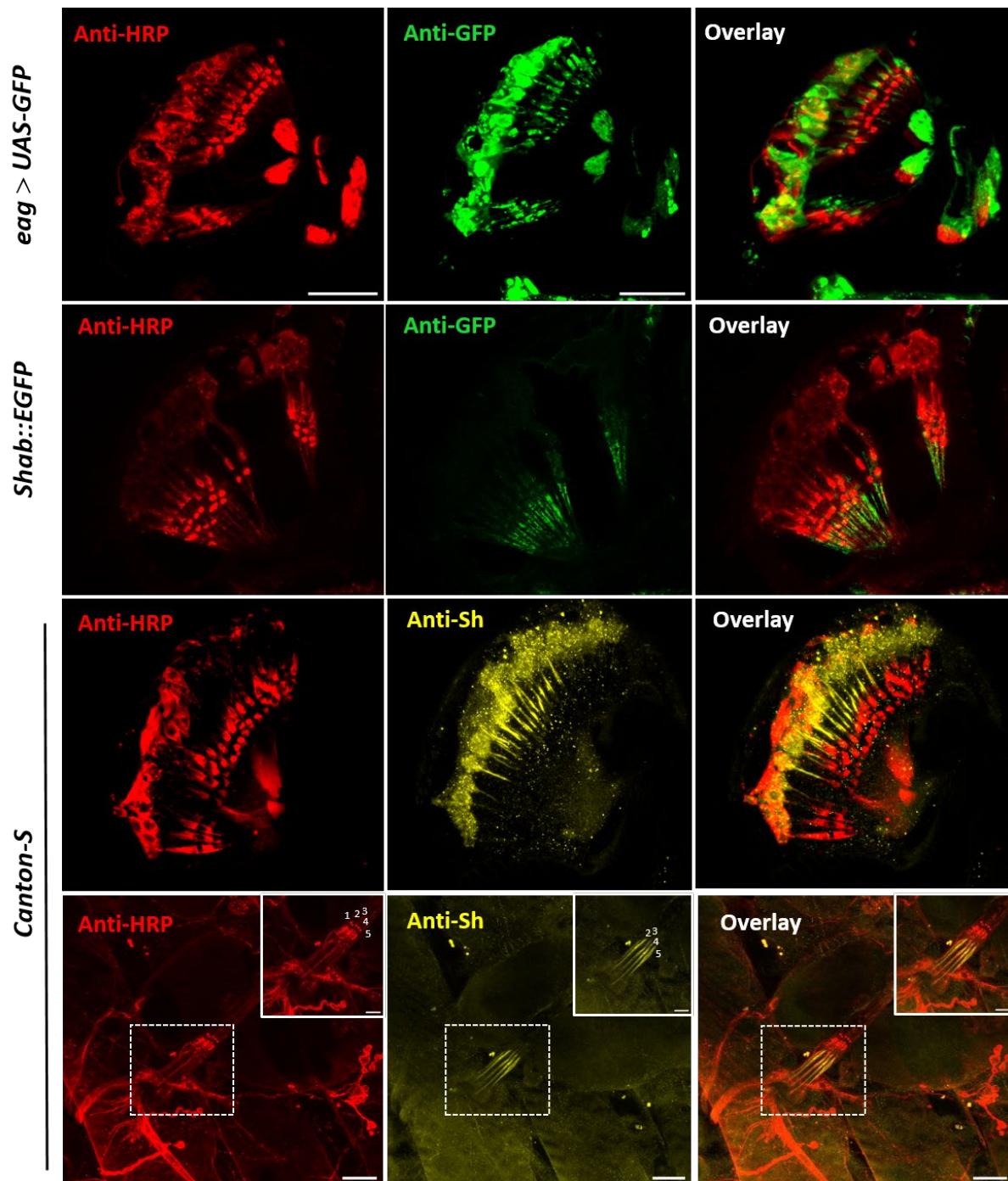


Fig. 39 Voltage-activated potassium channels expression in JO. Three Kv channels were studied to illustrate the expression in JO. The expression of *either-a go go (eag)* was performed by using Gal4/UAS system. *Shab* protein was localized by using *shab*-fused EGFP transgenic strain. *Shaker* channel were stained with *anti-Shaker* primary antibody in *Canton-S* background flies. Furthermore, the lch5 organ in 3rd larva stage were stained with anti-Shaker primary antibody to show the selective expression. Green: GFP signal. Red: HRP signal. Yellow: *Shaker* protein. Scale bar is 20 μ m.

1.3.3.3.2 Voltage-gated potassium channels in fly's hearing

The effect of various homologous potassium channels on fly's hearing at iBF has been discussed in Chapter 2, I concluded that the amplification gain was severely impaired in the absence of *Shab* (Kv2), which is encoded a delayed rectifier K⁺ channels and belongs to a member of *Shaker* channel family.

In electrical tuning, besides the Cav and BK channels involvement in turtle, other Kv channels have been established that they also participate in the tuning modulation, such as a delayed rectifier channel Kv3.1 in chick and A-type currents Kv in turtle, which are particular defined at low frequency oscillation (< 100 Hz) (Oberholtzer JC *et al.*, 1997; Oberholtzer JC *et al.*, 1995). In fly, a delayed rectifier channel Kv is encoded by *Shab* gene, and *Sh* channel can produce an A type current for electrical regulation, therefore *Shab* and *Sh* both are investigated with sequential frequencies stimuli. To access the specificity of Kv, *eag*, as another typical *eag* family channel, was also measured and discussed.

To eliminate the effects from other non-related genes, the progenies that carry either *Sh¹³³/Df(1)BSC⁴⁰⁵* or *Shab³/Df(3L)BSC⁴²⁸* were collected for measurement. The deleted *eag* locus strain by P element insertion was labelled as *eag^{Δfull}*. With the loss of these channels, only *Shab³/Df(3L)BSC⁴²⁸* showed a significantly reduced power ($261 \pm 156 \text{ nm}^2/\text{Hz}$) and shifted iBF to higher frequency ($395 \pm 60 \text{ Hz}$) comparing to control groups (Fig. 40 A and Fig. 53) in free fluctuation measurement. *Sh¹³³/Df(1)BSC⁴⁰⁵* and *eag^{Δfull}* mutants displayed a reduced fluctuation power, but no shift of iBF was observed (Fig. 40 A and Fig. 53). At iBF, sound-evoked amplification sensitivity gain was completely abolished in *Sh¹³³/Df(1)BSC⁴⁰⁵* (1.8 ± 0.3) and partly impaired in *Sh¹³³/Df(1)BSC⁴⁰⁵* and *eag^{Δfull}* mutants (3.2 ± 0.4 and 4.2 ± 0.5 respectively). With sequential frequencies stimuli, the arista displacement amplitude of *Shab³/Df* was linear to the magnitude of SPV in all stimulated frequencies, whereas the sensitivity gain of *Sh¹³³/Df(1)BSC⁴⁰⁵* and *eag^Δ* strains was gradually lost with the increasing of frequencies and the sound receiver became passive system at frequencies >450 Hz (Fig. 40 B). For mechanical response, the sensitivity gain at iso-intensities was plotted against frequencies and applied to SHM model. It was clear that the shift of iBF at iso-intensities was restricted in a small range at high frequency portion from 661 Hz to 768 Hz along with a fine rise of Q factor from 0.88 to 1.17 in *Shab³/Df(3L)BSC⁴²⁸* mutant. However, the change of iBF in *Sh¹³³/Df(1)BSC⁴⁰⁵* and *eag^{Δfull}* mutants were much higher than in *Shab³/Df(3L)BSC⁴²⁸*, individually ranging from 343 Hz to 820 Hz and from 290 Hz to 688 Hz with a similar variable Q factor from ca. 0.8 to ca. 1.2.

It was no exception that the phenotype of CAP response with sequential frequency stimuli in *Sh¹³³/Df(1)BSC⁴⁰⁵*, *Shab³/Df(3L)BSC⁴²⁸*, and *eag^{Δfull}* mutants was similar with control flies: (1) the maximum CAP amplitude at iBF did not differ from control flies (Fig. 40); (2) the maximum CAP amplitude gradually decreased with the rise of frequency within the tested acoustic SPV range; (3) the normalized CAP amplitudes at iso-intensities were superimposed together and displayed a V-shaped trend with a peak at ca. 250 Hz in all three mutants (Fig. 40 D). The CAP response at iso-displacement was different in the absence of *Sh* channel. At frequency < 200 Hz, the maximum CAP amplitude did not significant decrease in *Sh* null allele, but maintain slightly fluctuation around the CAP amplitude at iBF. After normalizing CAP amplitudes at iso-displacement, the different CAP versus frequency curves were superimposed together and the slightly decrease trend occurred to ca. 0.9 at frequency < 200 Hz

comparing to the sharply reduction in WT flies, as well as the *Shab³/Df(3L)BSC⁴²⁸* and *eag^{Δfull}* mutants (Fig. 40 D), determining that the

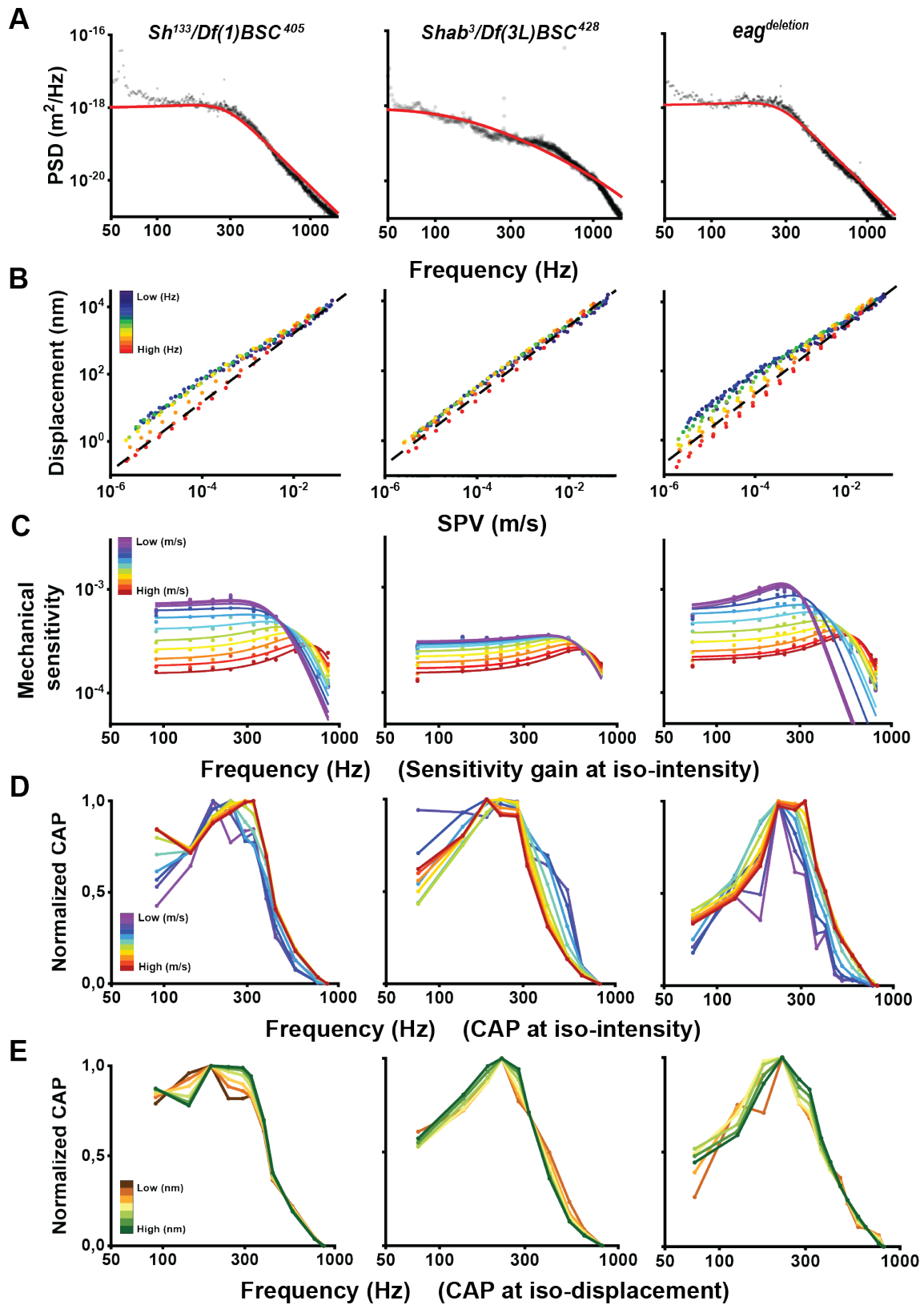


Fig. 40 Auditory performance in *Sh*, *Shab* and *eag* mutants at different frequencies. (A) Free fluctuation measurement from three mutated Kv channels strains *Shaker¹³³*, *Shab³*, and *eag^{Δfull}*. For *Sh* and *Shab*, the null alleles were crossed to

respective deficiency strain (*Df*) to eliminate the effect of genetic background. Black dots: PSD amplitude at each oscillating frequency. Red line: simple harmonic oscillation model fitting. (B) The arista displacement versus SPV at each frequency. Black dash line: linear system. (C) The mechanical sensitivity versus frequencies at iso-intensities. The gradient intensities were shown in gradient color and fitted with simple harmonic oscillation model. (D) and (E) The normalization of CAP amplitude at iso-intensities and iso-displacement. Data is from one representative animal of three to five examined flies (N= 3-5 per strain).

frequency that is lower than 100 Hz cannot be discriminated according to the difference of CAP amplitude in *Sh* channel null mutant. Taken together, the Kv channels in fly's ear, *Sh* channel particularly contributes to the CAP response at low frequency (<100 Hz), not the other Kv channels.

1.3.3.4 Other related genes (*Irk1*, *piezo*, *prestin*) in fly's hearing

Besides the Cav, BK, and Kv channels that modulate the electrical tuning, some other genes in vertebrate cochlea have been reported that contribute to the frequency discrimination, such as inward rectifier (Kir) channels, *prestin*, and *piezo*.

1.3.3.4.1 *Irk1*, *piezo*, *prestin* expression in JO

According to the frequency range of electrical resonance, the Cav/BK paired channels modulation is dominant when frequency is higher than 100 Hz. However, when frequency is lower than 100 Hz, Kir channels have also been tested to participate in the tuning regulation in chick. In *Drosophila* genome, three paralogs for human Kir have been found, named *Irk1*, *Irk2*, and *Irk3*, and these three channels express both in brain and JO (Fig. 41). Because of unviability of proper null alleles for *Irk2* and *Irk3* channels, only *Irk1* channel was measured and analysed. From Fig. 41, it shows that *Irk1* channel presents only in sub population of JO neurons.

Prestin, as a motor protein, is indispensable for frequency range extension across vertebrate species (R Fettiplace, 2020). Furthermore, *prestin* protein both exists in sensory neurons of mammalian cochlea (TD Weddell, 2011) and fly's ear (Fig. 41), but the effect of *prestin* in hearing is opposite. The absence or dysfunction of *prestin* leads to abolishment of auditory cochlea amplification in OHC, but not mechanical amplification in *Drosophila* JO (DF. Eberl, 2015).

Piezo is a mechanically gated cation channel that is essential in diverse mechanical stimulated electrophysiological properties. Wei Zhang demonstrated that *piezo* is selectively present in subset of 5 Lch5 neurons and is required for *Drosophila* larva to recognize high frequency sound. To access the effect of *piezo* channel in adult fly's ear, the expression of *piezo* channel in JO was addressed firstly. In contrast to the expression of *piezo* in lch5 neuron of larva stage, it is non-selective present in all JO neurons (Fig. 41).

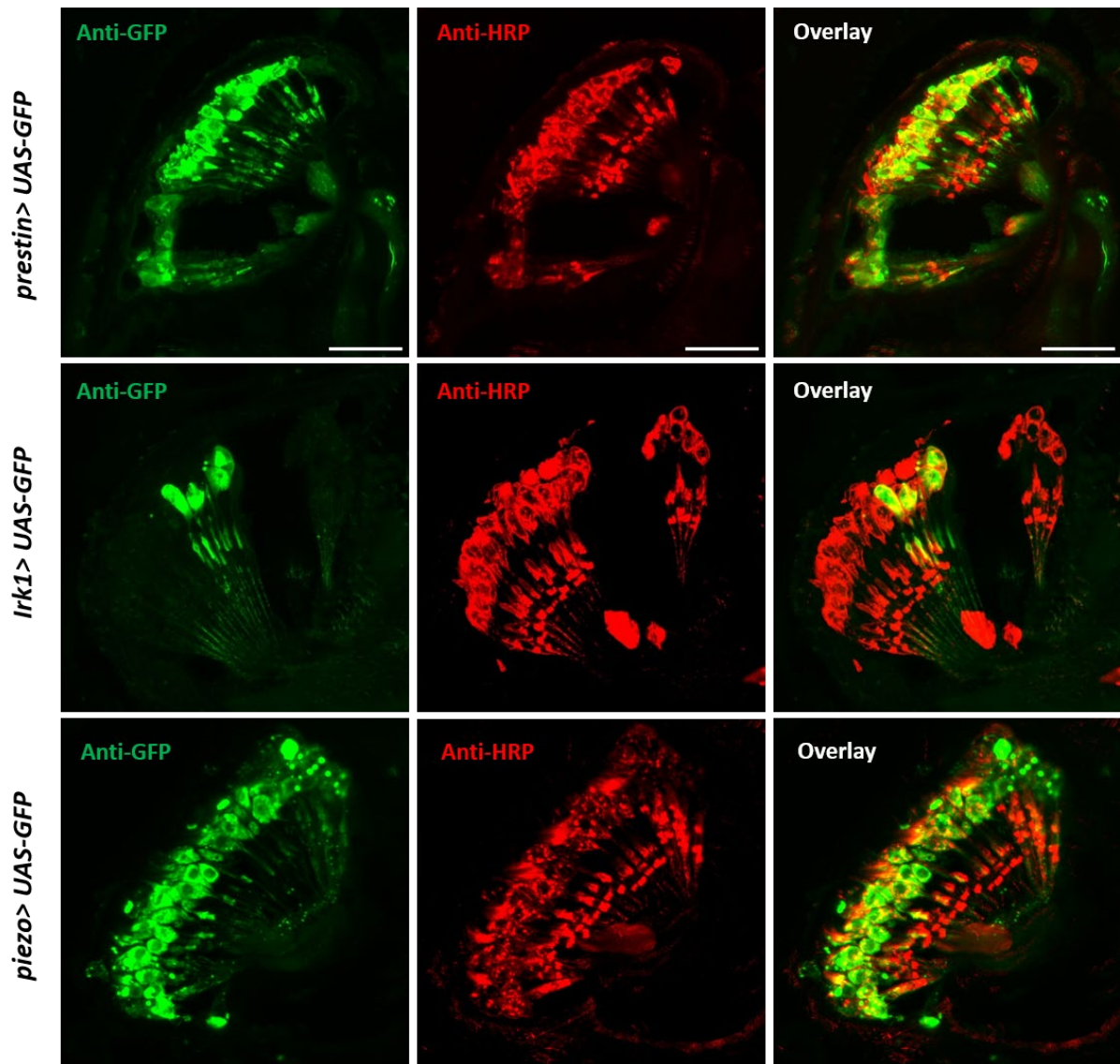


Fig. 41 *Irk1*, *prestin*, and *piezo* are expressed in JO. The respective Gal4 enhancer lines of *Irk1*, *prestin*, and *piezo* were crossed to UAS-GFP for establishment of expression in JO. *Prestin* and *piezo* were expressed in all JO neurons, but *Irk1* only presents in a subset of JO neurons. Green: GFP signal to show the gene expression. Red: HRP signal to illustrate the structure of chordotonal neurons. Scale bar is 20 μ m.

1.3.3.4.2 *Irk1*, *piezo*, *prestin* effects in fly's hearing

To access the hearing properties of these three genes, three mutants were utilized for functional measurement, *Irk1*^{M108404}, *prestin*³³⁹, and *piezo*^{KO}. The *Irk1*^{M108404} allele contains a mimic cassette, which inserts into the coding intron region of *Irk1* gene locus (long transcript isoforms) and theoretically interrupts gene transcription. But it is still notable that the short transcripts isoforms of *Irk1* are not blocked, which may not completely block *Irk1* channel functions. The *piezo*^{KO} mutant is an amorphic allele with the deletion of all 31 coding exons, resulting in a null allele or knock out of *piezo*. As for *prestin*³³⁹, it was generated by ends-out targeting approach with homologous recombination. Two in-frame stop codons were inserted into a coding exon, leading to a misexpression of *prestin* gene products.

In free fluctuation measurement, the sound receiver of *prestin*³³⁹ allele behaved normally without any power loss or iBF shift comparing to control flies. However, free fluctuation in *IrkI*^{MI08404} and *piezo*^{KO} alleles were partly weakened with a decreased power to $423 \pm 96 \text{ m}^2/\text{Hz}$ (Fig. 42 A, Table 11). Pure tone stimulation at iBF, the mechanical amplification of *prestin*³³⁹ was not affected at all (Fig. 42 B). *IrkI*^{MI08404} and *piezo*^{KO} alleles on the other hand exhibited a drop in sensitivity gain to 5.3 ± 0.7 (Fig. 42 B). Subsequently, the non-linear mechanical amplification gradually became linear with the rise of tonal frequencies for all three mutants (Fig. 42 B) as control flies. The iBF of sensitivity gain at iso-intensities all shift 530 Hz (from 210 Hz), 429 Hz (from 320 Hz), and 540 Hz (from 370 Hz) to high frequency region for *prestin*³³⁹, *piezo*^{KO}, and *IrkI*^{MI08404} alleles respectively.

Without exception, none of the tested alleles for *prestin*, *piezo* or *IrkI* exhibited affected antennal nerve response at iBF. With series frequency stimulation, null allele of *prestin*³³⁹ revealed no change in the electric tuning at either iso-intensities or iso-displacement of sound receptor neurons, with a resonance frequency of 258 Hz, in congruence with an iBF of $275 \pm 35 \text{ Hz}$. As for *piezo*^{KO}, and *IrkI*^{MI08404} alleles in Fig. 42 D and E, on the right side of apex, a sharply reduction to zero occurred for iso-intensities and iso-displacement like control flies. But on the left side of apex, the CAP amplitude changed in gradient along with displacement magnitude. In detail, *piezo*^{KO} flies exhibited that the lower displacement amplitude arista vibrated, the CAP response did not change compared to the maximum CAP response at iBF when frequency is lower than 100 Hz. In *IrkI*^{MI08404} flies, the trend was reversed with higher displacement amplitudes that arista produced led to relatively lower CAP response.

To sum up, *prestin*, as a motor protein, functions to maintain normal hearing in vertebrate, but has no effect on fly's hearing. The phenotype of *IrkI*^{MI08404} was not completely abolished, reflecting that *IrkI*^{MI08404} may be not a proper null allele because the short transcripts of *IrkI* potentially participate in the hearing regulation. Furthermore, it is surprising that *piezo* channel showed modulatory function in frequency tuning at low frequency in adult flies, which is opposite to its regulation in larva. The deeper mechanisms and reasons for this difference need more studies in future.

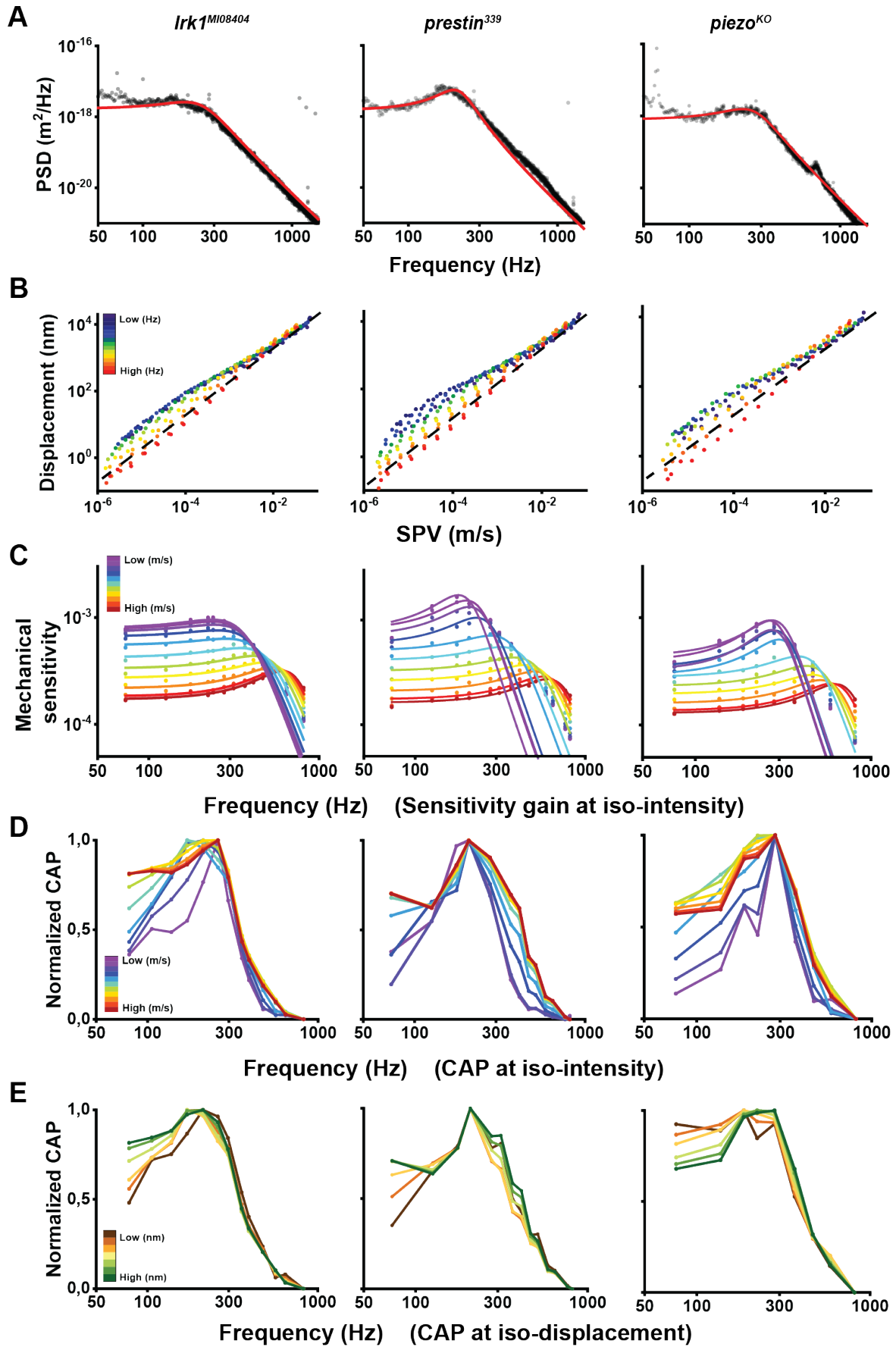


Fig. 42 Auditory performance in *Irk1*, *piezo*, and *prestin* mutants at different frequencies. (A) Free fluctuation measurement from three alleles, *prestin*³³⁹, *piezo*^{KO}, and *Irk1*^{M108404}. Black dots: PSD amplitude at each oscillating frequency. Red line: simple harmonic oscillation model fitting. (B) The mechanical response across frequencies. Black dash line: linear system. (C) The mechanical gain at iso-intensities versus frequencies curves. The gradient intensities were shown in gradient color and fitted with simple harmonic oscillation model. (D) and (E) The normalization of CAP amplitude at iso-intensities and iso-displacement. Data is from one representative animal of three examined flies (N=3).

1.3.4 Summary from genetic screen (Q factor and iBF)

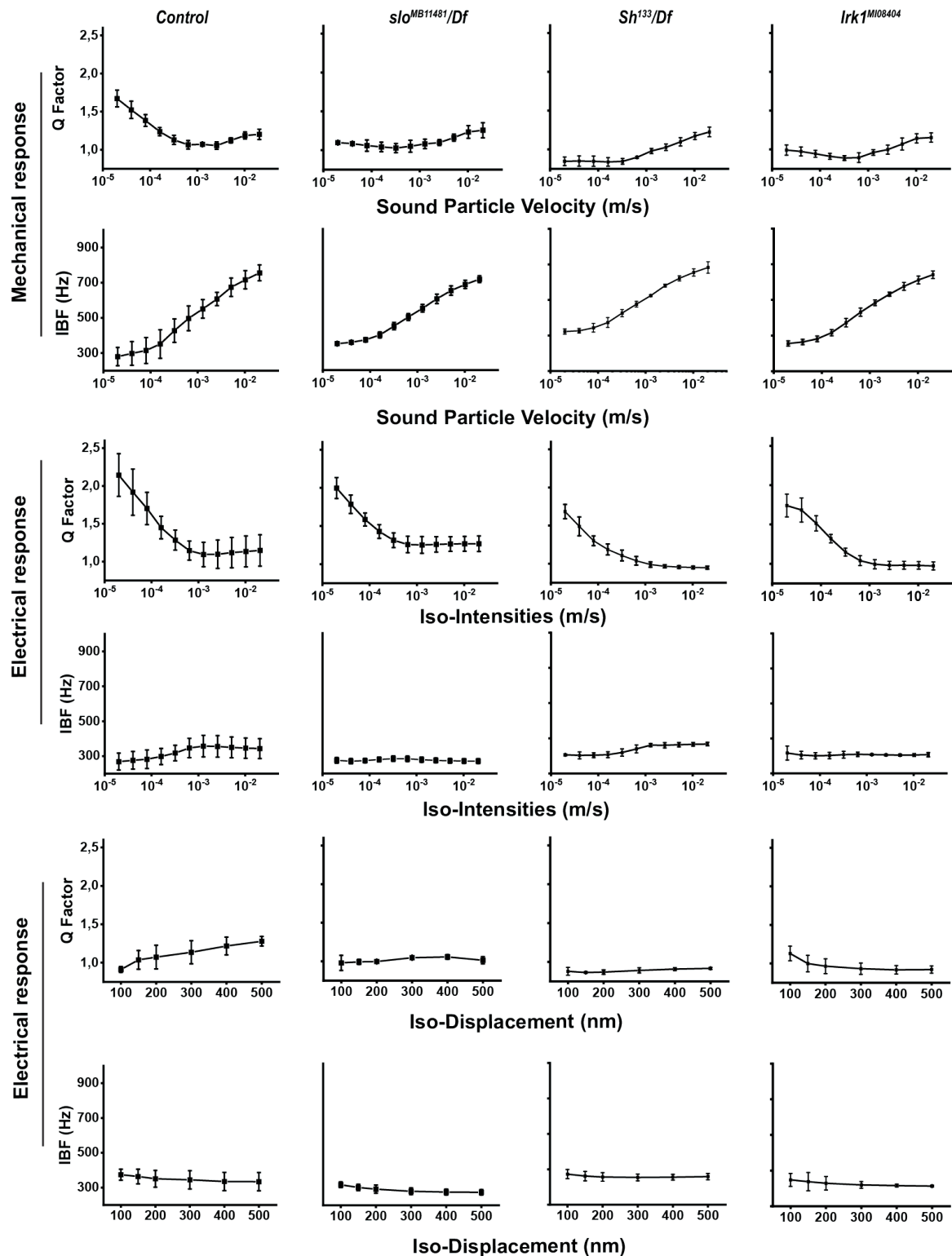


Fig. 43 Summary of factor Q factor and iBF for simple harmonic oscillation fitting. Data are shown as mean \pm 1SD (N=3-5).

According to the measurement of candidate genes from Fig. 22, it shows that only *slo* and *Shaker* channels contribute to electrical tuning when the frequency is lower than iBF. For mechanical response with series frequency stimulation, the Q factor is ranging from 1.61 ± 0.1 at lowest intensity to 1.1 ± 0.06 at highest intensity in control flies, whereas Q factor in *slo* channel mutant is ranging from 1.09 ± 0.01 to 1.25 ± 0.09 , and in *Sh* channel mutant is from 0.84 ± 0.05 to 1.22 ± 0.06 . But the change of iBF at iso-intensity is similar among these mutants. As for the electrical response, the difference is at iso-displacement. Q factor is increased from 0.9 ± 0.01 at 100 nm to 1.2 ± 0.06 at 500 nm, whereas both *slo* and *Sh* channels have *Shab*³/*Df(3L)BSC*⁴²⁸ fine change between 0.87 to 1.01 over displacement range (Fig. 43).

1.3.5 Alternative splicing in electrical tuning modulation

Up to here, I have tested the mechanical and electrical responses of different channels with series frequencies stimulation in fly's ear according to Fig. 22. Except for the influence of different channels, the other factor that modulates the electrical tuning is the ion channel kinetic properties, which is hypothetically modulated either by intracellular modulators or variation of distinct isoforms of ion channels (R. Fettiplace, 1999). BK channel, as the core component for electrical tuning modulation, is a good and well-established example in turtle cochlea (R. Fettiplace 1996). Five BK channel isoforms have been identified with particular localization within hair cells that contribute to frequency filtering, sharpen the tuning, and constitute a tonotopical map from 40 to 600 Hz. Meanwhile, other species in which electrical tuning occurs with similar mechanism, such as chick, have also been tested (Fuchs *et al.*, 1988; Fettiplace, 2020).

In fruit fly, *slowpoke* channel, as a BK channel family member, contains 7 transmembrane domains and 23 distinct isoforms that have been discovered till now. Although alternative splicing of *slo* channel happens in fly, whether this phenomenon occurs in JO is not addressed yet. To access this purpose, I carried out a RACE-PCR to determine whether the dominant isoform presents in JO or whether the phenotype of *slo* null allele results from the various isoforms. In contrast with the conventional one step 5'- RACE or 3'- RACE PCR to obtain full length cDNA sequence, I designed isoform specific primer pairs in middle of cDNA and used both 5'- RACE and 3'- RACE PCR to get amplified PCR product, then combined these two segments for full length cDNA sequence analysis.

From 5'- RACE and 3'- RACE products, five random colonies were picked up for final sequencing. As shown in Fig. 44, the combined sequences showed a unique arrangement from all five PCR products which was different from all annotated *slo* channel isoforms. It is no doubt that new isoforms are present in JO and the variation of *slo* channel presumably leads to differentiate of diverse frequency components. Importantly, it is also notable that the practical impossibility to address the

kinetic properties from signal JO neuron because of technical limitations restricts further clarification which *slo* isoform is dominant and their respective modulate mechanism (Schwarz *et al.*, 1988; Lagrutta *et al.*, 1994; Jones *et al.*, 1999).

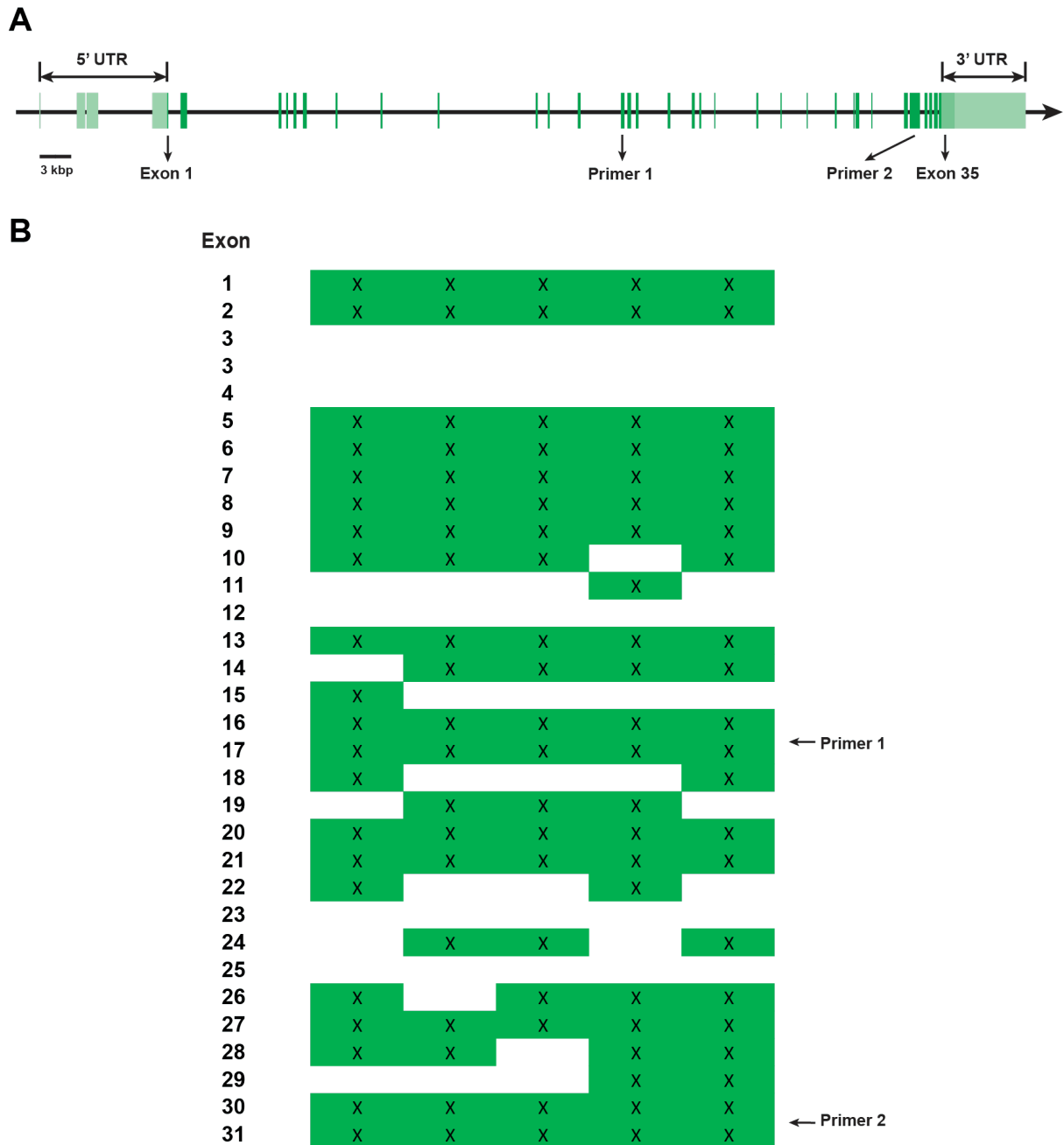


Fig. 44 Alternative splicing of *slowpoke* gene in JO. (A) The intron-exon structure of *slowpoke* gene. (B) The arrangement of *slo* transcripts from amplified RACE PCR products.

1.4 Discussion

As outlined in Fig. 22, I have tested different genes, which are identified and involved in the electrical frequency discrimination in vertebrate cochlea, to determine their participant and functional contribution in *Drosophila* frequency tuning in respect of mechanical and electrical response in this chapter. Summing up, some genes, like *slo* and *Sh*, which are present in particular subset of JO neurons potentially contribute to the electrical tuning of auditory JO neurons, especially at low frequencies, but not genes that non-selectively express in all JO neurons, like *Cav*, *eag*, and *prestin*.

1.4.1 Damped simple harmonic oscillation

The fly's sound receiver behaves like a SHO in the absence of sound and can be regarded as a resonator with sound stimuli, and applied to SHO model. In the vertebrate cochlea, two resonance behaviors, mechanically and electrically, are shown to be capable for frequency discrimination based on the partition of the frequency range. Electrical tuning with a damped electrical current is dominant when frequency is lower than 1 kHz. The damped resonance frequency relies on the density of paired Cav/BK channels that filter in hair cells.

In *Drosophila*, in regard to the mechanical response, the antennal receiver resonantly behaves like a moderately SHO within the wide range intensities stimulation, owing to the non-linear stiffness. As shown in control flies, the iBF at iso-intensity continuously rises with the increasing intensity additionally along with the decrease of corresponding sensitivity gain, whereas the sharpness of fitting curves at iBF is mildly affected. In contrast to flies with ablated AB or B JO neurons which exhibit no obvious iBF shift, it determines that the fly's ear mechanically responds to external sound at low frequency range and low intensities, and mechanical amplification gradually decreases with increasing frequencies or intensities.

As for electrical resonance, the current generated from the cochlear hair cells in chick or turtle is damped oscillating and this damped current behavior can tune the frequency up to 800 Hz in chick and 600 Hz in turtle respectively. In contrast with the evaluation of electrical current from single cochlear hair cell, the electrical response is recorded by monitoring the antennal extracellular nerve response (antennal CAP response) in flies. Furthermore, the tested frequency was defined up to ca. 800 Hz owing to the un-detectable CAP amplitude at higher frequencies in lab. An inverted V-shaped of CAP amplitude across frequencies at iso-displacements illustrates an electrical resonance behavior generating from JO neurons, and the CAP reaches relative maximum between 200 and 300 Hz, where the range of frequency is tuned in natural condition. At frequency range from 300 to 800 Hz, a shape drop of the CAP response observed in control, ablated class B neurons, and ablated class D neurons, but a shift to lower frequency in ablated AB neurons, tested that the different sub-population of auditory neurons exhibit different electrically tuned frequency, and this difference stems from a cell inherent

properties of JO neurons, which is agreement with the previous finding that the different subgroups of JO neurons shows frequency preference (E Matsuo *et al.*, 2014).

1.4.2 Frequency discrimination: from cells to genes

A cell-based inherent mechanism has shown that frequency preference does occur in JO by recording the calcium imaging in AMMC area: class A neurons modulate a wide range frequency from 100 Hz to 800 Hz, or even higher up to 1 kHz; class B neurons preferentially modulate the frequencies below 100 Hz; class D neurons mainly modulate middle frequency range (200 to 400 Hz) (Matsuo *et al.*, 2014). However, the frequency range associated with different JO neuron populations is not a precise classification. These sorted JO neurons synergistically sense frequencies, leading to an overlap occurrence but with different dominant frequency range. Except calcium imaging, recording the antennal CAP by using cell specific ablation assay provides an alternative way to address the different JO neurons' functions. In the absence of AB neurons, the generation of absolute CAP is severely impaired across all frequency range, but it is still detectable, and a remarkable rising CAP amplitude was observed when frequency was lower than 150 Hz. Class B neurons not only contribute to the low frequency (< 100 Hz), but also the middle frequency from 100 to 200 Hz comparing to no effects in the ablated class CE or class D strains from frequency spectrum. It is notable that cell-specific ablation assay can eliminate most of the respective neurons (A Kamikouchi *et al.*, 2006), but it is possible that some remaining neurons may contribute to the modulation. Except the modulation on the cellular level, participation of some channels or encoded proteins on frequency tuning within JO neurons is reasonable.

Comparing with the mechanical tuning that is endowed in the cochlea at frequency > 1 kHz and in which the mechanism is still under debate, electrical tuning, as the dominant mechanism at frequency < 1 kHz in non-mammals, involves multiple-types voltage gated channels, including Cav/BK channels as core component that regulates wide range frequency, and other Kir and Kv channels that assist at low frequency (< 100 Hz). In *Drosophila*, frequencies are decomposed in both Ich5 organ and JO. *piezo* channels seem implicated in high frequency tuning in Ich5 of larva (Zhang *et al.*, 2021). To address which channel modulates the frequency tuning in JO, I selected candidates with known involvement electric tuning in vertebrates, namely Cav, BK, Kir, and Kv channels, to investigate whether these homologous channels are also involved in the electrical tuning in adult fly. Of the tested candidates, only *slo* and *Sh* channels contribute to electrical tuning at frequencies below 150 Hz. Without *slo* and *Sh* channels, a relative higher CAP amplitude was acquired at that range.

Considering no observed differences in tested Cav (*Ca-a 1D*, *Ca-a 1T*, and *Ca-beta*), *Irkl*, *Shab*, and *eag* mutants, it may hypothetically say that either some unknown Cav channels or multiple channels modulate the Ca²⁺ influx to active the nearby *slo* channel in JO. Nevertheless, for electrical tuning, *Sh* channel is required, not other delayed rectifier *Shab* or *eag* channels. Meanwhile, there are also many

questions, such as how the different channels work together to promote electrical tuning remains to be addressed.

1.4.3 Gene-specific patterns of expression in JO

The JO neurons can be sorted into two groups according to the functions: sound-sensitive (class A/B/D) and wind/gravity sensitive (class C/E/D) neurons. With respect to these two distinct functions and their corresponding JO neurons, identification of genes or proteins particular in either sound or wind/gravity neurons attracts more attention. In regard to the fly's hearing, many genes have been identified to influence hearing.

For instance, *ato* is indispensable for the structural formation of JO. *NompA* is located in dendritic cap acts as a bridge to connect the sensory neurons and a2/a3-joint. Additionally, three TRP cation channels, *NompC*, *iav*, and *Nan*, implicate in the mechano-electrical transduction in chordotonal neurons with distinctive spatial location where *NompC* localizes at the apex of distal cilia, and *Nan* and *iav* co-localize at the proximal cilia as a heteromeric channel, and work synergistic. Two identical features from these genes: (1) loss of them leads to the deafness of fly hearing; (2) they all non-selectively express in all JO neurons. Because of the occurrence of frequency tuning in class A/B/D neurons, finding out genes that are expressed in such subgroups and contribute to the electrical tuning is reasonable.

From the tested candidate genes for electrical tuning measurement, the electrical tuning in JO is not related to the genes that are non-selectively expressed in all JO neurons, such as *Cav* channels, *Shaker*, and *eag* channels, but the genes that are present in subset of auditory JO neurons, like *slo* and *Sh* channels. Although *Irkl* channel is present in sub-population of JO neurons, the inappropriate tested mutant is an uncertain factor that may leads to unconvincing results.

1.4.4 Diversification of channel gating kinetic

Electrical tuning originates from a delayed activation of Kv channels, causing a damped electrical oscillation because of the negative feedback regulation in cochlea (R. Fettpiac, 1999). The rate of frequency oscillations depends on not only the density of BK channels, but also the various gating kinetic of channels. There are several factors that contribute to the diversification of channels, such as diverse genes, homomeric or heteromeric channels, and variation of alternative splicing, etc.

As the core component in electrical tuning, the different species of BK channels with distinct gating kinetic that cover most of frequency range are identified in turtle and chick (R. Fettpiac, 1999). Meanwhile, the different variants with respective gating kinetic of *slo* channel also present in *Drosophila*. The variation of *slo* isoforms in JO may lead to the diverse expression (Fig. 45). Not only *slo* channel, but also the alternative splicing of *Sh* channel leads to multiple K⁺ channel components. In

fly, electrical tuning occurs and both *slo* and *Sh* make contribution at low frequency. As for the variation of gating kinetic, except *slo* channel, the variation resulting from *Sh* channel is equal to be considered.

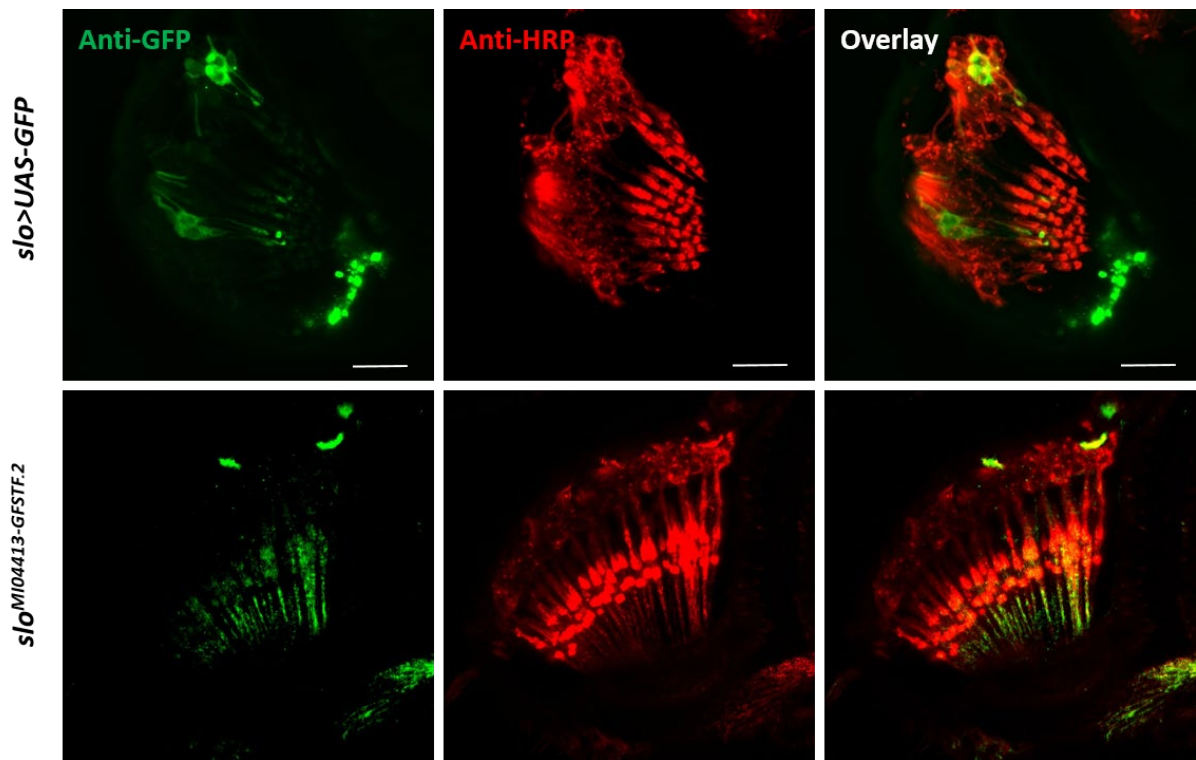


Fig. 45 Two types of strains for *slo* channel expression. Upper one: conventional Gal4 enhancer line. Below one: *slo* channel with a fused EGFP tag. Scale bar is 10 μ m.

Chapter 2.

Genetic screen of potassium channels in Johnston's Organ (JO)

2.1 Introduction

2.1.1 Background and genetic screen in *Drosophila*

Hearing, as one aspect of basic sensory modalities, plays an essential role to receive information from the environment and to maintain interspecies communication. Hearing impairment has been regarded as the most common sensory deficit, and the etiologies are diverse from environmental factors to genetic dysfunction, such as prolonged exposure with loud noise, viral infection in the ear, aging, or heredity, etc. Although hearing defects caused by some environmental factors can be prevented or avoided by early intervention, the etiologies originating from the disruption of hereditary information are raising challenges. Therefore, identification of potential pathogenic genes that contribute to hearing impairment in temporal and spatial heterogeneity, and searching for the pathogenic mechanisms and clinical therapies for these genes are important (A. Dror, 2010; Eyken, 2007).

Drosophila melanogaster, as a powerful model organism, has been used in genetic and biological research for decades. To identify the novel genes that may modulate fly hearing, performing a genetic screen only in the 2nd segment of the *Drosophila* antenna is a suitable approach. Previous lab colleagues, Senthilan (Senthilan *et al.*, 2012) and Natasha Zhang (unpublished data), have individually conducted genetic screens in JO using two different strategies, a whole-organ knockout method based on *atonal* deficit and cell-specific ablation method as shown in Fig. 46.

Atonal (*ato*), as a developmental protein, is crucial for the chordotonal lineage of JO. Flies carrying the null *ato* allele, *ato*¹/*Df*(3R)*p*¹³, fail to form JO. Taking advantage of this whole-organ ablation, genes explicitly expressed in JO can be screened and delineated by comparing with control groups (Fig. 46 A). From this screen, not only 274 *Drosophila* auditory organ genes have been found, but also more than 21 genes showed impaired effects on fly hearing (Senthilan *et al.*, 2012). In a cell-specific ablation assay, Natasha Zhang introduced a targeted method to ablate specific sub-population of JO neurons using the Gal4/UAS system. The Gal4 enhancer lines containing specific JO neurons promoters (AB, CE, or all JO neurons) are crossed to a UAS-ricin line to drive the expression of the toxic ricin in particular chordotonal neurons to ablate neurons, then, the remaining neurons or cells can be isolated and subjected to the downstream genetic screen and data analysis (Fig. 46 B).

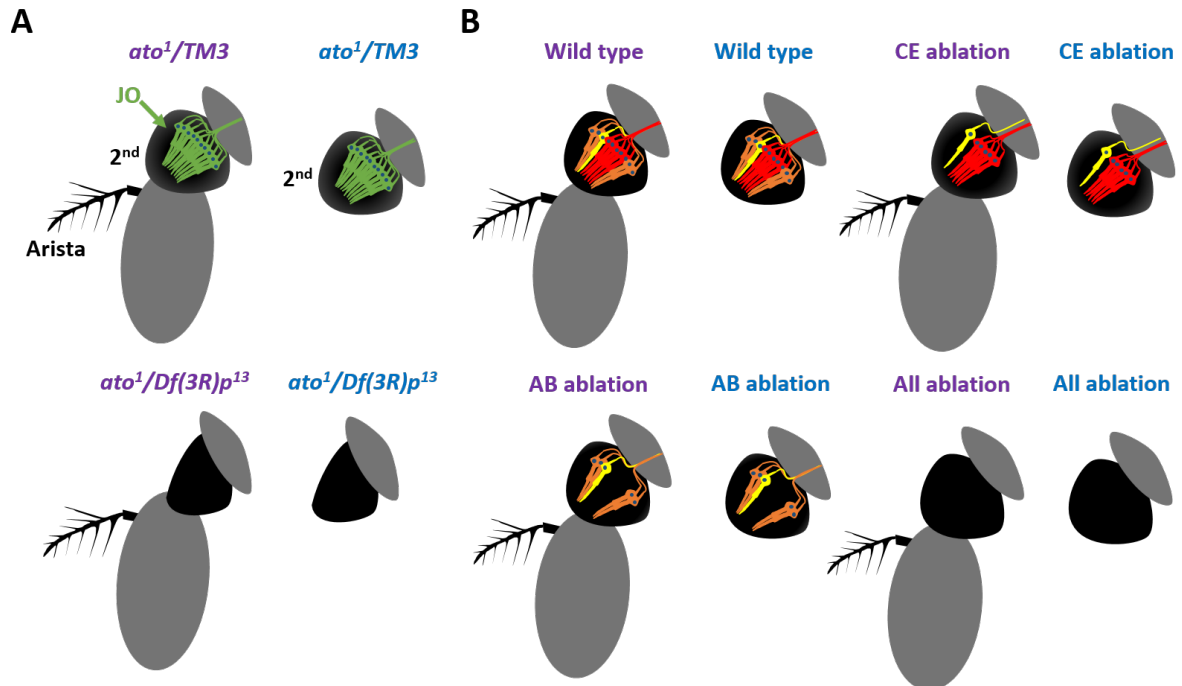


Fig. 46 Diagram of two strategies for genetic screen in JO. (A). Whole-organ knockout methods: up left shows the control with normal JO and bottom left shows *ato* null mutants with loss of JO (color in purple). RNA was extracted from 2nd segment antenna from control and null allele mutants, then subjected to downstream genetic screen (upright and bottom right, color in blue). (B). Cell-specific ablation methods: the whole antenna (color in purple) shows normal morphology of JO after chordotonal neurons ablation, but different functional cluster of sensory neurons for downstream genetic screening (AB neurons color in red; B neurons color in yellow; CE neurons color in orange). RNA extraction was performed as same as in (A) and total RNA was subjected to downstream RNA sequencing (color in blue).

My work in this section started from the subsequent data analysis of genetic screen from Natasha Zhang (Table. 10), to further characterize these genes and determine whether they affect the JO functions and the mechanisms. Firstly, I assessed the expression pattern of these candidates in JO utilizing fluorescent report assay and antibody staining. From the JO staining results, the expression of these genes can be sorted into three groups: (1) no expression in JO neurons (*wtrw*); (2) expression in all JO neurons (*Rdl*, *CG15270*, *eag*); (3) expression in a subset of JO neurons (*slowpoke*, *Shaker*, *nAcha5*) (Fig. 47). Furthermore, taking into account the limitation of availability of proper null mutants and manipulation, I narrow down the candidate genes and mainly focus on the genes of potassium channels (*slowpoke*, *Shaker*, and *eag*).

Table 9. Candidate genes from cell-specific ablation genetic screen

Candidate genes	Expression In JO
<i>slowpoke (slo)</i>	+/-
<i>shaker (sh)</i>	+
<i>ether a go-go (eag)</i>	+
<i>nAChRα5</i>	+/-
<i>resistant to dieldrin (rdl)</i>	+
<i>water witch (wtrw)</i>	-
<i>CG15270</i>	+
<i>CG1090</i>	?
<i>Ionotropic receptor 60a (Ir60a)</i>	?

(+/-: expression in subset of JO neurons; +: expression in all JO neurons; -: no expression in JO neurons; ?: not decided)

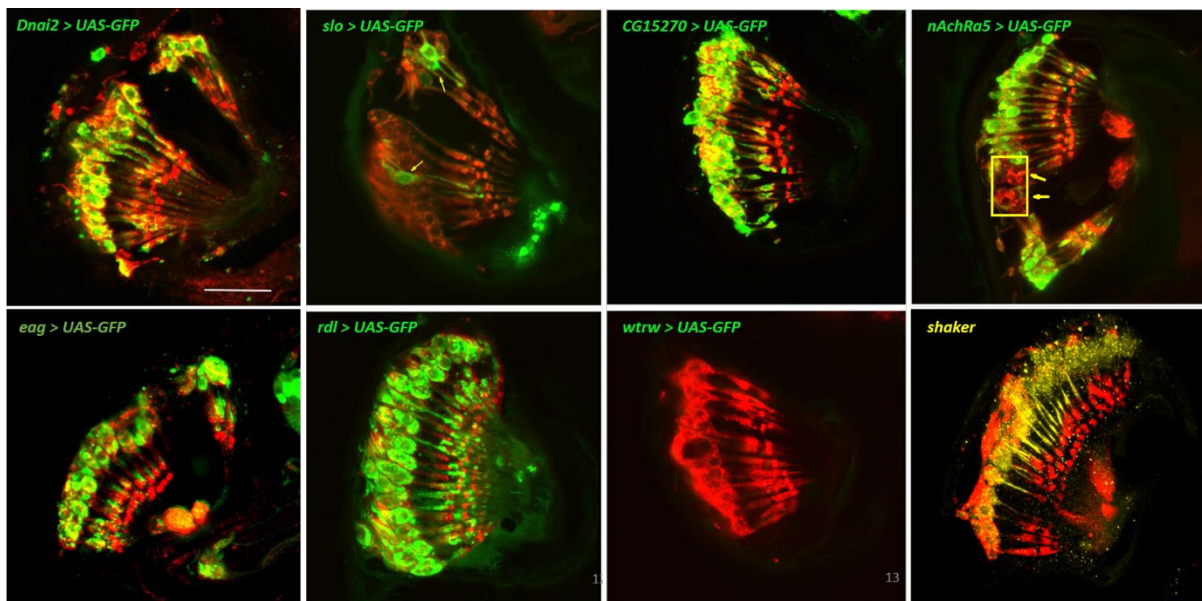


Fig. 47 Expression of candidate genes in JO. Adult 2nd antennal segment was subjected to immunohistological staining (details shown in method section). All images are shown in overlap with HRP and GFP signals. Neurons were stained with HRR (color in red) and expression of candidate genes were labelled with GFP (color in green). *Shaker* channels were stained with anti-Sh antibody in *Canton-S* background (color in yellow). Arrowheads indicate un-stained neurons. Scare bar is 20 μ m.

2.1.2 Potassium channels: diversity, classification, and physiology

The physiological process that all biological organisms perceive environmental (physical or chemical) stimuli and generate biological responses depends on the ability of specialized cells to receive, process, and transmit signals through specific mechanisms. The rapid signal conversion in the cell membrane is modulated by ion channels, which allow particular ions to flow through the ion-impermeable membrane as a result of the electrical potential difference between the intra- and extra-cellular membranes. Based

on the species of ions passing through the membrane, the ion channels can be classified into chloride channels, sodium channels, potassium channels, calcium channels, proton channels, and non-selective cation channels. Alternative categories from other aspects have also been described, such as the mechanisms of gating, number of pores or transmembrane domains, and localization of the protein.

As a comparison, potassium (K^+) channels are not only the biggest, most diverse group, but also the most broadly distributed functional channels compared to other types of channels. Subtypes of K^+ channels can be classified based on the number of transmembrane (TM) domains from K^+ channel monomer (Fig. 48). Subgroups of 2TM, 4TM, 6TM, 7TM, and 8TM (first found in yeast) have been identified, moreover more subsets for each subgroup have been founded according to their different electrophysiological properties or stimulus to activate K^+ channels (C. Tian *et al.*, 2014; Maljevic, 2013; Gonzalez, 2012).

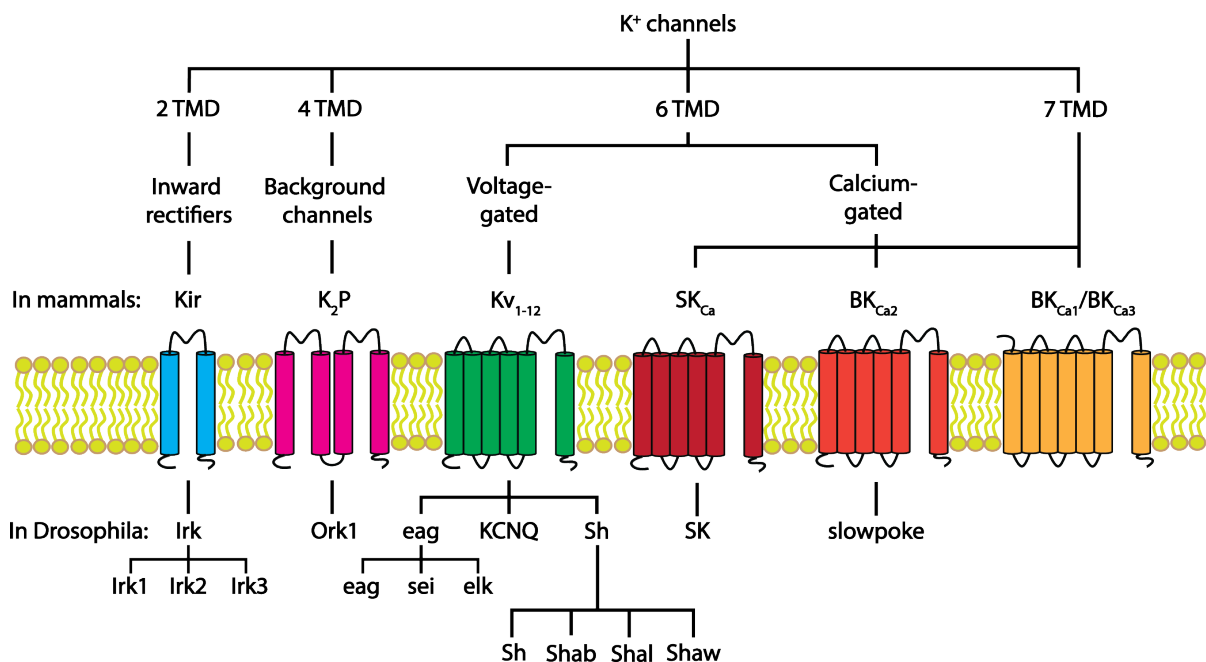


Fig. 48 Classification of K^+ channels monomer by transmembrane domain. The monomer K^+ channels can be fundamentally classified into five subgroups according to the number of transmembrane domains: 2TM, 4TM, 6TM, 7TM, and 8TM (only found in yeast). In mammals, all 2TM, 4TM, 6TM and 7TM are discovered with more subsets respectively. The homologous genes of these K^+ channels are also widely expressed in *Drosophila*.

The physiological functions of K^+ channels that particularly conduct potassium ions across the membrane, so-called electrochemical gradient, are based on two main features: one is rapid and selective to reduce needed channels and avoid depletion of the ionic gradient. The other one is the alteration of conductance as a result of stimuli, to maintain cellular homeostasis. Malfunctions of K^+ channels manifest various pathological symptoms and illnesses, ranging from the cardiovascular system, like cardiac arrhythmia, to neurological diseases, such as epilepsy and deafness. To prevent and avoid occurrence of K^+ channels-caused diseases, it is better to understand and deeply clarify where the

K^+ channels contribute to cells and the mechanisms of how these channels regulate the electrophysiological activities.

2.1.3 Potassium channels: recirculation in cochlea

In the signalling transduction of nervous system, potassium (K^+) channels are critical components and participate in many cellular processes, such as repolarization of neuronal cells, neuronal action potential waveform, extracellular signalling between neurons (transmitter release), and axonal conduction. In the mechanistic study of K^+ channels in sensory organs, hearing perception is one good established example, which is regulated by multiple cell types and K^+ channels (Zdebik *et al.*, 2009).

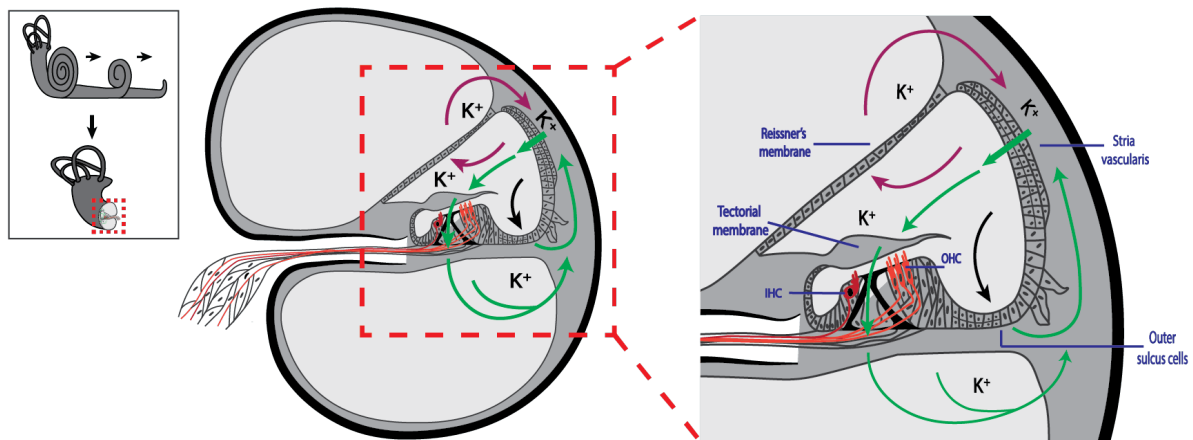


Fig. 49 Diagram of potassium ion recirculation in human coiled cochlea. Illustration of K^+ cycling model in human cochlea. In physiological state, the cochlea is a fluid-filled semicircular canal. The scala media contains high concentration of K^+ secreted from stria vascularis and maintains a high endocochlear potential (EP) which is important for the generation of auditory current (green pathway). The other two alternative K^+ recycling paths pass through either Reissner's membrane or accessory supporting cells to back to stria vascularis. Images are modified from (Zdebik, 2009).

In vertebrates, the ear detects sound waves and the conversion of signals from mechanical movement into electrical signals occurs in the cochlea. The formation of auditory electrical signals relies on the change of ionic gradients with a unique organization between the inside and outside of hair cells. In the sensory hair cells of cochlea, the process is modulated by the MET channels on the stereocilia, which allow the inflow of K^+ into sensory hair cells for the depolarizing current. In the absence of sound, a high K^+ concentration secreted by the stria vascularis is maintained in the scala media, as well as the surrounding the apical membrane and MET channels of hair cells, to keep a high positive endocochlear potential (EP), which is required for hearing sensitivity (Zdebik *et al.*, 2009; Szuts *et al.*, 2018). With the external sound input, the vibrations of basilar membrane caused by the fluid movement in cochlea lead to the bending of stereocilia on the tip of hair cells, which stretches the tip links between stereocilia to open transduction channels and allow the K^+ entry into hair cells. Afterward, this unique ionic modulation leads to a change of membrane potentials for the generation of electrical signals (Fig. 50).

K^+ can influx into hair cells through MET channels and efflux at the basal side of hair cells mediated by multiple K^+ -conducting channels, including KCNQ, BK, or KCNJ channels (Beisel *et al.*, 2005; Cazals *et al.*, 2015; Xia *et al.*, 2020). To maintain K^+ homeostasis in the cochlea, three models are established to explain how the released K^+ from hair cells subsequently are recycled and removed to stria vascularis, K^+ cycling via open perilymph, via gap junctions, or K^+ buffering (Fig. 49). Apart from this K^+ recirculation pathway, there are two major K^+ recycling modulations. One is that K^+ in the scala media passes through Reissner's membrane into scala vestibule perilymphatic fluid, and then recycles to stria vascularis (Fig. 49 arrowhead color in purple), the other pathway is that K^+ accomplishes the recycling by transmission between supporting cells (Fig. 49 arrowhead color in black). These discoveries mentioned above clearly show the importance of K^+ channels in the regulation of hearing. However, it should be also aware that, although some assumptions and evidence in animal models have identified the concept for K^+ recycling in the cochlea, there are still alternative explanations and mechanisms to further be investigated and characterized.

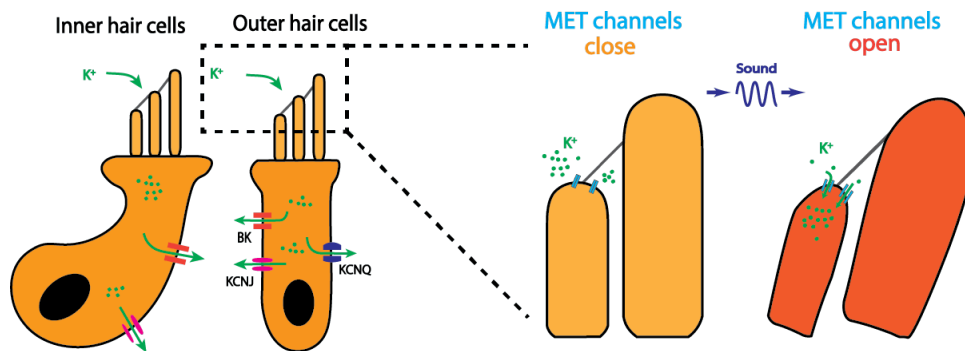


Fig. 50 Potassium channels in Outer and Inner hair cells. Two types of sensory hair cells are the core components that contribute to the conversion of signals from mechanical vibration to electrical nerve signals. The MET is located at the apex of stereocilium in hair cells. When the short stereocilium bends to long stereocilium with stimulation, the stretched membrane can open the MET to allow the K^+ influx into hair cells, leading to the ion gradient composition and generating the current (right image). Other K^+ channels located at the base of hair cells will recycle K^+ ion back to the semicircular canal and maintain ionic homeostasis.

2.1.4 Potassium channels: diversity and functions in *Drosophila*

Drosophila melanogaster has been studied as a model organism over decades to extend our knowledge and understanding in biological research, including the big breakthrough in the field of K^+ channels. Since the first K^+ channel gene, *Shaker*, was identified and cloned from *Drosophila*, the understanding is widely enriched not only in the diversity of different K^+ channels families, but also in the functional properties of homologous genes in different species ranging from *Drosophila* to mammals, as well as advancement in various research disciplines. For instance, benefiting from the discovery of *Shaker* channel (known as Kv1), other major Kv channels families have been subsequently identified by gene screening analysis in *Drosophila*, such as Kv2 (*Shab*), Kv3 (*Shaw*), Kv4 (*Shal*), Kv10 (*ether-a-go-go*), Kv11 (*sei*), Kv12 (*elk*), and K_{Cav} (*SK and slo*). Later on, their homologs were also found in mammals.

Other K⁺ channel family members, like Kv7, K_{2P}, or Kir channels were first identified in mammals. However, paralogs can be also found in *Drosophila* as well, like *KCNQ* (Kv7), *Ork1* (K_{2P}), and *Irk* (Kir) (Fig. 48) (Frolov *et al.*, 2012).

Functions of K⁺ channels seem to be evolutionarily conserved between species, because channelopathy found in human diseases is related to over 60 homologous genes of channels in the fly (Kass, 2005; Cavaliere & Hoage, 2011). The functions of K⁺ channels are diverse on the fly. For instance, *Shaker* and *Shab* channels are both involved in the generation of action potential, photoreceptor performance, and synaptic transmission (Ueda & Wu, 2006; Vahasoyrinki *et al.*, 2006). As for the other two *Shaker*-related family members, *Shaw* channel is related to the control of body mass and lethality, whereas *Shal* channel can modulate the repetitive firing and larvae locomotion (Ping *et al.*, 2011). In contrast with the rapid action and deactivation of the *Drosophila Shaker* channel, *KCNQ* channel can be slowly activated and deactivated, and is involved in the embryonic development and fly's heartbeat (Wen *et al.*, 2005). Moreover, unlike other K⁺ channels, *eag* not only can act as a partner subunit to other channels, but also has distinctive features with voltage and pH sensation because of its cyclic nucleotide C-terminus (Gutman *et al.* 2005). As for the calcium-activated K⁺ channels, loss of *slo* channel can cause neural and motor disorder, and loss of SK channel can lead to hypersensitive nociception behaviors in larva (DM Gertner, 2014; Atkinson *et al.*, 2000). To sum up, studies of K⁺ channel mutations in *Drosophila* are essential for advance for the understanding of human disorders and pathophysiology.

2.1.5 Aims: potassium channels in the *Drosophila* hearing organ

The knowledge of K⁺ channels in the vertebrate cochlea is well studied, but not in the *Drosophila*'s ear. In this chapter, I performed a K⁺ channel screen and mutant analysis of these channels to test the hearing perception in the *Drosophila* ear to address three main questions: (1) Which K⁺ channels are abundant and distributed in the *Drosophila* ear; (2) How are K⁺ channels expressed in neurons and their cellular localization; (3) Which K⁺ channels affect hearing perception and the potential mechanisms of modulation.

2.2 Results

2.2.1 Homologous genes of K⁺ channels in *Drosophila*

Considering the structural diversity, numerous functional K⁺ channels can be grouped into three structural families: (1) the inward rectifier (Kir) family, monomers encoded by 15 different genes contain two transmembrane (TM) domains that assemble one pore, and they form as tetramers in the physiological state; (2) the two-pore four TM domain K⁺ channels (K_{2P}) family (also called background channels). This family is encoded by 14 different genes in mammals and are assembled as dimers for

modulation; (3) the six TM domains K⁺ channels with one formed pore as the biggest subfamily, tetrameric is assembled to form a conserved ion-selectivity pore region to regulate the passage of ions. This 6TM domain families not only include functional channels, containing *Shaker* (Kv1), *Shab* (Kv2), *Shaw* (Kv3), *Shal* (Kv4), *KCNQ* (Kv7), *ether-a-go-go* (Kv10), *erg* or *sei* (Kv11), and *elk* (Kv12) subfamily (also known as voltage-gated K⁺ channels), but also non-functional channels, including Kv5, Kv6, Kv8, and Kv9. Besides these three categories, there are some K⁺ channels that particularly are activated by Ca²⁺ ion, and they are the small conductance (SK_{Ca}) Ca²⁺-activated K⁺ channels that belong to the 6TM domain family and the large conductance (BK_{Ca}) Ca²⁺-activated K⁺ channels. Unlike the other K⁺ channel, the BK_{Ca} subgroups can further be classed into BK_{Ca1} and BK_{Ca3} containing 7TM domains, and BK_{Ca2} containing 6TM domains (Fig. 48).

The homologous genes of these different subfamilies of K⁺ channels are all present in *Drosophila*. As shown in Fig 48, inwardly rectifying (*Irk*) potassium channels belong to the Kir family and have three sub-channels, including *Irk1*, *Irk2*, and *Irk3*. Open rectifier K⁺ channel 1 (*Ork1*) belongs to the K_{2P} family and currently is the only identified K_{2P} channel in *Drosophila*. As for the functional Kv and BK channels (*slowpoke*), they are all present in *Drosophila*. From this discovery, it shows that properties of high homology and wide distributions of K⁺ channels are similar both in mammals and the *Drosophila* system.

2.2.2 Distribution of K⁺ channels in the 2nd segment of antenna

The multiplicity mediated by K⁺ channels indicates that the modulations may differ based on the diversity of distribution and abundance of K⁺ channels in living organisms. Therefore, it is essential to identify the expression level of interesting genes in the targeted organ in a temporal and spatial pattern. In *Drosophila*, I performed the RT-PCR assay to screen for homologous K⁺ channel genes in the 2nd segment of the antenna and head (without antenna) to check the existence of K⁺ channels (Fig. 51).

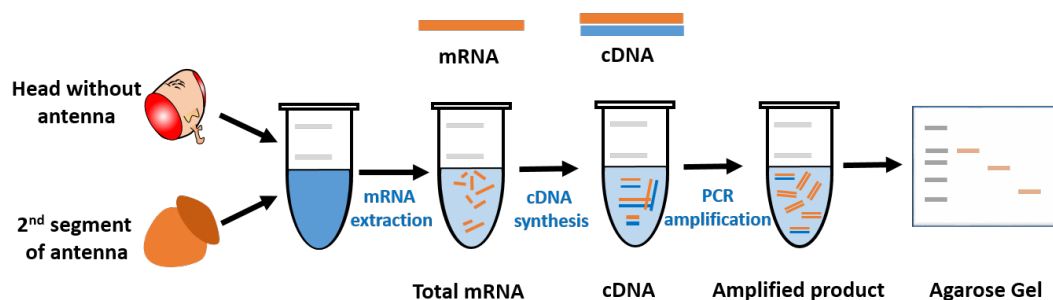


Fig. 51 Diagram of RT-PCR for K⁺ screening in *Drosophila*. The heads without antenna or second segment of antenna are dissected from *Drosophila* and projected to downstream mRNA extraction and cDNA synthesis. The manipulations are provided by the commercial kits (see in Methods and Materials section). After cDNA synthesis, the nucleic acid fragment of K⁺ channel genes is amplified by using gene-specific primers respectively (see the primer list for each individual K⁺ gene). Afterwards, the amplified PCR products are identified in 1% agarose gel by checking the size of each targeted gene.

All different kinds of K^+ channel families were encoded and displayed a broad distribution in the *Drosophila* brain. However, the abundance of some K^+ channel genes slightly differed. *Slowpoke* and *Ork* channels are expressed less compared to other channels in the brain (Fig. 52 A). As for the expression of K^+ channels in JO, the expression pattern was not different compared to the expression in the brain, besides *Ork1* channel. Because *Ork1* gene was less detectable and showed a virtually weak PCR band under the same experimental conditions (Fig. 52 B). The low expression of *Ork1* channels in JO indicated that JO functions may be *Ork1* channel independent.

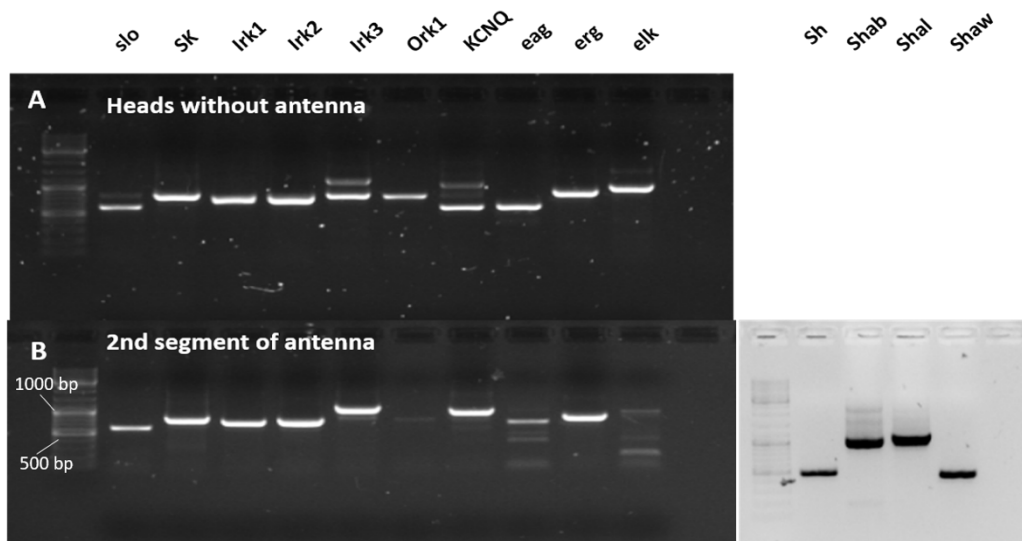


Fig. 52 The expression of K^+ channel genes in heads (without antenna) and second segment of antenna. (A) 15 heads were used for total RNA extraction and 500 ng total RNA were subjected to cDNA synthesis. 1 μ l volume from cDNA reaction mix was added into total 25 μ l PCR reaction mix for 35 cycles of amplification. Then, 15 μ l from PCR reaction mix were loaded into 1% agarose gel to detect the band on desired size. (B) 150 pairs of 2nd segment of antenna were used for total RNA extraction, and the subsequent steps were same as in (A). The flies used for whole steps are 5 to 7 days old.

2.2.3 Effects of mutation in K^+ channels on fly hearing

Numerous studies have proven that many types of K^+ channels participate in the modulation of hearing in mammals. Kir 4.1, KCNE1, and KCNQ1 channels present in stria vascularis to regulate the secretion of K^+ into stria media, and loss of these channels can lead to profound deafness. In the aspect of hearing for K_{2P} channels, some K_{2P} channels exhibit unique expression levels at different growth periods in the rat cochlea nucleus and show that they are may deafness-associated (G. Holt, 2006). In 2015, Yves Cazals proved that only $K_{2P5.1}$, which is abundant in outer sulcus cells for K^+ recycling, is necessary for hearing, not other K_{2P} channels. Moreover, $Kv7$ and K_{Ca} expressed in hair cells regulate the efflux of K^+ either to contribute to K^+ conductance or to participate in the electrical resonance for frequency discrimination in turtles respectively.

In this section, hearing in K^+ channel mutants is analyzed by measuring the free fluctuations of the antennal sound receiver and its sound-induced displacement. From RT-PCR results, it demonstrated that homologous genes of K^+ channels are widely expressed in JO. In this part, the performances of K^+

channel mutants in hearing are identified by measuring the free fluctuation and sound-evoked response of the antennal sound receiver. (*Ork1* was excluded due to low gene expression levels in the JO, and *Irk3* was omitted due to the lack of a proper *null* allele for analysis.)

In free fluctuation measurement, wild-type flies (*w¹¹¹⁸* and *Canton-S*) displayed the highest fluctuation power at 1191.2 ± 264.1 nm²/Hz (*Canton-S*) and 1612 ± 307.1 nm²/Hz (*w¹¹¹⁸*) respectively, with the iBF at 296 ± 39.6 Hz (*Canton-S*) and 226 ± 30.5 Hz (*w¹¹¹⁸*). However, the passive motions of arista caused by ablation of auditory neurons (class AB neurons) in JO, displayed dramatically decreased power to 72.8 ± 40.7 nm²/Hz, and the best frequency shifted to a higher frequency compared to control flies, 429.6 ± 40.4 Hz (Fig. 53, Table 10). From the tested K⁺ mutated alleles, they can be classified into three categories according to the change of power compared to control flies: (1) no significant effect (*Elk*, *Irk2*, *SK*, *Shal*, and *Shaw*); (2) mildly impaired (*sei*, *Irk1*, *slo*, and *KCNQ*); (3) significant impaired (*eag*, *Sh*, and *Shab*) (Fig. 53 and Table 10). However, only two null alleles, *Shaker¹³³* and *Shab³*, the best frequency (iBF) significantly shifted to the higher frequency (Fig. 53 B).

Table 10. Free fluctuation measurement in *wild-type* flies and K⁺ channel mutants

Category	Genes	Power (nm ² /Hz)	iBF (Hz)
Wild type	<i>Canton-S</i>	1191.2 ± 264.1	296 ± 39.6
	<i>w¹¹¹⁸</i>	1612 ± 307.1	226 ± 30.5
No effect	<i>Elk^{MI02485}</i>	756.2 ± 216	256.8 ± 25.4
	<i>Irk2G8690</i>	655.4 ± 217.3	301.6 ± 22.1
	<i>SK^{MB03486}</i>	968 ± 211	252.1 ± 30.1
	<i>Shal^{DN}</i>	1388 ± 488	218.4 ± 30.6
	<i>Shaw^{DN}</i>	556 ± 148	260.4 ± 16.4
	Mildly impaired (*/**)	<i>sei^{HP21840}</i>	444 ± 287.2
<i>Irk1^{MI08404}</i>		423 ± 96	287.1 ± 23.1
<i>slo^{MB11481}/Df</i>		395 ± 144	286.4 ± 40.1
<i>KCNQ³⁷⁰</i>		369 ± 48	284.1 ± 45.5
Significant impaired (***)	<i>eag^{Afull}</i>	189 ± 35.3	349.5 ± 24.2
	<i>Sh¹³³</i>	93 ± 2.3	525.2 ± 17.2
	<i>Shab³</i>	236 ± 166	574 ± 55.7

Data are shown as a mean \pm 1SD (N=5).

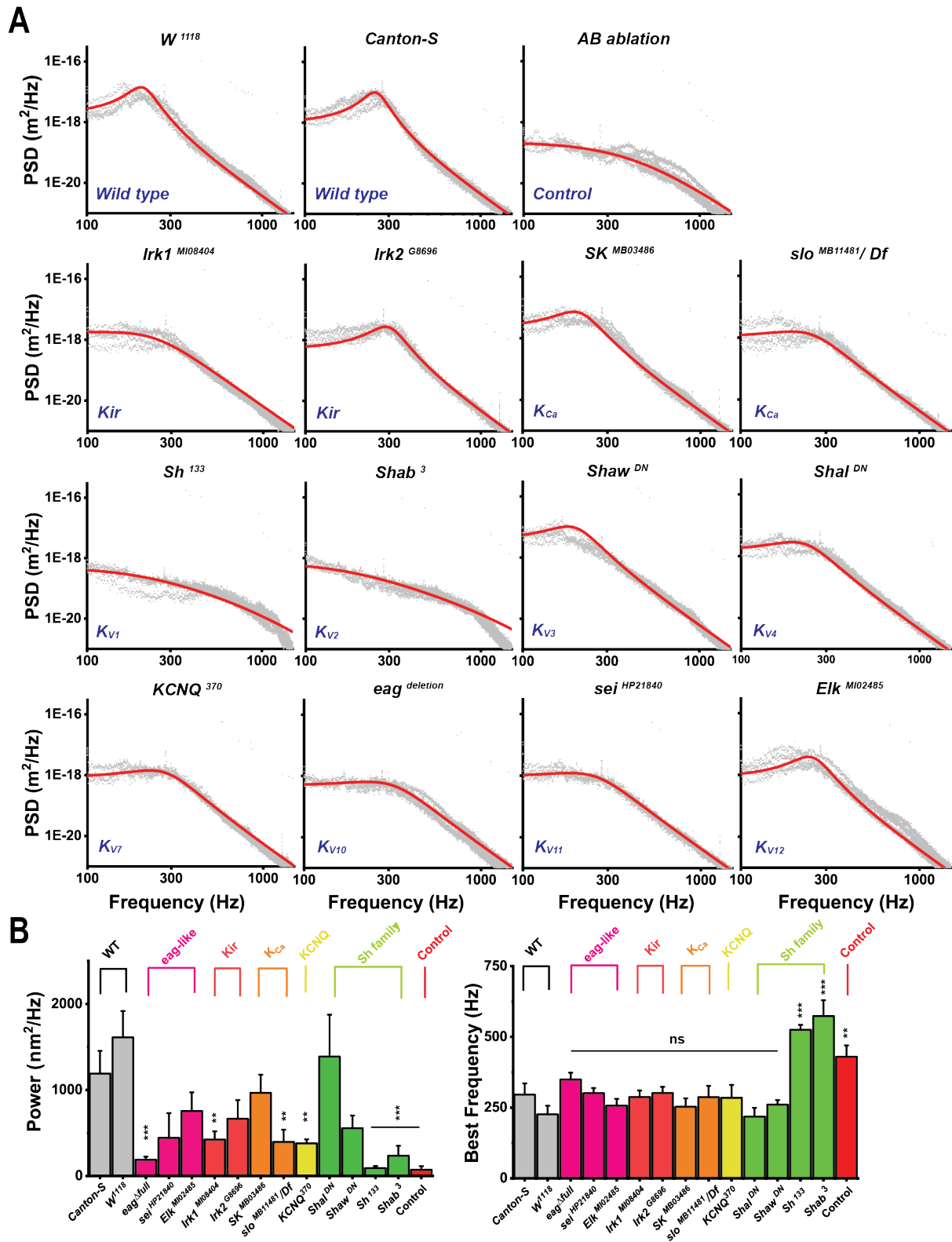


Fig. 53 Free fluctuation measurement in K⁺ channel mutants. Five to seven days old flies from each genotype were employed to measure the power spectral density of antenna vibration in the absence of sound stimulation. (A) Power spectra for each K⁺ mutated alleles. Gray trace, spectrum for five animals per strain; Red trace, the fit of spectrum with harmonic oscillator. (B) Principal parameters from PSD measurement for each genotype: power (Left) and best frequency (Right). The gray shows wild type flies and positive control with ablated AB neurons is color in red. Other experimental groups show and are labelled in different color. Data are shown as mean \pm 1SD (N=5). Two-tailed Mann Whitney U-test is used for statistical analysis between control groups and K⁺ mutants, and Bonferroni correction is used to correct for multiple comparisons, ns: not significant ($P > 0.05$), $0.05 > P > 0.01$, $0.01 > P > 0.001$.

With the pure tone stimuli at iBF, in control flies, the sound-evoked arista displacement displayed a compressive nonlinearity with sound particle velocity (SPV), enhancing mechanical sensitivity when sound is faint. The corresponding calculated mechanical amplification gain was 9.9 (w^{1118}) and 12.4 (*Canton-S*). In contrast to control flies, nonlinear mechanical amplification was completely lost (gain at 1.7 ± 0.2) in flies with ablated auditory AB neurons, with a linearity of antenna passive system (Fig. 54). For the tested K^+ channel alleles, five of twelve strains behave normally (*Elk*, *SK*, *Irk2*, *Shaw*, and *Shal*). And mechanical amplification was mildly impaired in the other five strains (*Irk1*, *slo*, *eag*, *KCNQ*, and *sei*). In the absence of *Sh* (gain at 1.6 ± 0.2) or *Shab* (gain at 1.5 ± 0.2) channels, the mechanical sensitivity was abolished when the sound is faint under the same intensity stimuli (Fig. 54).

In parallel to the mechanical response measurement, CAP responses from the antennal nerve were recorded at iBF. The absolute maximum CAP amplitude generated from sound stimulation was not significantly different between control flies and K^+ mutated alleles (Fig. 55 C). Moreover, after plotting normalized CAP amplitudes against either sound particle velocity or displacement, the resulting CAP-intensity or CAP-SPV curves were practically identical in all strains (Fig. 55). The decreased CAP response or significant right shift of CAP-SPV or CAP-displacement curves can only be observed in ablated auditory neurons strain (Fig. 55). Till now, the loss of *Sh* or *Shab* channels can only affect the mechanical sensitivity in *Drosophila* hearing, but not the nerve response.

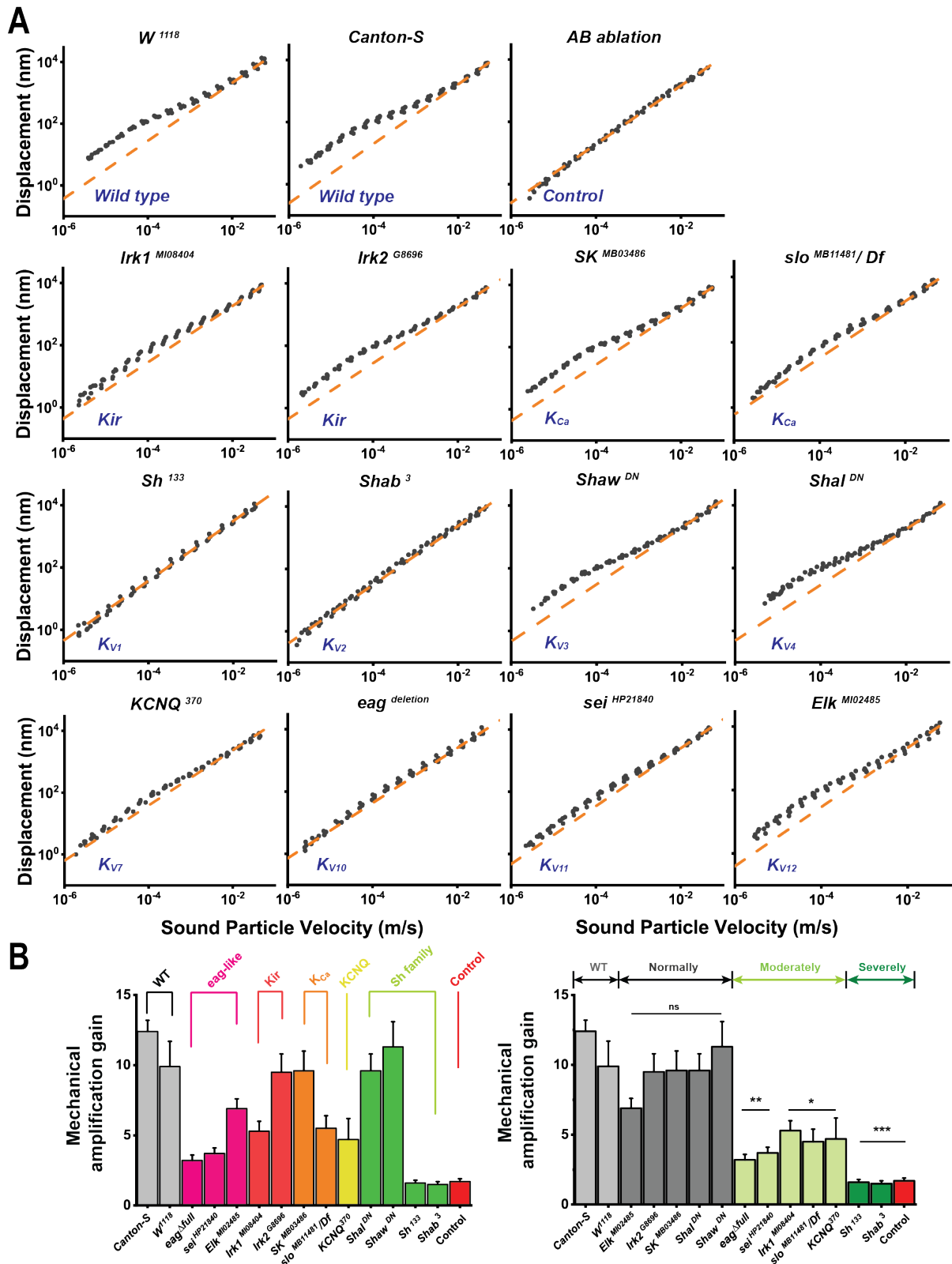


Fig. 54 Mechanical response from sound intensity measurement in K^+ channel mutants at iBF. Five to seven days old flies from each genotype were employed for measurement with pure tone stimulation. (A) Sound-evoked antennal displacement response versus SPV at iBF. Gray trace: displacement at corresponding intensity, five animals per strain. (B) The corresponding mechanical amplification gain was calculated from (A). The graphs were generated by two categories: one is based on the number of TM domains (Left); the other one is made by the value of gain, severely (gain < 3); mildly (3 < gain < 6). Data are shown as mean \pm 1SD (N=5). Two-tailed Mann Whitney U-test is used for statistically significant analysis, and Bonferroni correction is used to correct for multiple comparisons (N=5) * P < 0.05, ** P < 0.01, *** P < 0.001.

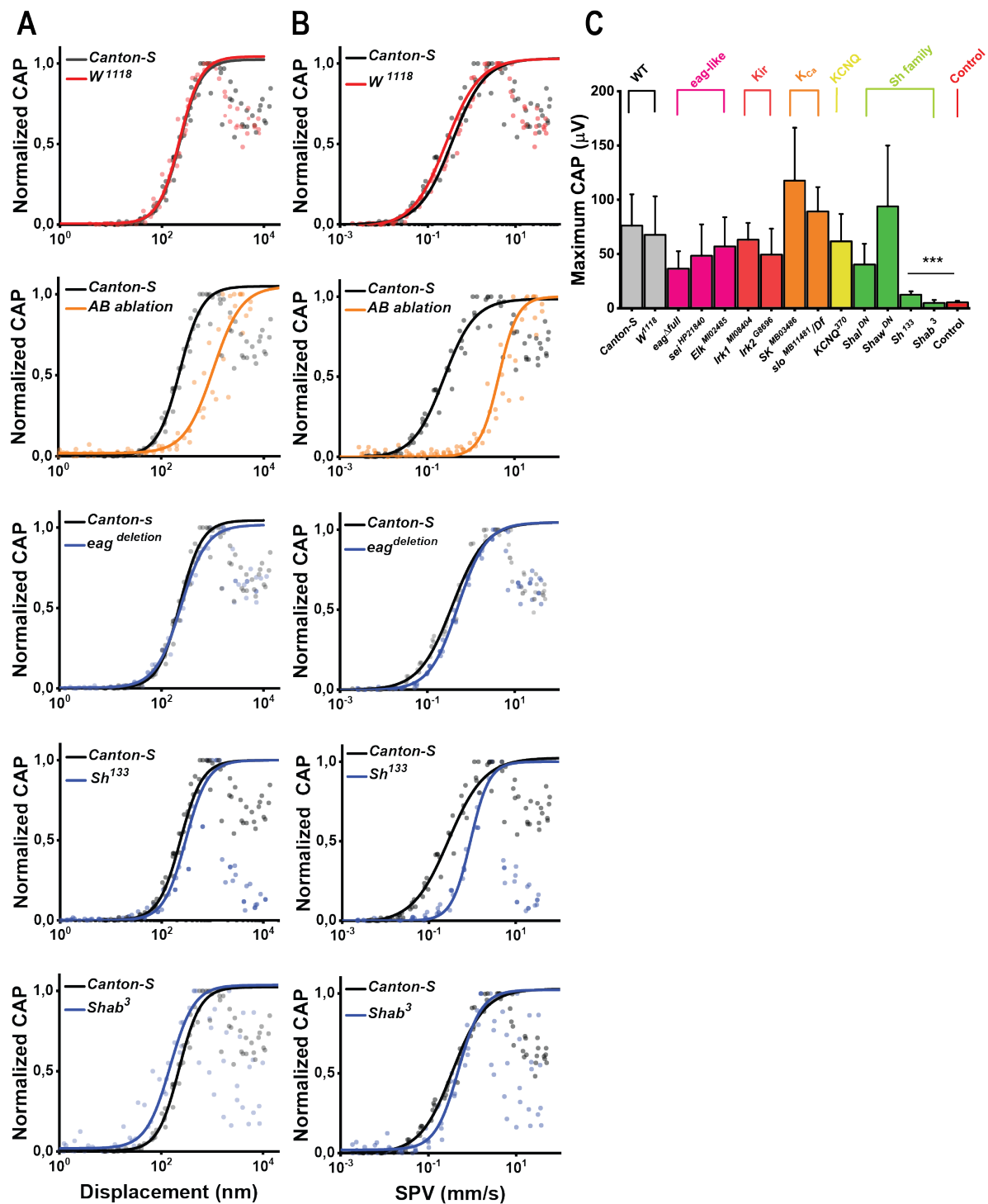


Fig. 55 Electrical response from sound-evoked measurement in K^+ channel mutants at iBF. (A) CAP-Displacement and (B) CAP-Sound Intensity curves were graphed by plotting CAP amplitude against displacement or intensity and normalization is to eliminate the difference from different flies. Black dots and curves: *Canton-S* fly measurement; Red dots and curves: *w¹¹¹⁸* fly measurement; Brown dots and curves: AB neurons ablated flies measurement; (C) The corresponding CAP amplitudes were recorded and channels are classified based on the TM domain in graph (top). Response thresholds at particle (middle) and displacement (bottom) were calculated and shown in graphs. Data are shown as mean \pm 1SD (N=5). Two-tailed Mann Whitney U-test is used for statistically analysis and Bonferroni correction is used to correct for multiple comparisons (n=5), * $P < 0.05$, ** $P < 0.01$, *** $P < 0.001$.

2.2.4 Requirements of *Shaker* or *Shab* channel for *Drosophila* hearing?

The mechanical amplification in *Drosophila* hearing was severely impaired in *Sh*¹³³ or *Shab*³ mutant, but the CAP response was not affected. *Sh*¹³³ is a missense mutation in the core region of *Sh* channel, which leads to a non-functional channel. The *Shab*³ allele contains two deletions, leading to a frameshift with multiple stop codons, rendering this effectively a *null* allele (C.F Wu, 2006; (Hegde *et al.*, 1997)). To avoid possible phenotypes of possible side-effects from the genetic background (*e.g.* unknown side-mutations or inbreeding effects), the measurements were performed not only by using homozygous mutant allele, but also heterozygous null allele, which was accompanied by a corresponding deficiency allele spanning the gene of interest region.

In contrast to *Sh*¹³³/*Sh*¹³³ flies, mechanical amplification (gain, power) in *Sh*¹³³/*Df(1)BSC*⁴⁰⁵ flies was partially restored to 4.2 ± 0.5 (gain) and 455 ± 144 nm²/Hz (power) (Fig. 57). Additionally, the best frequency of *Sh*¹³³/*Df(1)BSC*⁴⁰⁵ flies (263.8 ± 27.3 Hz) was indistinguishable from wild-type flies. The maximum CAP was not different between *Sh*¹³³/*Df(1)BSC*⁴⁰⁵ (86.1 ± 39.9 μ v) and control flies (*Canton-S*, 76.1 ± 28.8 μ v). However, the auditory performance in *Shab*³/*Shab*³ flies and *Shab*³/*Df(3L)BSC*⁴²⁸ flies (gain at 1.8 ± 0.3 ; power at 261 ± 156 nm²/Hz) were identical. It turns out that the abolishment of mechanical amplification in *Drosophila* hearing may be *Shab* channel dependent. Because there was no effect in hearing electrical transduction, it was not surprising that the morphology of JO neurons in the *Shab*³ allele was integral (Fig. 56).

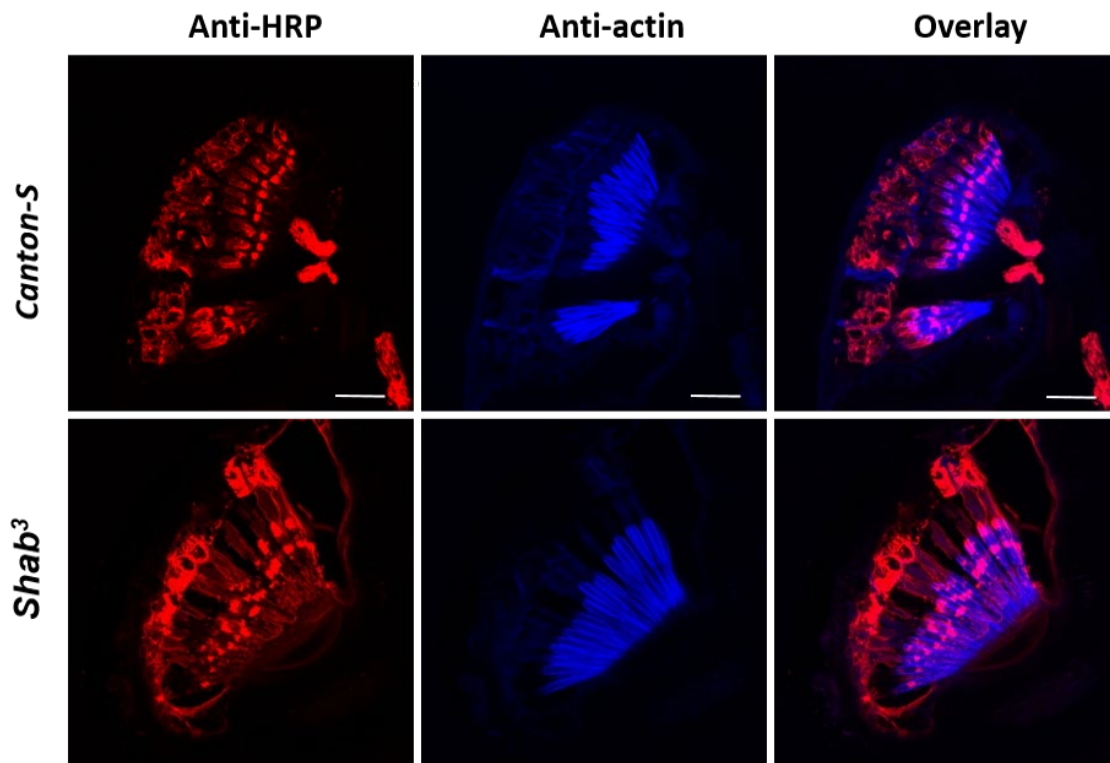


Fig. 56 Morphology of JO neurons in *wild-type* flies and *Shab*³ mutants. In Canton-S flies (*WT*) and *Shab* mutant, the chordotonal neurons in JO were stained with anti- HRP (color in red), the F-actin was stained with anti-phalloidin (color in blue), the overlapped pictures were shown on the right side. Scale bar is 10 μ m.

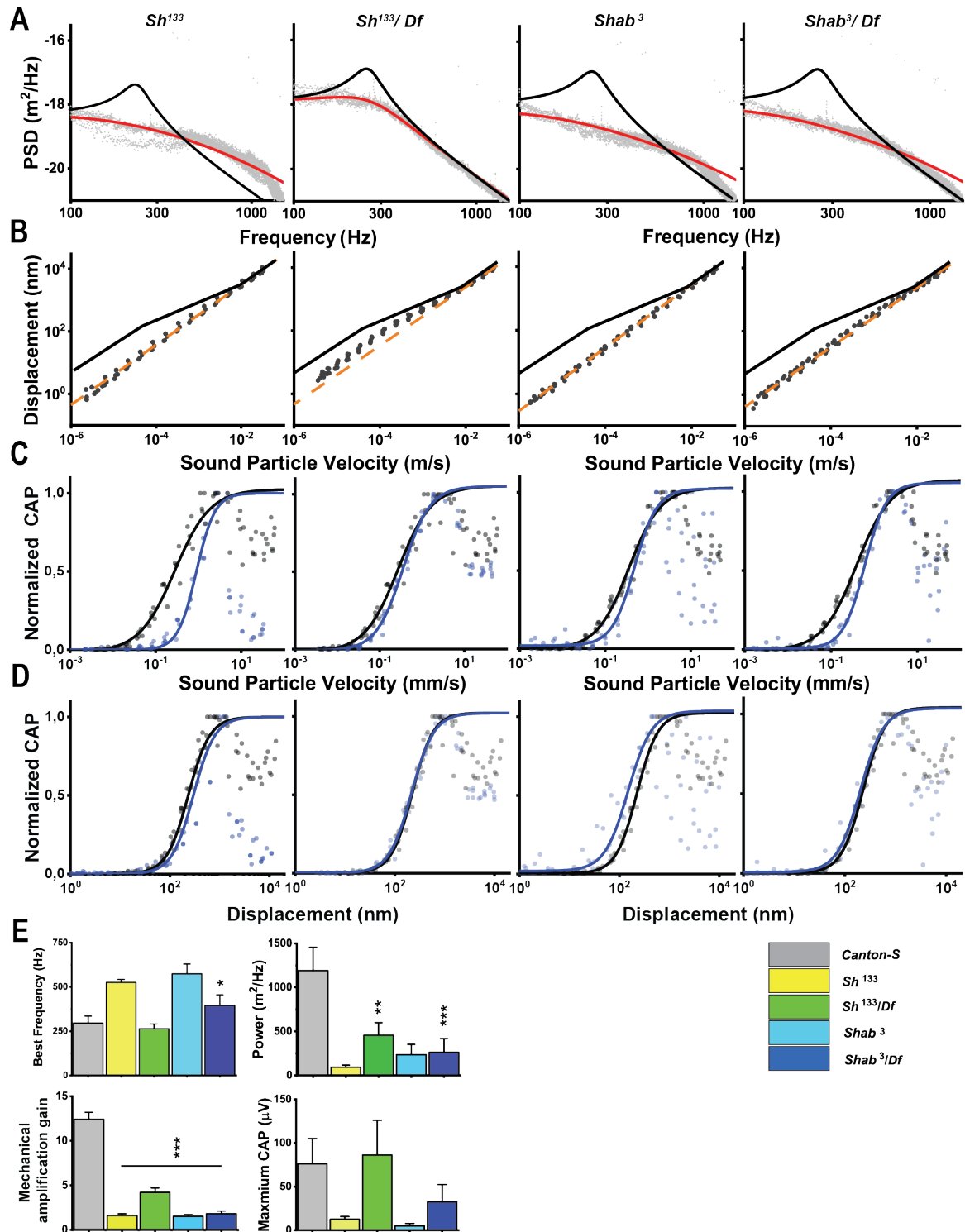


Fig. 57 Auditory performance in *Shake* and *Shab* mutants. (A) Free fluctuation measurement of *Sh*¹³³, *Shab*³, *Sh*¹³³/*Df*(1)*BSC*⁴⁰⁵, and *Shab*³/*Df*(3*L*)*BSC*⁴²⁸. Gray trace, spectrum for five animals per strain; Red trace, the fitting of spectrum with harmonic oscillator; Black trace, the fit of spectrum with harmonic oscillator in wild type flies. (B) Arista displacement versus SPV at iBF. Gray trace: displacement at corresponding intensity, five animals per strain. Brown dash trace: passive linear trend originating from high intensity stimuli; Black trace, modelling trend of displacement in wild type flies. (C) (D) Normalization of CAP amplitude versus SPV and Displacement. Black trace, wild type flies; Blue trace, experimental flies.

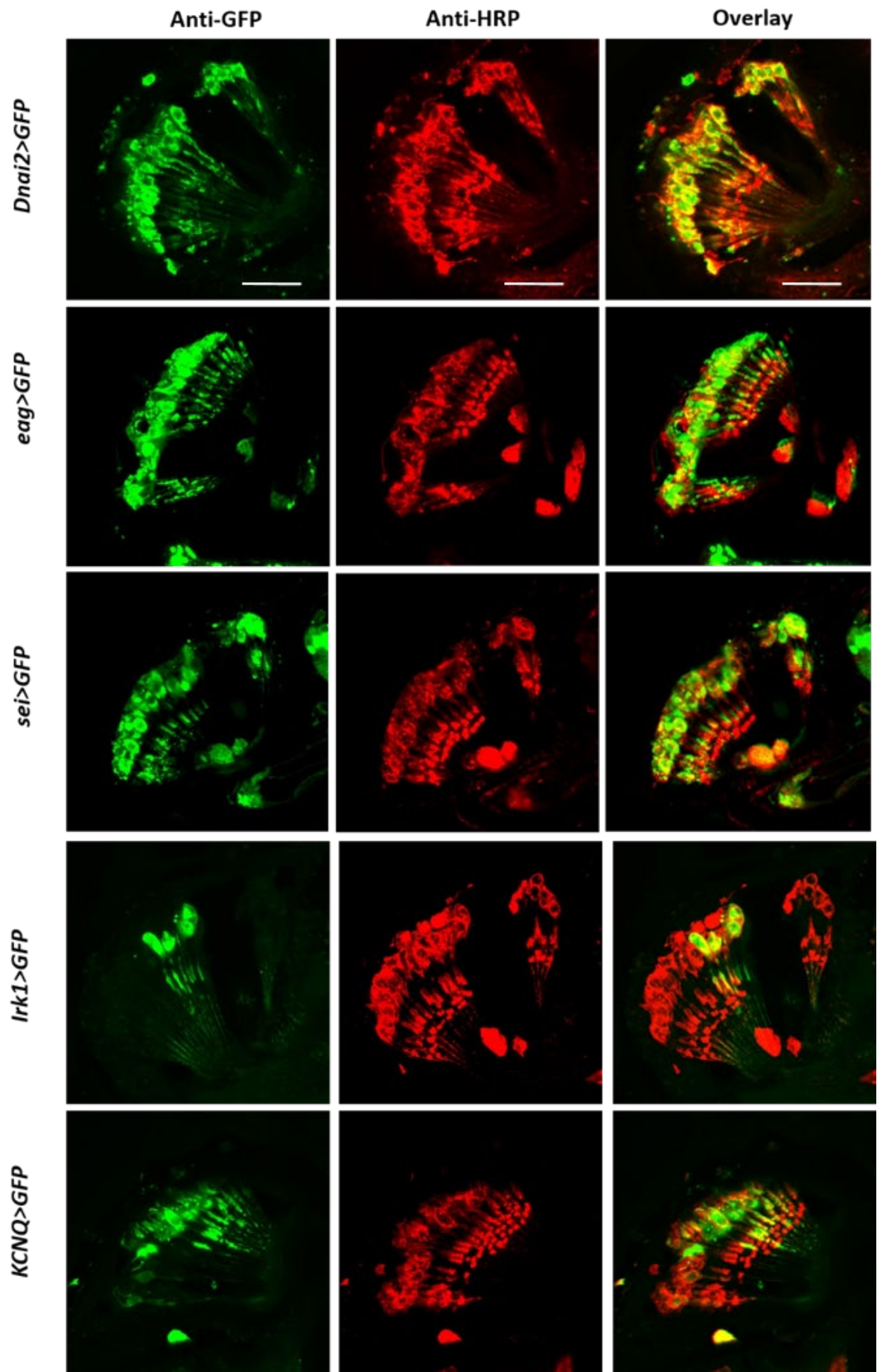
(E) Parameters from hearing measurement for each strain: power, mechanical amplification gain, maximum CAP, and best frequency. The different groups were labelled in color shown in right side. Data are shown as mean \pm 1SD (N=5). Two-tailed Mann Whitney U-test is used for statistically analysis between different groups and Bonferroni correction is used to correct for multiple comparisons (N=5) * $P < 0.05$, ** $P < 0.01$, *** $P < 0.001$.

2.2.5 Expression of potassium channels in JO

To further explore the characteristics of K⁺ channels in JO, it is indispensable to know whether these channels express in chordotonal neurons or supporting cells, and their cellular localization. By clarifying the localization in JO, this would imply the fact that how K⁺ ion entries into neurons and modulates the membrane current in auditory signal transmission. To probe K⁺ channels in JO, the Gal4/UAS system was carried out by expressing GFP reporter protein under the control of K⁺ channel Gal4 enhancer lines. The primary antibody staining against specific channels and EGFP-fusion transgenic insertion strain are also used to reveal the expression of K⁺ channels in JO.

Because preliminary results showed that *Elk*, *Irk2*, *SK*, *Shaw*, and *Shal* had no effect on hearing, the expression of these channels was not tested. *Dnai2* is a well-established protein that is non-selectively present in all chordotonal neurons in JO as shown the GFP signals in Fig. 58. The tested K⁺ channels, including *slo*, *Irk1*, *eag*, *sei*, *KCNQ*, *Sh*, and *Shab*, were all expressed in chordotonal neurons, not in the supporting accessory cells in JO, but with distinctive expression patterns: (1) non-selective expression in all neurons, including *eag*, *sei* and *Shab* channels; (2) restricted expression in a subset of JO neurons, including *Irk1*, *slo*, *KCNQ*, and *Sh* channels; (3) different cellular localization, *Sh* and *Shab* channels (Fig. 58).

Shaker channel is localized in the sensory dendrites of JO neurons. *Shab* channel can be found in the cilia of practically all JO neurons. The JO hosts ca. 500 sensory neurons, sorted into 5 subgroups from A to E with distinctive sub-population of JO neurons. The K⁺ channels (*slo*, *KCNQ*, *Sh*, and *Irk1*) not only displayed selective expression in JO neurons, but also presented in unequal neuron numbers. From this discovery, it could be predicted that the distinct expressions of these K⁺ channels may have their own unique functions which currently are still unknown.



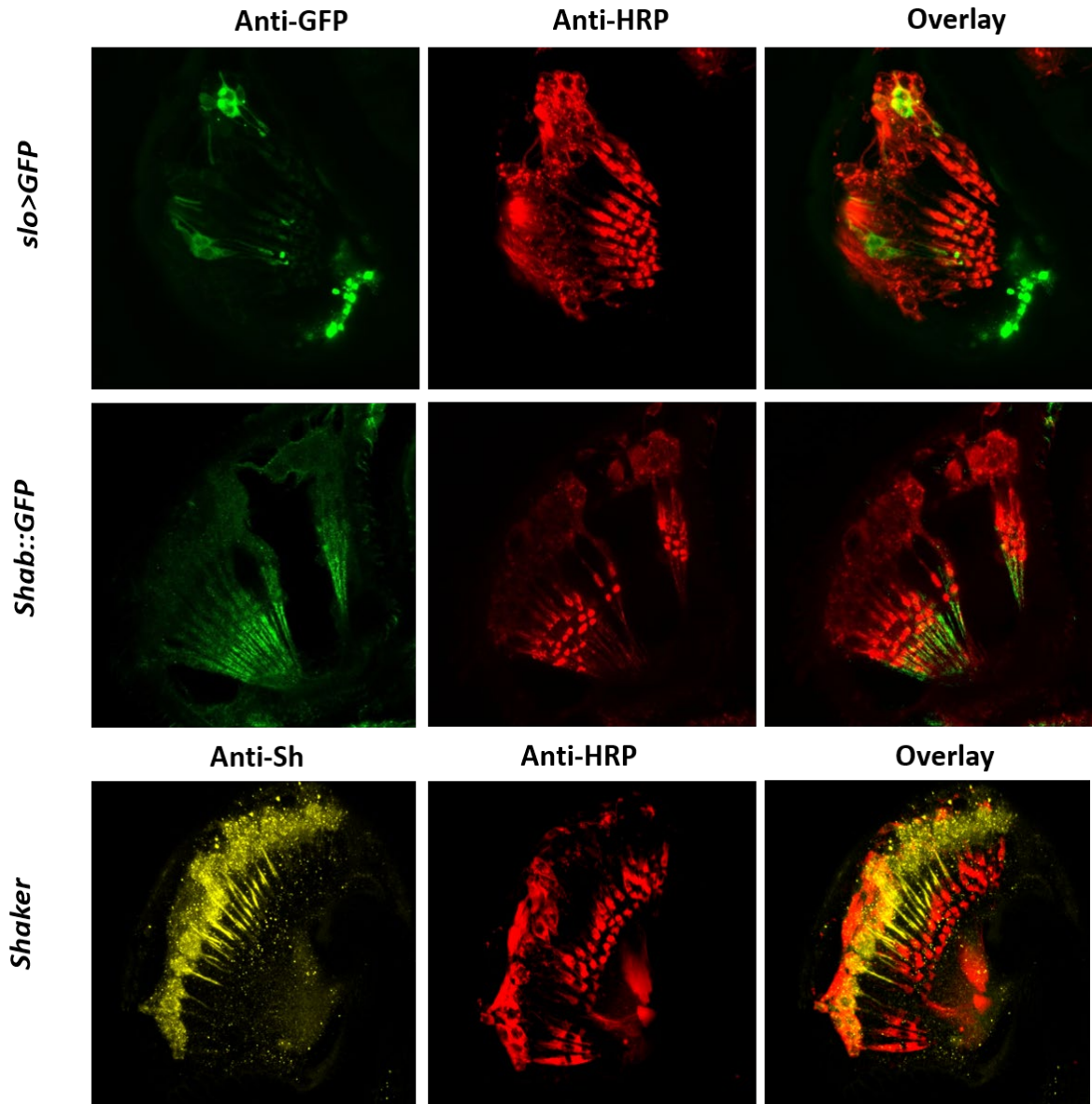


Fig. 58 Expression of tested potassium channels in JO. The morphology of chordotonal neurons was stained with anti-HRP as shown in red color. The merged images indicated the channel expression throughout the JO neurons. A transgenic insertion strain contained a fusion EGFP construct in *Shab* locus was used to check the expression. An anti-*Sh* antibody was used to probe the *Sh* channel as shown in yellow color. Scale bar is 20 μ m.

2.3 Discussion

Judging from the expression and phenotypes of K^+ channels in JO, this chapter implicates several potassium channels in fly hearing, extending the number of ion channels that are implicated in JO neuron function.

2.3.1 Genetic parallels of K^+ channels in *Drosophila* and Vertebrate ears

In vertebrate, K^+ channels are required for normal hearing. For instance, Kir and *KCNQ* channels are found in the stria vascularis, where they regulate the secretion of K^+ into stria media to maintain the high concentration of K^+ ions. Additionally, *KCNQ* on the basal side of hair cells assists the K^+ to cycle back to endolymph. Lack of them can result in hearing impairment. *Drosophila* JO is a multicellular structure, containing sensory neurons, scolopale cells, CAP cells, and ligament cells. Likewise, the homologs of different types of K^+ channel families are present in *Drosophila*. Furthermore, these tested channels are also present in the *Drosophila* JO, but the abundance of different K^+ sub-channels or families differs. Compared to the high expression of *Orkl* channel in the *Drosophila* head, its presence in JO is scarcely detectable. Kir and *KCNQ*, homologous genes to human Kir and *KCNQ* family, are high abundance both in the *Drosophila* head and JO, and the impaired hearing in *Irkl* and *KCNQ* mutated strains demonstrated that they may participate in the hearing modulation of antenna. Furthermore, dysfunctions of *Drosophila eag* and *sei* channels lead to a partial failure of hearing, but their effects and function in the vertebrate cochlea are still not addressed yet. Seven of fourteen tested homologous K^+ genes are related to auditory impairment in *Drosophila* ear. This gives a view that the electrophysiological property of hearing is multi-K channels participant both in the vertebrate cochlea and *Drosophila* JO.

Comparing to the high K^+ concentration in the perilymph of the vertebrate cochlear, it is assumed to have a K^+ enriched receptor lymph in the scolopale space around the sensory neurons of the JO (Eberl, 2004; M. Roy et al., 2013). The maintenance of ionic composition in scolopale space is modulated by ion channels, including K^+ channels, to control the inflow and outflow of ions into cells for electrophysiological activities. However, the mechanism of how these K^+ channels activation and deactivation are still elusive.

2.3.2 Expression of K^+ channels in the *Drosophila* ear

Unlike the different expressions of deafness-associated K^+ channels in various types of cells in the cochlea, all tested seven K^+ channels are expressed in the chordotonal neurons, not in surrounding supporting cells. However, all homologous K^+ channels are present in JO from RT-PCR screen. This difference between these two methods may originate from the limitation of tested numbers, failure of Gal4 enhancer lines, or other un-discovered K^+ channels. Except for the sensory neurons, the

importance of ion channels in the regulation of auditory transduction from supporting cells is irrefutable either in cochlea or JO. For example, some Na⁺/K⁺-ATPase subunits, ATPa and Nrv2 which modulate the exchange of Na⁺ and K⁺ ions, are expressed in scolopale cells, and they are hearing-associated. The loss of Na⁺/K⁺-ATPase function leads to deafness. This finding supports the idea that the hearing modulation involves multiple ion channels and cell types. Taking into consideration the different expressions of tested K⁺ channels in JO neurons, the widespread expression of *eag*, *sei*, and *Shab* channels in all JO neurons may lead to universal functions, but the distinct expression of *Irkl*, *KCNQ*, and *slo* channels in a particular subset of neurons can further to reveal the specific function of these JO neurons in cell inherent pattern. Compared to the morphology and architecture of categorized class A/B/D JO neurons, the expression of K⁺ channels in the sub-population of JO neurons rises an idea that they may involve in the different aspects of hearing modulation, like *slo* and *Shaker* channels involvement in low auditory frequency.

2.3.3 Role of Kv2 in mammals hearing and *Shab* in *Drosophila*

To sum up the hearing performance of K⁺ channels in *Drosophila*, none of the analyzed mutated alleles disrupted the conduction of auditory nerve signals, but the restrictions are defined in the mechanical amplification of hearing. For the mutants' phenotypes (*Irkl*, *KCNQ*, *Sh*, and *slo*), it seems to be understandable that the mechanical amplification was partly impaired because of their expression in subpopulation of ca. 500 JO neurons. As for *eag* and *sei* channels, they are present in all JO neurons, but the null alleles did not completely abolish the hearing function. This may be due to some other channels or proteins also involve in the modulation according to the fact that *eag* channel may interplay as a modulating subunit with other channels or binds to cyclic nucleotide to function in a physiological state (Wilson *et al.*, 1998; Tsai *et al.*, 2012).

Compared to other K⁺ channels, the complete loss of mechanical amplification was only observed in the *Shab*³ null allele, which gives the view that the control of amplification in hearing requires *Shab* channel. *Shab*, known as *Shaker cognate b* or Kv2, is the second isolated K⁺ channel following the identification of first *Shaker* K⁺ channel in *Drosophila*. *Shab* channel allows for sustained K⁺ efflux from cells with a delay after depolarization to generate a delayed rectifier current (Vahasoyrinki *et al.*, 2006)). For the hearing perception of Kv2 family, the loss of Kv2.1 channel in zebrafish can impair inner ear development. As the key transcription gene, it is crucial for K⁺ metabolism, cilia development, and protein trafficking in the ear. Moreover, Ian D. Forsythe reported that the hearing loss resulting from acoustic over-exposure can be rescued by the presence of Kv2.2 channel in mice (Forsythe, 2013). In the *Drosophila* ear, the results showed that *Shab* channel is a cilium component in chordotonal neurons and essential for the mechanical amplification of hearing. Considering the genetic parallels and functional analysis between the *Drosophila* eye and ear, the lack of components that participate in the phototransduction cascade can also lead to hearing defects, such as rhodopsin and TRP channels.

Because of the abundance of *Shab* channel in the photoreceptor and JO neurons, the functions of *Shab* channel in vision and hearing can bring new insight as a new candidate channel.

2.3.4 Achievements and questions to be answered?

In summary, this chapter implicates K^+ channels fly hearing by: (1) testing the presence of K^+ channel genes in JO; (2) investigating the expression and localization of these channels in JO; (3) examining hearing in K^+ channel mutants. Many questions still remain: (1) how, for example, are the electrophysiological properties and characteristics of K^+ current modulated? (2) how do the mutations tested affect sound responses? (3) How do the different K^+ channels interact? Further studies will be required to address these issues.

List of references

- A. C. Crawford., R. Fettiplace (1981) An electrical tuning mechanism in turtle cochlear hair cells. *The Journal of Physiology*, **312**, 377-412
- Adams, M.D., Celniker, S.E., Holt, R.A., Evans, C.A., Gocayne, J.D., Amanatides, P.G., Scherer, S.E., Li, P.W., Hoskins, R.A. & Galle (2000) The genome sequence of *Drosophila melanogaster*. *Science*, **287**, 2185-2195.
- A. J. Hudspeth, R. S. Lewis (1988) Kinetic analysis of voltage- and ion-dependent conductances in saccular hair cells of the bull-frog, *Rana catesbeiana*. *The Journal of Physiology*, **400**, 237-274
- Albert, J.T. & Kozlov, A.S. (2016) Comparative Aspects of Hearing in Vertebrates and Insects with Antennal Ears. *Current Biology*, **26**, R1050-R1061.
- Alberti, P.W. (2001) The anatomy and physiology of the ear and hearing. *Occupational exposure to noise: Evaluation, prevention, and control*, 53-62.
- Ashmore, J., Avan, P., Brownell, W., Dallos, P., Dierkes, K., Fettiplace, R., Grosh, K., Hackney, C., Hudspeth, A. & Jülicher (2010) The remarkable cochlear amplifier. *Hearing Research*, **266**, 1-17.
- Beisel, K.W., Rocha-Sanchez, S.M., Morris, K.A., Nie, L., Feng, F., Kachar, B., Yamoah, E.N. & Fritsch, B. (2005) Differential expression of KCNQ4 in inner hair cells and sensory neurons is the basis of progressive high-frequency hearing loss. *Journal of Neuroscience*, **25**, 9285-9293.
- Bennet-Clark, H.C. (1989) Songs and the Physics of Sound Production Cricket behavior and neurobiology. *Cornell University Press*, pp. 227-261.
- Berg, R.E. & Stork, D.G. (2005) The Physics of Sound. Pearson Prentice Hall.
- Birmingham, N.A., Hassan, B.A., Price, S.D., Vollrath, M.A., Ben-Arie, N., Eatock, R.A., Bellen, H.J., Lysakowski, A. & Zoghbi, H.Y (1999) *Math1*: an essential gene for the generation of inner ear hair cells. *Science*, **284**, 1837-1841.
- Beurg, M., Fettiplace, R., Nam, J.-H. & Ricci, A.J (2009) Localization of inner hair cell mechanotransducer channels using high-speed calcium imaging. *Nature Neuroscience*, **12**, 553-558.
- Boekhoff-Falk, G. (2005) Hearing in *Drosophila*: development of Johnston's organ and emerging parallels to vertebrate ear development. *Developmental Dynamics*, **232**, 550-558.
- Caldwell, J.C. & Eberl, D.F (2002) Towards a molecular understanding of *Drosophila* hearing. *Journal of Neurobiology*, **53**, 172-189.
- Cazals, Y., Bevendut, M., Zanella, S., Brocard, F., Barhanin, J. & Gestreau, C. (2015) KCNK5 channels mostly expressed in cochlear outer sulcus cells are indispensable for hearing. *Nature Communication*, **6**, 8780.
- de Boer, E. & Nuttall, A.L. (2000) The mechanical waveform of the basilar membrane. II. From data to models--and back. *Journal of the Acoustical Society and America*, **107**, 1487-1496.
- Dhasakumar S Navaratnam., Laura Escobar., Manuel Covarrubias. & J.Carl Oberholtzer (1995) Permeation Properties and Differential Expression across the Auditory Receptor Epithelium of an Inward Rectifier K Channel Cloned from the Chick Inner Ear. *The Journal of Biological Chemistry*, **270**, 19238-19245.
- Dhasakumar S Navaratnam., Thomas J Bell., Tu Dinh Tu., Erik LCohen. & J.Carl Oberholtzer (1997) Differential Distribution of Ca-Activated K Channel Splice Variants among Hair Cells along the Tonotopic Axis of the Chick Cochlea. *Neuron*, **19**, 1077-1085.

- Effertz, T., Wiek, R. & Göpfert, M.C (2011) NompC TRP channel is essential for Drosophila sound receptor function. *Current Biology*, **21**, 592-597.
- Ekdale, E.G (2016) Form and function of the mammalian inner ear. *Journal of Anatomy*, **228**, 324-337.
- Erichsen, S., Zuo, J., Curtis, L., Rarey, K. & Hultcrantz, M (1996) Na, K-ATPase α - and β -isoforms in the developing cochlea of the mouse. *Hearing Research*, **100**, 143-149.
- Fettiplace, R. (2017) Hair Cell Transduction, Tuning, and Synaptic Transmission in the Mammalian Cochlea. *Comprehensive Physiology*, **7**, 1197-1227.
- Fettiplace, R. (2020) Diverse Mechanisms of Sound Frequency Discrimination in the Vertebrate Cochlea. *Trends in Neuroscience*, **43**, 88-102.
- Fettiplace, R. & Fuchs, PA (1999) Mechanisms of hair cell tuning. *Annual review of physiology*, **61**, 809.
- Fettiplace, R (2011) Hair cell transduction, tuning, and synaptic transmission in the mammalian cochlea. *Comprehensive Physiology*, **7**, 1197-1227.
- Fettiplace, R (1987) Electrical tuning of hair cells in the inner ear. *Trend in Neuroscience*, **10**, 421-425.
- Field, L.H. & Matheson, T. (1998) Chordotonal organs of insects. *Advances in Insect Physiology*. Elsevier, pp. 1-228.
- Fischer, J.A., Giniger, E., Maniatis, T. & Ptashne, M (1988) GAL4 activates transcription in Drosophila. *Nature*, **332**, 853-856.
- Freegarde, T. (2012) Introduction to the Physics of Waves. *Cambridge University Press*.
- Fritsch, B. & Beisel, K W (2001) Evolution and development of the vertebrate ear. *Brain Research bulletin*, **55**, 711-721.
- Fuchs, P., Nagai, T. & Evans, M G (1988) Electrical tuning in hair cells isolated from the chick cochlea. *Journal of Neuroscience*, **8**, 2460-2467.
- Getachew, G (2018) A review of simple harmonic motion for mass spring system and its analogy to the oscillations in lc circuit. *c*, **6**.
- Goepfert, M.C. & Hennig, R.M (2016) Hearing in insects. *Annual Review Entomology*, **61**, 257-276.
- Göpfert, M. & Robert, D (2003) Motion generation by Drosophila mechanosensory neurons. *Proceedings of the National Academy of Science*, **100**, 5514-5519.
- Göpfert, M., Stocker, H. & Robert, D (2002) atonal is required for exoskeletal joint formation in the Drosophila auditory system. *Developmental Dynamics*, **225**, 106-109.
- Gopfert, M.C. & Hennig, R.M. (2016) Hearing in Insects. *Annual Review of Entomology*, **61**, 257-276.
- Göpfert, M.C. & Robert, D (2002) The mechanical basis of Drosophila audition. *Journal of Experimental Biology*, **205**, 1199-1208.
- Göpfert, M.C. & Robert, D (2001) Turning the key on Drosophila audition. *Nature*, **411**, 908-908.
- Green, D.M. (2021) *An introduction to hearing*. Routledge.
- Grinnell, A.D (1969) Comparative physiology of hearing. *Annual Review of Physiology*, **31**, 545-580.
- Grothe, B., Pecka, M. & McAlpine, D. (2010) Mechanisms of sound localization in mammals. *Physiological Review*, **90**, 983-1012.
- Hales, K.G., Korey, C.A., Larracuente, A.M. & Roberts, D (2015) Genetics on the fly: a primer on the Drosophila model system. *Genetics*, **201**, 815-842.

- Hall, J.C (1994) The mating of a fly. *Science*, **264**, 1702-1714.
- Hauko, R. & Repnik, R (2019) Damped harmonic oscillation: Linear or quadratic drag force?, *American Journal of Physics*, **87**, 910-914.
- Hoy, R.R. & Robert, D (1996) Tympanal hearing in insects. *Annual Review of Entomology*, **41**, 433-450.
- Hu, Y., Jia, Y., Deng, T., Liu, T. & Zhang, W (2021) Molecular Mechanisms for Frequency Specificity in a Drosophila Hearing Organ. *bioRxiv*.
- Ishikawa, Y., Fujiwara, M., Wong, J., Ura, A. & Kamikouchi, A. (2019) Stereotyped Combination of Hearing and Wind/Gravity-Sensing Neurons in the Johnston's Organ of Drosophila. *Frontiers of Physiology*, **10**, 1552.
- Jones, E., Gray-Keller, M. & Fettiplace, R (1999) The role of Ca²⁺-activated K⁺ channel spliced variants in the tonotopic organization of the turtle cochlea. *The Journal of Physiology*, **518**, 653.
- Kamikouchi, A., Inagaki, H.K., Effertz, T., Hendrich, O., Fiala, A., Göpfert, M.C. & Ito, K (2009) The neural basis of Drosophila gravity-sensing and hearing. *Nature*, **458**, 165-171.
- Kamikouchi, A., Shimada, T. & Ito, K. (2006) Comprehensive classification of the auditory sensory projections in the brain of the fruit fly *Drosophila melanogaster*. *Journal of Comparative Neurology*, **499**, 317-356.
- Keegan, L., Gill, G. & Ptashne, M (1986) Separation of DNA binding from the transcription-activating function of a eukaryotic regulatory protein. *Science*, **231**, 699-704.
- Kruth, P. & Stobart, H. (2007) *Sound*. Cambridge University Press.
- Lagrutta, A., Shen, K.Z., North, R.A. & Adelman, J.P. (1994) Functional differences among alternatively spliced variants of Slowpoke, a Drosophila calcium-activated potassium channel. *Journal of Biological Chemistry*, **269**, 20347-20351.
- Lai, J.S.-Y., Lo, S.-J., Dickson, B.J. & Chiang, A.S (2012) Auditory circuit in the Drosophila brain. *Proceeding of The National Academy of Science*, **109**, 2607-2612.
- Laptev, I.A., Raevskaya, N.M., Filimonova, N.A. & Sineoky, S.P. (2018) The piggyBac Transposon as a Tool in Genetic Engineering. *Applied Biochemistry and Microbiology*, **53**, 874-881.
- Lee, J., Moon, S., Cha, Y. & Chung, Y.D (2010) Drosophila TRPN (= NOMPC) channel localizes to the distal end of mechanosensory cilia. *Plos One*, **5**, e11012.
- Lu, Q., Senthilan, P.R., Effertz, T., Nadrowski, B., Göpfert, M.C (2009) Using Drosophila for studying fundamental processes in hearing. *Integrative and Comparative Biology*, **49**, 674-680.
- Mason, M.J (2016) Structure and function of the mammalian middle ear. II: Inferring function from structure. *Journal of Anatomy*, **228**, 300-312.
- Matsuo, E., Seki, H., Asai, T., Morimoto, T., Miyakawa, H., Ito, K. & Kamikouchi, A. (2016) Organization of projection neurons and local neurons of the primary auditory center in the fruit fly *Drosophila melanogaster*. *Journal of Comparative Neurology*, **524**, 1099-1164.
- Matsuo, E., Yamada, D., Ishikawa, Y., Asai, T., Ishimoto, H. & Kamikouchi, A. (2014) Identification of novel vibration- and deflection-sensitive neuronal subgroups in Johnston's organ of the fruit fly. *Frontiers of Physiology*, **5**, 179.
- Metaxakis, A., Oehler, S., Klinakis, A. & Savakis, C. (2005) Minos as a genetic and genomic tool in *Drosophila melanogaster*. *Genetics*, **171**, 571-581.
- Mirzoyan, Z., Sollazzo, M., Allocca, M., Valenza, A.M., Grifoni, D. & Bellosta, P. (2019) *Drosophila melanogaster*: A Model Organism to Study Cancer. *Front Genet*, **10**, 51.

- Nadrowski, B., Effertz, T., Senthilan, P.R. & Gopfert, M.C. (2011) Antennal hearing in insects--new findings, new questions. *Hearing Research*, **273**, 7-13.
- Narda, R.D (1966) Analysis of the stimuli involved in courtship and mating in *D. malerkotliana* (Sophophora, Drosophila). *Animal Behaviour*, **14**, 378-383.
- Newsome, T.P., Asling, B. & Dickson, B (2000) Analysis of *Drosophila* photoreceptor axon guidance in eye-specific mosaics. *Development*, **127**, 851-860.
- Nigel S. Atkinson, Robert Brenner, Whei-meih Chang, Jennette Wilbur, James L. Larimer and Joyce Yu (2000) Molecular Separation of Two Behavioral Phenotypes by a Mutation Affecting the Promoters of a Ca-Activated K Channel. *The Journal of Neuroscience*, **20**, 2988-2993.
- Oxenham, A.J. (2018) How We Hear: The Perception and Neural Coding of Sound. *Annu Rev Psychol*, **69**, 27-50.
- P. A Fuchs., M. G. Evans (1990) Potassium currents in hair cells isolated from the cochlea of the chick. *The Journal of Physiology*, **429**, 529-551.
- Pacheco, D.A., Thiberge, S.Y., Pnevmatikakis, E. & Murthy, M. (2021) Auditory activity is diverse and widespread throughout the central brain of *Drosophila*. *Nature Neuroscience*, **24**, 93-104.
- Phelps, C.B. & Brand, A.H (1998) Ectopic Gene Expression in *Drosophila* Using GAL4 System. *Methods*, **14**, 367-379.
- Plack, C.J. (2018) *The sense of hearing*. Routledge.
- Pollack, I (1948) Effects of high pass and low pass filtering on the intelligibility of speech in noise. *The Journal of the Acoustical Society of America*, **20**, 259-266.
- R.A. Eatock., M, Saeki & M.J Hutzler (1993) Electrical resonance of isolated hair cells does not account for acoustic tuning in the free-standing region of the alligator lizard's cochlea. *The Journal of Neuroscience*, **13**, 1767-1783
- Rebollo, R., Romanish, M.T. & Mager, D.L (2012) Transposable elements: an abundant and natural source of regulatory sequences for host genes. *Annual review of genetics*, **46**, 21-42.
- Riabinina, O., Dai, M., Duke, T. & Albert, J.T. (2011a) Active process mediates species-specific tuning of *Drosophila* ears. *Current Biology*, **21**, 658-664.
- Riabinina, O., Dai, M., Duke, T. & Albert, J.T (2011b) Active process mediates species-specific tuning of *Drosophila* ears. *Current Biology*, **21**, 658-664.
- Rosowski, J.J (2013) Comparative middle ear structure and function in vertebrates. *The Middle Ear*, 31-65.
- Roy, M., Sivan-Loukianova, E. & Eberl, D.F (2013) Cell-type-specific roles of Na⁺/K⁺ ATPase subunits in *Drosophila* auditory mechanosensation. *Proceedings of the National Academy of Science*, **110**, 181-186.
- Ryder, E. & Russell, S (2003) Transposable elements as tools for genomics and genetics in *Drosophila*. *Briefings in Functional Genomics*, **2**, 57-71.
- Ryan G. Kavlie., Janice L. Fritz., Florian Nies., Martin C. Göpfert., Dominik Oliver., Joerg T. Albert. & Daniel F. Eberl (2015) Prestin is an anion transporter dispensable for mechanical feedback amplification in *Drosophila* hearing. *Journal of Comparative Physiology A*, **201**, 51-60
- Sataloff, J. & Sataloff, J (2005) *The Physics of Sound*. 2.
- Scanes, C.G. (2018) Animal Perception including differences with humans. *In Animals and human society*. Elsevier, pp. 1-11.

- Schwarz, T.L., Tempel, B.L., Papazian, D.M., Jan, Y.N. & Jan, L.Y (1988) Multiple potassium-channel components are produced by alternative splicing at the Shaker locus in *Drosophila*. *Nature*, **331**, 137-142.
- Senthilan, P.R., Piepenbrock, D., Ovezmyradov, G., Nadrowski, B., Bechstedt, S., Pauls, S., Winkler, M., Möbius, W., Howard, J. & Göpfert, M.C (2012) *Drosophila* auditory organ genes and genetic hearing defects. *Cell*, **150**, 1042-1054.
- Shorey, H (1962) Nature of the sound produced by *Drosophila melanogaster* during courtship. *Science*, **137**, 677-678.
- Spiehl, H.T. (1952) Mating behavior within the genus *Drosophila* (Diptera). Bulletin of the AMNH; v. 99, article 7.
- Stocker, R.F (1994) The organization of the chemosensory system in *Drosophila melanogaster*: a review. *Cell and tissue research*, **275**, 3-26.
- Szuts, V., Jarabin, J.A., Nagy, N., Otvos, F., Nagy, R., Nagy, A., Halasy, K., Rovo, L., Szell, M. & Kiss, J.G. (2018) Altered Potassium Ion Homeostasis in Hearing Loss. *Ion Channels in Health and Sickness*.
- Tan, X., Beurg, M., Hackney, C., Mahendrasingam, S. & Fettilplace, R. (2013) Electrical tuning and transduction in short hair cells of the chicken auditory papilla. *Journal of Neurophysiology*, **109**, 2007-2020.
- Theodosiou, N.A. & Xu, T (1998) Use of FLP/FRT system to study *drosophila* development. *Methods*, **14**, 355-365.
- Todi, S.V., Sharma, Y., Eberl, D.F (2004) Anatomical and molecular design of the *Drosophila* antenna as a flagellar auditory organ. *Microscopy research and technique*, **63**, 388-399.
- Tong, H., Kopp-Scheinflug, C., Pilati, N., Robinson, S.W., Sinclair, J.L., Steinert, J.R., Barnes-Davies, M., Allfree, R., Grubb, B.D., Young, S.M., Jr. & Forsythe, I.D. (2013) Protection from noise-induced hearing loss by Kv2.2 potassium currents in the central medial olivocochlear system. *Journal of Neuroscience*, **33**, 9113-9121.
- von Schilcher, F (1976) The function of pulse song and sine song in the courtship of *Drosophila melanogaster*. *Animal Behaviour*, **24**, 622-625
- Weber, P.C., Cunningham III, C.D. & Schulte, B.A (2001) Potassium recycling pathways in the human cochlea. *The Laryngoscope*, **111**, 1156-1165.
- Windmill, J.F. & Jackson, J.C. (2016) Mechanical specializations of insect ears *Insect hearing*. Springer, pp. 125-157.
- Xia, X., Zhang, Q., Jia, Y., Shu, Y., Yang, J., Yang, H. & Yan, Z. (2020) Molecular basis and restoration of function deficiencies of Kv7.4 variants associated with inherited hearing loss. *Hearing Research*, **388**, 107884.
- Xu, Z.-Q.J., Zhang, Y., Luo, T., Xiao, Y. & Ma, Z (2019) Frequency principle: Fourier analysis sheds light on deep neural networks. *arXiv preprint aiXiv*
- Yack, J (2004) The structure and function of auditory chordotonal organs in insects. *Microscopy research and technique*, **63**, 315-337.
- Yamaguchi, M. & Yoshida, H (2018) *Drosophila* as a model organism. *Drosophila Models for Human Diseases*, 1-10.
- Yamanaka, K., Maruyama, Y., Tsuji, T. & Nakamoto, K (2001) Resonance frequency and Q factor mapping by ultrasonic atomic force microscopy. *Applied Physics Letters*, **78**, 1939-1941.

- Yin, T.C.T., Smith, P.H. & Joris, P.X. (2019) Neural Mechanisms of Binaural Processing in the Auditory Brainstem. *Compr Physiol*, **9**, 1503-1575.
- Yorozu, S., Wong, A., Fischer, B.J., Dankert, H., Kernan, M.J., Kamikouchi, A., Ito, K. & Anderson, D.J. (2009) Distinct sensory representations of wind and near-field sound in the *Drosophila* brain. *Nature*, **458**, 201-205.
- Yufei Hu., Yinjun Jia., Tuantuan Deng., Ting Liu. & Wei Zhang (2021) Molecular Mechanisms for Frequency Specificity in a *Drosophila* Hearing Organ, bioRxiv
- Zdebik, A.A., Wangemann, P. & Jentsch, T.J. (2009) Potassium ion movement in the inner ear: insights from genetic disease and mouse models. *Physiology (Bethesda)*, **24**, 307-316.
- Zhang, W., Yan, Z., Jan, L.Y. & Jan, Y.N (2013) Sound response mediated by the TRP channels NOMPC, NANCHUNG, and INACTIVE in chordotonal organs of *Drosophila* larvae. *Proceedings of the National Academy of Science*, **110**, 13612-13617.

List of abbreviations

AMMC	antennal mechanosensory and motor center
CAP	compound action potential
JO	Johnston's organ
a1:	1 st antennal segment; scape
a2:	2 nd antennal segment; pedicel
a3:	3 rd antennal segment; funicle
GFP	green fluorescence protein
RFP	red fluorescent protein
iBF	individual best frequency
cDNA	complementary DNA
UAS	upstream activating sequence
RT-qPCR	Quantitative reverse transcription PCR
FFT	Fast Fourier Transform
FLP	Flippase
FRT	Flippase Recognition Target
Lch5	lateral pentaloscolopidial chordotonal organ
MTC	mechanotransduction channel
<i>nompC</i>	no mechanoreceptor potential C
<i>ato</i>	atonal
<i>Dnai2</i>	dynein, axonemal, intermediate chain 2 GFP green
<i>JO15</i>	GAL4 driver for sound-receptors
<i>NP6250</i>	GAL4 driver for gravity/wind-receptors
<i>eag</i>	ether a go-go
<i>Sh</i>	shaker
<i>Shab/Shaw/Shal</i>	Shaker cognate b/w/l
<i>slo</i>	slowpoke
<i>Elk</i>	Eag-like K ⁺ channel
<i>Irk1/Irk2/Irk3</i>	Inwardly rectifying potassium channel 1/2/3
<i>Ork1</i>	Open rectifier K ⁺ channel 1
<i>SK</i>	small conductance calcium-activated potassium channel
<i>cac</i>	cacophony
<i>Ca-α1D</i>	Ca ²⁺ -channel protein α_1 subunit D
<i>Ca-α1T</i>	Ca ²⁺ -channel protein α_1 subunit T
<i>Ca-β</i>	Ca ²⁺ -channel-protein- β -subunit

List of Figures

Fig. 1	Diagram of sound generation and two types of sinusoidal waves.....	7
Fig. 2	Diagram of different sound waveforms.....	8
Fig. 3	Frequency response curve from different filters.....	9
Fig. 4	Three harmonic motion	10
Fig. 5	Illustration of hearing process in human ear.....	12
Fig. 6	Two types of ears in insects.....	14
Fig. 7	The mechanics of hearing in <i>Drosophila</i> ear.....	17
Fig. 8	Chordotonal neurons in JO and 3 rd stage larva.....	18
Fig. 9	Auditory circuit in <i>Drosophila</i> brain.....	19
Fig. 10	Category of JO neurons.....	20
Fig. 11	Frequency preference of auditory JO neurons	21
Fig. 12	Sound generation and frequency discrimination	23
Fig. 13	Frequency discrimination on basilar membrane of coiled cochleae.....	24
Fig. 14	Different cochlea structure and mechanism of electrical tuning	26
Fig. 15	Comparison of auditory frequency components process in vertebrate and fly ear.....	26
Fig. 16	Illustration of Gal4/UAS system in <i>Drosophila</i>	28
Fig. 17	SMARTer (RACE-PCR) cDNA synthesis	32
Fig. 18	Illustration of FLP/FRT system.....	36
Fig. 19	Parental generation crossing for cell specific ablation	37
Fig. 20	Fixation of fly and LDV measurement setup	40
Fig. 21	Illustration of two recordings for <i>Drosophila</i> sound receiver.....	41
Fig. 22	Workflow for fly hearing performance measurement	45
Fig. 23	Anatomy of JO in fly's ear	46
Fig. 24	Free fluctuation of antenna in <i>wild-type</i> fly without sound.....	47
Fig. 25	Sound-evoked intensity measurement in <i>wild-type</i> fly at iBF.....	48
Fig. 26	Mechanical and electrical response in <i>wild-type</i> fly with series frequencies stimulation	50
Fig. 27	Mechanical sensitivity in <i>wild-type</i> fly at isolated intensity.....	51
Fig. 28	Electrical response in <i>wild-type</i> fly at iso-intensity	52
Fig. 29	Electrical response in <i>wild-type</i> fly at iso-displacement.....	53
Fig. 30	Cross-section staining of JO neurons with different driver lines in adult flies.....	54
Fig. 31	Whole antenna mounting with nuclear-RFP labelling and 3D reconstruction	55
Fig. 32	Brain projection of JO neurons.....	55
Fig. 33	Auditory performance in ablated JO neurons strains at different neurons	57
Fig. 34	RT-PCR result for <i>Ca-a 1D</i> mRNA in the 2 nd segment of antenna.....	59
Fig. 35	Voltage-gated calcium channels expression in JO	58
Fig. 36	Auditory performance in <i>Ca-a 1D</i> , <i>Ca-alt</i> , and <i>Ca-beta</i> mutants at different frequencies..	61

Fig. 37	Calcium-activated potassium channel (BK) expression in JO.....	62
Fig. 38	Auditory performance in <i>slowpoke</i> channel mutant at different frequencies	63
Fig. 39	Voltage-activated potassium channels expression in JO	65
Fig. 40	Auditory performance in <i>Sh</i> , <i>Shab</i> , and <i>eag</i> mutants at different frequencies	67
Fig. 41	<i>Ikr1</i> , <i>prestin</i> , and <i>piezo</i> expression in JO	69
Fig. 42	Auditory performance in <i>Irk1</i> , <i>piezo</i> , and <i>prestin</i> mutants at different frequencies	71
Fig. 43	Summary of Q factor and IBF for simple harmonic oscillation fitting	72
Fig. 44	Alternative splicing of <i>slowpoke</i> gene in JO	74
Fig. 45	Two-type strains for <i>slo</i> channel expression	78
Fig. 46	Diagram of two strategies for genetic screen in JO	80
Fig. 47	Expression of candidate genes in adult JO	81
Fig. 48	Classification of K ⁺ channels monomer by transmembrane domain.....	82
Fig. 49	Diagram of human cochlea cross-section and recirculation of potassium ion in coiled cochlea.....	83
Fig. 50	Potassium channels in Outer and Inner hair cells.....	84
Fig. 51	Diagram of RT-PCR for K ⁺ screening in <i>Drosophila</i>	87
Fig. 52	The expression of K ⁺ channel genes in heads (without antenna) and second segment of antenna.....	87
Fig. 53	Free fluctuation in K ⁺ channels mutants flies.....	90
Fig. 54	Mechanical response from sound intensity measurement in K ⁺ channel mutant at iBF	92
Fig. 55	Electrical response from sound-evoked measurement in K ⁺ channel mutant at iBF	93
Fig. 56	Morphology of JO neurons staining in <i>Wild type</i> and <i>Shab</i> mutants.....	94
Fig. 57	Auditory performance in <i>Shake</i> and <i>Shab</i> mutants.....	95
Fig. 58	Expression of potassium channels in JO	98

List of Tables

Table 1.	PCR primer list for K ⁺ channel screen	30
Table 2.	Denatured total RNA reaction mix	33
Table 3.	Buffer mix and Master mix	33
Table 4.	5' or 3' RACE cDNA synthesis Mix	33
Table 5.	RACE PCR reaction mix and PCR program	34
Table 6.	Primer list for identification of <i>slowpoke</i> transcript isoforms	35
Table 7.	Fly strains in this thesis	37
Table 8.	Antibody used in this thesis	44
Table 9.	Candidate genes from cell-specific ablation genetic screen	81
Table 10.	Free fluctuation measurement in <i>wild-type</i> flies and K ⁺ channel mutants	89

Acknowledgements

Here, I would like to take this opportunity to express my respect and appreciation to all people I have met in Germany, South Korea, and China. Without your kind and generous support, I would never go this far in my scientific career.

Firstly, I want to thank my doctoral supervisor, Prof. Dr. Martin Göpfert, who offers me this precious chance to work in such a wonderful lab for the past four years even though I have zero experience in *Drosophila* and auditory research. He was always there in the lab to support me, provide generous advice and comments, and discuss results and projects. His support and invaluable patience enable me to accomplish my doctoral study completely and timely. I would like to show my gratitude to the members of my thesis committee meeting, Prof. Dr. Andre Fiala, and Dr. Jan Clemens for their constructive comments and kind help. Furthermore, I want to thank Prof. Dr. Andrea Stumpner, Prof. Dr. Carolin Wichmann, and Prof. Dr. Nicola Strenzke for their interest to look through my dissertation and participate in my thesis defense.

Major thanks to Dr. Philipp Hehlert for his scientific introduction and training, advice and comments about my projects, and generous help with my dissertation. He is like my mentor, and I do learn a lot from him. I would also like to thank Dr. Radoslaw Katana, Dr. Narges Bodaghabadi, and Majid Bahader for their supportive ideas, discussions, and corrections. Moreover, thanks to Dr. Natascha Zhang, Dr. Thomas Efferts, Dr. Debra Yasemin Knorr, Nicola Schwedhelm Domeyer, Stephanie Pauls, Silvia Gubert, and Hanna Pies for their scientific and technical assistance to make my projects run smoothly. Thanks to Gudrun Matthes for working on my contract.

It is a great honour to appreciate my mentors before I came to Germany. Thank you Prof. Dr. Hojae Bae, Prof. Dr. Keyong-Man Kim, and Prof. Sun Bo as my scientific pioneer.

Lastly, I would like to give my deep appreciation to my parents, brother, and sister for their unconditional love and support. I miss you so much! Time flies, but the only person, who has always been by my side for the past ten years, is my wife, Ying Wang. She always believes in me, supports me, and helps me go through all the difficulties from college to doctorate, from friendship, relationship, to final marriage bonds.

谢谢你们所有人的支持与帮助 (Thank you) !!!

Curriculum Vitae

Personal details:

Name: Xiaowei Zhang
Date of birth: December 20, 1990
Place of birth: Changzhi City, Shanxi Province, China
Nationality: Chinese

Education:

10.2018 – Present PhD Student, Georg-August-Universität Göttingen (Germany)
Department of Cellular Neurobiology
Supervised by Prof. Dr. Martin Göpfert
PhD Thesis title: Molecular Mechanisms of Sound Frequency
Discrimination in the *Drosophila* Ear

10.2014 – 08.2016 Master Student, Chonnam National University (South Korea)
Department of Molecular Pharmacology
Supervised by Prof. Dr. Kyeong-man Kim

10.2010 – 08.2014 Bachelor Student, Changchun University of Chinese Medicine (China)
Major in Chemistry and Pharmacy

Working Experience:

04.2017 – 09.2018 Research assistant, Konkuk University (South Korea)
Department of Stem Cell and Regenerative Biotechnology
Supervised by Prof. Dr. Hojae Bae

Skills:

Molecular biology: RNA and DNA manipulations (extraction, cDNA synthesis, RACE-PCR, qPCR, cloning, plasmid construction, Western blot, ELISA, 2D/3D cell culture, Immunohistochemistry, Fluorescence microscope

Chemistry: HPLC, Gas chromatography, Chemical basic operation, biological activity detection

Publications:

Ongoing preparation: Evidence for BK channel-dependent electrical tuning in the *Drosophila* hearing organ

Previous publication: **Xiaowei Zhang**, ThiHnag Le, Xiaohan Zhang, Mei Zheng, Kyeong-Man Kim. (2016) Palmitoylation on the carboxyl tail is required for the selective regulation of dopamine D2 versus D3 receptors, BBA- Biomembrane. 1858, 2152-2162.

Ningning Sun, **Xiaowei Zhang**, Xiaohan Zhang, Kyeong-Man Kim. (2017) The EGF receptor inhibits the signaling of dopamine D3receptor through the phosphorylation of GRK2 on tyrosine residues, BBRC. 489, 515-522.

Xiaowei Zhang, Hee Jeong Yoon, Min Gyeong Kang, Hojae Bae. (2018) Identification and evaluation of cytotoxicity of peptide liposome incorporated citron extracts in an in vitro system, Int. J. Mol. Sci. 2018, 19, 626.